Distortional Lateral Torsional Buckling of Doubly Symmetric Wide Flange Beams

by
Ramin Arizou
Under the supervision of
Dr. Magdi E. Mohareb

Thesis submitted to the University of Ottawa
in partial fulfillment of the requirements for the
Master of Applied Science in Civil Engineering

Department of Civil Engineering
Faculty of Engineering
University of Ottawa

To my beloved parents,

Roudabeh, and Abdulghafour

and

in the memory of my grandmother

Acknowledgment

I would not be able to finish this thesis without the continuous support of my supervisor, Dr. Magdi Mohareb. His vast knowledge, creative and critical thinking, experience, and most importantly, his kind and vibrant personality, not only have helped me in this endeavor but also inspired me to push my limits and gain academic confidence. I would like to express my gratitude to the Natural Science and Engineering Research Council of Canada (NSERC) for financial support.

I would like to send my love and appreciation to my colleagues Ahamad, Samer, and Cao, who accepted me and became my closest friends throughout this work. Their advice and motivations have been extremely invaluable for me.

I also would like to thank my uncle's family, Sami, Shokoufa, Matin, Mohammad, and Arash, whose emotional support made me stronger. My heart goes to my parents Roudabeh and Abdulghafour, and to my siblings, Ghazal and Benyamin. I am so lucky to have my family with me.

Abstract

Distortional lateral-torsional buckling theories assume that the flanges remain undistorted, while the web is free to distort as a thin plate. Most theories adopt a cubic polynomial distribution along the web height to relate the lateral displacement of the web to the displacements and angles of twist both flanges. The present study develops a family of finite element solutions for the distortional buckling of wide flange beams in which the flanges are assumed to remain undistorted. In contrast to past theories, the lateral displacement distribution along the web height is characterized by superposing (a) two linear modes intended to capture the classical non-distortional lateral-torsional behavior and (b) any number of user-specified Fourier terms intended to capture additional web distortion. In the longitudinal direction, all displacement fields characterizing the lateral displacements are taken to follow a cubic distribution.

The first contribution of the thesis develops a finite element formulation that is able to replicate the classical non-distortional lateral torsional buckling solutions when the distortional modes are suppressed while enabling more accurate predictions for distortional lateral torsional buckling compared to those solutions based on the conventional cubic interpolation of the lateral displacement. The formulation is used to conduct an extensive parametric study to quantify the reduction in critical moments due to web distortion relative to the classical non-distortional predictions in the case of simply-supported beams, cantilevers, and beams with an overhang. The solution is then used to generate interaction curves for beams with an overhang subjected to various proportions of uniformly distributed and point loads.

The second contribution of the thesis adds two additional features to the formulation (a) to capture the destabilizing effect due to the load height relative to the shear center and (b) a module that incorporates any number of user-defined multi-point kinematic constraints. The additional features are employed to investigate the effect of load height, bracing height, and combined effects thereof in practical design problems. A distortional indicator is then introduced to characterize the distribution of web distortion along the beam span as the beam undergoes distortional lateral buckling. A systematic design optimization technique is then devised to identify the location(s) along the span at which the addition of transverse stiffeners would maximize the critical moment capacity.

Table of Contents

List of Figures

List of Tables

Chapter 1: Introduction

1.1. General

Laterally unsupported beams with doubly symmetric cross-sections subjected to loading inducing bending about the strong axis are subjected to longitudinal normal stresses that subdivide the cross-section into a tension portion and a compression portion. An increase in loading will eventually lead to beam failure through one of a few possible modes. If the beam has a short span relative to the cross-section depth, the stresses may attain the nominal yielding stress of the material, which leads to a material mode of failure, whereas if the beam is comparatively long, experimental observations (e.g., [1-4]) suggest the beam buckles. This failure mode is characterized by a tendency of the compression portion of the cross-section to undergo lateral displacement, along with the tendency of the tensile portion of the cross-section to resist lateral displacement. In a simply-supported beam, this leads to a lateral displacement of the cross-section in which the compression flange moves more than the tension flange (i.e., the section undergoes twisting of the cross-section). This failure mode is known as lateral torsional buckling (LTB), and it is the scope of the present thesis.

The kinematics of LTB may be characterized by four states (Fig. 1-1). These are:

1. **The undeformed state**: in which no loading is applied and the beam retains its un-deformed shape.
2. **State of equilibrium under reference loads**: In this state, the beam is subjected to a reference load $q(z)$. Under loading, the beam reaches equilibrium by undergoing a vertical deformation $v(z)$.
3. **State of onset of buckling**: The reference load is increased by a scaler λ. For loading $\lambda q(z)$, the beam reaches a neutral state of equilibrium, at which is it has a tendency to undergo LTB under no increase in loading.
4. **Buckling State**: The beam undergoes LTB characterized by lateral displacements and twist.

The classical approach (Fig. 1-1) in modeling LTB is based on the Vlasov thin-walled beam theory [5]. This theory is characterized by two simplifying assumptions (i) cross-section moves as a rigid disk in its plane throughout deformation, and (ii) shear strains within the section mid-surface are negligible. Since the classical approach does not account for the cross-sectional distortion, it will be referred to as non-distortional LTB in this thesis. However, for thin-walled beams with comparatively short spans, stocky flanges, and/or slender webs, web distortion may take place (e.g., [6-8]). An approach that accounts for cross-sectional distortion throughout buckling is to model both flanges as Vlasov beams connected to a flexible web represented as a thin plate. We refer to such solution types as distortional LTB.

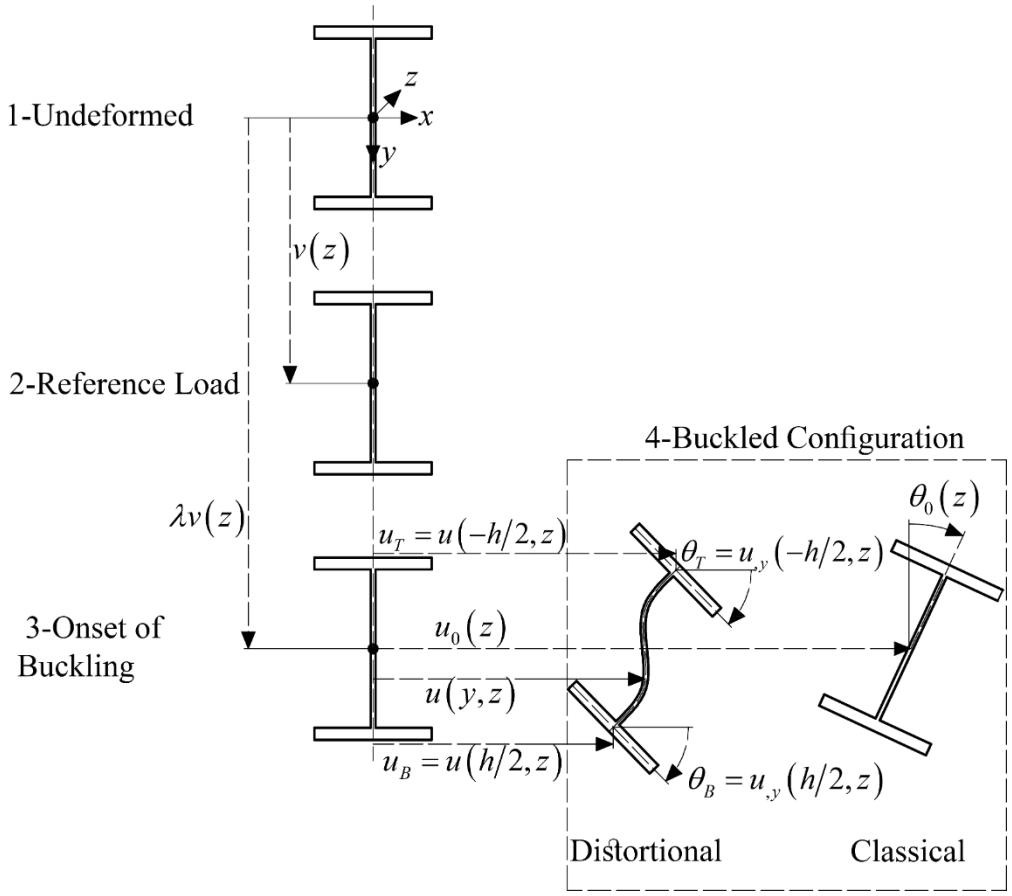

Fig. 1-1: Stages of deformation

Energy methods such as the principle of virtual work, the stationary complementary energy, and total potential energy may be used to formulate the equilibrium (or neutral stability) conditions associated with the LTB behavior of a beam. In this thesis, the total potential energy functional is adopted to obtain the discretized form of the conditions of neutral stability of doubly symmetric wide flange beams throughout lateral-torsional buckling. According to the principle of stationary potential energy, the beam is in equilibrium if no change occurs in the system's total potential energy for an arbitrary variation of the displacement fields that satisfies

the problem's essential boundary conditions. This virtual displacement is obtained from infinitesimal variations of the true configuration of the structure [9]. Therefore, by setting the first variation of the total potential energy of the beam throughout buckling to zero, the equilibrium state corresponding to the onset of buckling is obtained.

The advantage of the principle of stationary potential energy is that the need for deriving the governing differential equations of LTB is obviated, which comes in handy when the governing differential equations of the body are complex and/or cannot be solved conveniently. In LTB problems, closed-form solutions are not typically available for general cases involving various boundary and loading conditions. For this reason, numerical approaches such as the Rayleigh-Ritz, finite integrals, finite strip, and finite element methods may be used. In Chapter 2 of this thesis, a finite element formulation is developed in which the displacement field of the web throughout buckling is related to modes of deformation, which account for both non-distortional and distortional deformation of the web. The principle of stationary potential energy is evoked with respect to the amplitude of the modes of deformation and yields the beam's equilibrium conditions at the onset of buckling. The remainder of this chapter briefly explains the prerequisites, approaches, and principles used throughout this work.

1.2. Principle of Stationary Potential Energy

In the most general form, the displacement field of a three-dimensional elastic body can be expressed as functions of the axes x, y and z; i.e.,

$$u = u(x, y, z), \qquad v = v(x, y, z), \qquad w = w(x, y, z) \tag{1.1a-c}$$

in which u is displacement along x-axis; v is displacement along y-axis, and w is displacement along z-axis. Under the small strain assumption, the strains are related to the displacement fields through

$$\begin{aligned} &\varepsilon_x = \frac{\partial u}{\partial x}, && \varepsilon_y = \frac{\partial v}{\partial y}, && \varepsilon_z = \frac{\partial w}{\partial z} \\ &\gamma_{xy} = \frac{\partial u}{\partial y} + \frac{\partial v}{\partial x}, && \gamma_{yz} = \frac{\partial v}{\partial z} + \frac{\partial w}{\partial y}, && \gamma_{zx} = \frac{\partial u}{\partial z} + \frac{\partial w}{\partial x} \end{aligned} \tag{1.2a-f}$$

Based on Hooke's law for linear isotropic material, the stress components are obtained as

$$\begin{aligned}
\sigma_x &= (\xi + 2\eta)\varepsilon_x + \xi\varepsilon_y + \xi\varepsilon_z \\
\sigma_y &= \xi\varepsilon_x + (\xi + 2\eta)\varepsilon_y + \xi\varepsilon_z \\
\sigma_z &= \xi\varepsilon_x + \xi\varepsilon_y + (\xi + 2\eta)\varepsilon_z \\
\tau_{xy} &= \eta\gamma_{xy} \\
\tau_{yz} &= \eta\gamma_{yz} \\
\tau_{zx} &= \eta\gamma_{zx}
\end{aligned} \tag{1.3a-f}$$

in which ξ and η are elastic Lama constants, and are related to the Modulus of Elasticity *E*, and the Poisson's Ratio μ through

$$\begin{aligned}
\xi &= \frac{\mu E}{(1+\mu)(1-2\mu)} \\
\eta &= \frac{E}{2(1+\mu)}
\end{aligned} \tag{1.4a-b}$$

The strain energy stored throughout deformation *U* is obtained by the product of the strain components and their corresponding stress components integrated over the volume of the elastic body, i.e.,

$$U = \frac{1}{2}\iiint_V \left(\varepsilon_x\sigma_x + \varepsilon_y\sigma_y + \varepsilon_z\sigma_z + \gamma_{xy}\tau_{xy} + \gamma_{yz}\tau_{yz} + \gamma_{zx}\tau_{zx}\right)dV \tag{1.5}$$

The work gained by the external is obtained by the product surface tractions p_x, p_y ,and p_z and their corresponding displacement integrated over the surface of the elastic body; i.e.,

$$V = -\iint_S \left(p_x^S u + p_y^S v + p_z^S w\right)dS \tag{1.6}$$

The total potential energy Π of the system is obtained by summing the internal strain energy *U* and the load potential energy *V* , i.e.,

$$\Pi = U + V \tag{1.7}$$

The body is in equilibrium when the total potential energy is in a stationary condition, which is known as the principle of stationary potential energy. The stationarity condition is obtained by setting to zero the first variation of the total potential energy with respect to displacement fields, i.e.,

$$\delta\Pi = 0 \tag{1.8}$$

1.3. Kinematics of Beam Theories and Thin-plate Theory

In the present thesis, three types of analyses have been conducted. The conventional Euler-Bernoulli beam theory is employed for the pre-buckling analysis, characterized by deformation from stage 1 to 2 in Fig. 1-1–. It is assumed that the flanges remain undistorted throughout buckling. Hence, they are modeled by the Vlasov thin-walled beam theory. In contrast, the web is assumed free to distort throughout buckling, hence modeled by the Kirchhoff thin plate bending theory. Herein, the kinematics of each theory are briefly explained, and based on the discussion provided in Section 1.2, total potential energy expressions are provided for the pre-buckling analysis and those required for buckling analysis of the flanges and the web.

1.3.1. Euler-Bernoulli Beam Theory

The Euler-Bernoulli beam theory assumes (i) planes normal to the centerline remain normal during the deformation, and (ii) the deflections are small (Fig. 1-2a). By these assumptions, the displacement fields are simplified as

$$\begin{aligned} w(z,y) &= w_0(z) - y\frac{dv(z)}{dz} \\ v(y,z) &= v(z) \end{aligned} \tag{1.9}$$

where $w_0(z)$ is the longitudinal displacement at the beam centroid and $v(z)$ is the transverse displacement. It notable that the first assumption omits shear deformation. Given the kinematics introduced in Eq.1.9, the pre-buckling total potential energy Π_p for a beam subjected to an arbitrary transverse load $q(z)$ that induces bending about the major principal x axis (Fig. 1-2b), is given by

$$\Pi_p = \int_{z=0}^{L} EI_x \left(\frac{\partial^2 v}{\partial z^2}\right)^2 dz - \frac{1}{2}\int_0^L q(z)v(z)\,dz \tag{1.10}$$

in which $I_x = t_W h^3/12 + bt^3/6 + bth$ is the moment of inertia of the beam about the axis x. The cross-sectional dimensions b, t, d and t_W are defined in Fig. 1-2c.

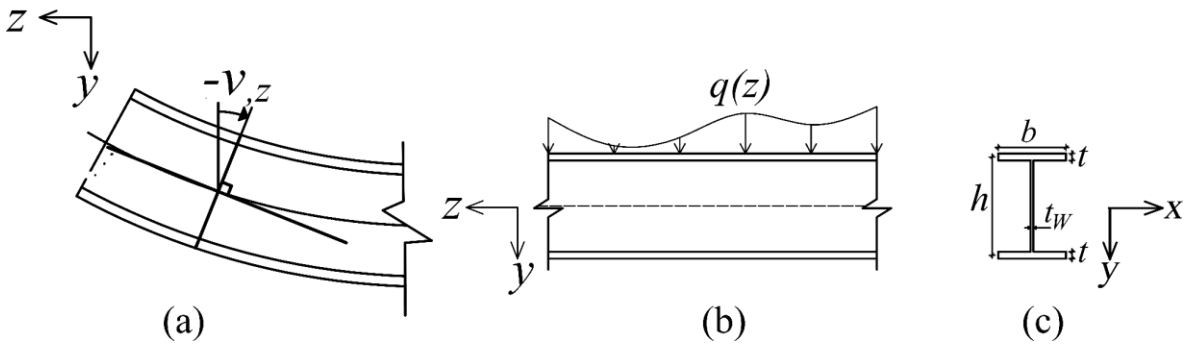

Fig. 1-2: (a) Kinematics of Euler-Bernoulli beam theory (b) Doubly-symmetric I beam subjected to arbitrary load $q(z)$, and (c) cross-sectional dimensions

1.3.2. Vlasov Thin-walled Beam Theory

In contrast to circular shafts, when a wide flange beam undergoes twist, it exhibits non-uniform longitudinal displacements that do not lie in a single plane, a phenomenon known as warping. Vlasov [5] developed a theory for open thin-walled members subjected to a combination of flexure and torsion. The Vlasov theory accounts for the effect of warping induced by torsion. Vlasov derived the kinematics of the thin-walled members based on three assumptions: (i) the beam cross-section has rigid movement. (ii) the shear strain at the middle surface is negligible, and (iii) The angle of twist of the cross-section is small.

Fig. 1-3a shows a doubly symmetric wide flange beam in which the shear center and centroid of the cross-section coincide at point O. Under the Vlasov assumptions, the displacements $(\bar{u},\bar{v},\bar{w})$ for a point $\left[x(s),y(s),\bar{\omega}(s)\right]$ lying on the mid-surface can be expressed in terms of shear center displacements $u(z)$, $v(z)$, and $w(z)$, and the angle of twists of the cross-section $\theta(z)$ of the section z, i.e.,

$$\begin{aligned}
\bar{u}(s,z) &= u(z) - y(s)\theta(z) \\
\bar{v}(s,z) &= v(z) + x(s)\theta(z) \\
\bar{w}(s,z) &= w(z) - x(s)\frac{\partial u(z)}{\partial z} - y(s)\frac{\partial v(z)}{\partial z} - \bar{\omega}(s)\frac{\partial \theta(z)}{\partial z}
\end{aligned} \tag{1.11a-c}$$

in which $\bar{\omega}(s) = x(s)\,y(s)$ is the sectorial coordinate defined for doubly symmetric beams. Throughout lateral-torsional buckling (i.e., in going from state 3 to 4 in Fig. 1-1), a thin-walled beam undergoes no additional transverse displacements displacement nor longitudinal displacements, and hence one obtains

$$\bar{u}(s,z) = u(z) - y(s)\theta_z(z)$$
$$\bar{v}(s,z) = x(s)\theta_z(z) \qquad \text{(1.12a-c)}$$
$$\bar{w}(s,z) = -x(s)\frac{\partial u(z)}{\partial z} - \bar{\omega}(s)\frac{\partial \theta_z(z)}{\partial z}$$

In this case, from Eq.1.12a-c by substituting into the total potential energy Π of a beam (Eq.1.7), performing the integrals over the area, one obtains (e.g., [10, 11])

$$\Pi = \frac{1}{2}\int_0^L \left(EI_y u_{,zz}^2 + EC_w\theta_{,zz}^2 + GJ\theta_{,z}^2\right)dz + \int_0^L M(z)u\theta'' dz \qquad (1.13)$$

where G is the shear modulus, E is Young's modulus, I_y is the weak axis moment of inertia for the flanges, C_w is the warping constant, J is the Saint-Venant torsional constant, and $M(z)$ is the major axis bending moment. In this thesis, the bending in the pre-buckling analysis is assumed to induce normal stresses $\sigma(z)$ on the flanges that are uniform at y and x axes while varying in z axis (Fig. 1-3b). The flanges are assumed to remain undistorted throughout buckling and thus modeled by the Vlasov beam theory.

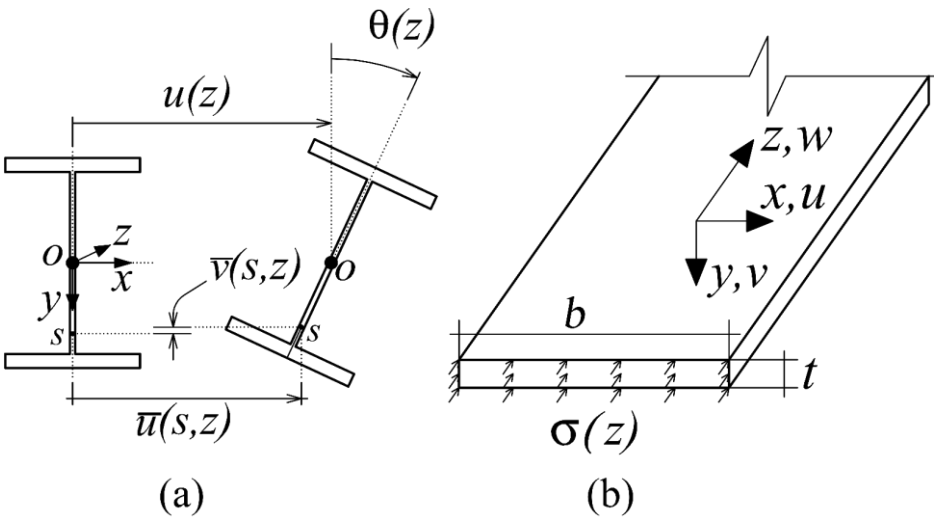

Fig. 1-3: (a) Kinematics of Vlasov theory (b) Flanges modeling scheme

1.3.3. Thin Plate Theory

While the Vlasov theory accounts for the warping effect, it neglects possible web distortion. Nevertheless, for beams with relatively small spans, slender webs, and/or stocky flanges, the LTB may lead to considerable web distortion. For this reason, the web is modeled as a Kirchhoff thin plate in this thesis. The Kirchhoff plate theory assumes that (i) a straight line normal to the mid-surface remains normal to the mid-surface throughout deformation, (ii)

straight lines normal to the mid-surface remain straight throughout deformation, (iii) the thickness of the plate does not change throughout deformation, and (iv) only the in-plane normal stresses and in-plane shear stresses are assumed to contribute to the internal strain energy while the contribution of other stress components is negligible. Assuming the plate undergoes flexure around y and z axes, one obtains the kinematics of Kirchhoff plate theory as ([12])

$$u = u(y,z); \quad v = -xu_{,y}; \quad w = -xu_{,z} \tag{1.14a-c}$$

Substituting Eq.1.14 into the strain components appearing in Eqs.1.2b, c and e yields

$$\varepsilon_z = -xu_{,zz}; \quad \varepsilon_y = -zu_{,yy}; \quad \gamma_{yz} = -2u_{,yz} \tag{1.15a-c}$$

A simplifying assumption in plate theory is to omit σ_x, τ_{xz} and τ_{xy}. The remaining stress components are obtained based on generalized Hooke's law, i.e.,

$$\sigma_z = \frac{E}{1-\mu^2}\left(\varepsilon_z + \mu\varepsilon_y\right); \quad \sigma_y = \frac{E}{1-\mu^2}\left(\varepsilon_y + \mu\varepsilon_z\right); \quad \tau_{yz} = \frac{E}{1+\mu}\gamma_{yz} \tag{1.16a-c}$$

By substituting Eqs.1.15 and 1.16 into the strain energy expression appearing in Eq.1.5, and taking integral with respect to x axis, the strain energy of a plate may be expressed as

$$U = \frac{D}{2}\iint\left[u_{,zz}^2 + u_{,yy}^2 + 2\mu u_{,yy}u_{,zz} + 2(1-\nu)u_{,yz}^2\right]dydz \tag{1.17}$$

in which $D = Et^3/12\left(1-\mu^2\right)$ is the flexural rigidity of the plate. For a thin-plate subjected to variable normal stress and t denotes the plate thickness. If the plate is subjected to normal membrane force per unit length N_y, and shear membrane force per unit length N_{xy}, as the plate buckles, the potential energy gained by forces N_y and N_{xy} are determined by

$$V = \frac{1}{2}\iint\left(N_z u_{,z}^2 + 2N_{xy}u_{,z}u_{,y}\right)dydz \tag{1.18}$$

Noting that $N_z = t\sigma(y,z)$ and $N_{yz} = t\tau(z)$ Eq.1.18, can be re-written as

$$V = \frac{t}{2}\iint\left[\sigma u_{,z}^2 + 2\tau u_{,z}u_{,y}\right]dzdy \tag{1.19}$$

The total potential energy of the plate is obtained from the summation of the internal strain energy appearing in Eq.1.17, and the load potential energy gain appearing in Eq.1.19 , i.e.,

$$\Pi = \frac{D}{2}\iint\left[u_{,zz}^2 + u_{,yy}^2 + 2\mu u_{,yy}u_{,zz} + 2(1-\nu)u_{,yz}^2\right]dydz + \frac{t}{2}\iint\left[\sigma u_{,z}^2 + 2\tau u_{,z}u_{,y}\right]dzdy \qquad (1.20)$$

The normal stress σ is assumed positive when in tension. Therefore, the potential energy gained by σ, as provided by Eq.1.20 is positive.

1.4. Scope of the Thesis and Motivation

1.4.1. Investigation of Conventional Distortional LTB Theories

The LTB buckling of doubly symmetric wide flange beams with relatively small spans, slender webs, and/or stocky flanges may be associated with significant web distortion. Classical buckling theories are based on the Vlasov thin-walled member theory and do not capture the distortional effect. The majority of the studies on distortional LTB of wide-flange members assume that the flanges remain undistorted, while the web undergoes distortion throughout buckling. In this thesis, we retain this assumption. While the distribution of lateral displacement along the web height is conventionally related to the lateral displacement and angles of twist of the flanges through cubic polynomials (e.g., [13-17]), this thesis develops a more robust approach leading to a new finite element formulation in which the distribution of the lateral displacement of the web is characterized by two types of modes of deformation, namely, non-distortional modes and distortional modes. By using this novel finite element formulation, the present work provides a basis to assess the adequacy of previous distortional buckling theories.

1.4.2. Effect of Distortion on LTB Resistance

To complement previous studies (e.g., [8, 18, 19]), the present work adopts the new formulation to investigate the influence of cross-sectional geometry and beam spans on reducing LTB capacity associated with the web distortion.

1.4.3. Transverse Stiffeners as Means of Suppressing Web distortion

The presence of a transverse stiffener at a given cross-section tends to suppress distortion at the stiffener location by enforcing equal angles of twist for the flanges while preventing the web from bending within the plane of the cross-section, and consequently increase the buckling resistance of doubly symmetric wide-flange beams (Fig. 1-4). Within this context, the present work provides (i) a modeling technique to suppress web distortion at a given cross-section in order to account for stiffeners that may be present at the section, (ii) identify the cross-sections along the span where the web exhibits the most distortion, and (iii) develop a practical design

approach to optimize the location of transverse stiffeners that would maximize the LTB capacity of the member.

1.4.4. Summary of Features

In summary, the finite element formulation provided in the present study incorporates

- Web distortional effect
- Load Height Effect
- A general kinematic constraint capable of simulating the effect of transverse stiffeners in suppressing web distortion, lateral braces that are offset from the flange locations, etc.

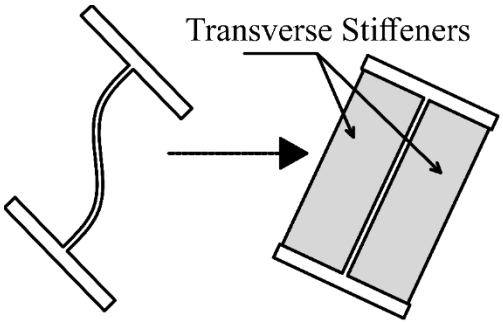

Fig. 1-4: Effect of transverse stiffeners

1.5. Overview of the Thesis

The present chapter provided fundamental concepts, techniques, and approaches adopted throughout the thesis. Chapters 2 and 3 are written in paper format, each including their stand-alone literature review.

In Chapter 2, a unified finite element formulation is developed for both distortional and non-distortional LTB of doubly symmetric wide flanges beams. Through an extensive parametric study, the influence of web slenderness, section aspect ratio, the flanges slenderness, and beam length on distortional and non-distortional LTB is investigated for (i) simply-supported beams subjected to mid-span point load, (ii) simply-supported beams subjected uniformly distributed load, and for (iii) cantilevers subjected to tip-placed point load (iv) simply-supported beams with a single overhang subjected to a tip-placed point. Examples are solved to demonstrate the dependence of the buckled configuration for a cantilever on its span. Finally, interaction curves are provided for simply-supported beams with a single overhang.

In Chapter 3, the finite element formulation is augmented to incorporate two additional features a) the load height effect and b) the inclusion of a kinematic constraint feature. Examples are solved to investigate the effect of lateral bracing on the non-distortional and distortional LTB. Several examples are provided to investigate the effect of the position of load height and lateral

bracing on distortional and non-distortional LTB. Finally, a practical approach for the optimized design of transverse stiffeners will be presented and then applied for a simply-supported beam and a simply-supported beam with an overhang.

Chapter 4, provides a summary of the work and outlines its various features. The observations and conclusions of the study are summarized. Finally, recommendations for future research and extension of the work will be provided.

1.6. References

[1] B. Bose, The influence of torsional restraint stiffness at supports on the buckling strength of beams, Structural Engineer. Part B 60(4) (1982).
[2] M. Wakabayashi, T. Nakamura, Buckling of laterally braced beams, Engineering Structures 5(2) (1983) 108-118.
[3] S. Kitipomchai, P.F. Dux, N.J. Richter, Buckling and Bracing of Cantilevers, Journal of Structural Engineering 110(9) (1984) 2250-2262.
[4] M. Assadi, W. Roeder Charles, Stability of Continuously Restrained Cantilevers, Journal of Engineering Mechanics 111(12) (1985) 1440-1456.
[5] V.Z. Vlasov, Thin-walled elastic beams, National Technical Information Service1961.
[6] S. Rajasekaran, D.W. Murray, Coupled Local Buckling In Wide-Flange Beam-Columns, 1973.
[7] C.P. Johnson, M.K. Will, Beam Buckling By Finite Element, 1974.
[8] G.J. Hancock, Local, distortional and lateral buckling of I-beams, 1978.
[9] J.N. Reddy, Energy Principles and Variational Methods in Applied Mechanics, Wiley2002.
[10] R.S. Barsoum, R.H. Gallagher, Finite element analysis of torsional and torsional–flexural stability problems, International Journal for Numerical Methods in Engineering 2(3) (1970) 335-352.
[11] C.M. Wang, S. Kitipornchai, On stability of monosymmetric cantilevers, Engineering Structures 8(3) (1986) 169-180.
[12] E. Ventsel, T. Krauthammer, E. Carrera, Thin plates and shells: theory, analysis, and applications, Appl. Mech. Rev. 55(4) (2002) B72-B73.
[13] M. Roberts Terence, G. Azizian Zaven, Instability of Thin Walled Bars, Journal of Engineering Mechanics 109(3) (1983) 781-794.
[14] M. Roberts Terence, G. Azizian Zaven, Influence of pre-buckling displacements on the elastic critical loads of thin walled bars of open cross section, International Journal of Mechanical Sciences 25(2) (1983) 93-104.
[15] M.M. Attard, General non-dimensional equation for lateral buckling, Thin-Walled Structures 9(1-4) (1990) 417-435.
[16] Y.L. Pi, N.S. Trahair, Prebuckling deflections and lateral buckling. I: theory, Journal of structural engineering 118(11) (1992) 2949-2966.
[17] Y.L. Pi, N.S. Trahair, Prebuckling deflections and lateral buckling. II: applications, Journal of Structural Engineering 118(11) (1992) 2967-2985.
[18] G.J. Hancock, M.A. Bradford, N. Trahair, Web distortion and flexural-torsional buckling, 1979.
[19] M.A. Bradford, N.S. Trahair, Distortional Buckling of I-Beams, 1981.

Chapter 2: Finite Element Formulation for Distortional Lateral Buckling of Beams

Abstract

The present study develops a finite element formulation for the distortional buckling of wide flange beams. The formulation characterizes the distribution of the lateral displacement along the web height by superposing (a) two linear modes intended to capture the classical non-distortional lateral-torsional behavior and (b) any number of user-specified Fourier terms intended to capture additional web distortion. All displacement fields characterizing the lateral displacements are taken to follow a cubic distribution in the longitudinal direction. A separation of variables technique is effectively achieved by exploiting the properties of the matrix Kronecker product. The finite element solution developed is shown to replicate accurately (a) the classical non-distortional lateral-torsional buckling solutions, (b) previously developed distortional buckling solutions based on cubic interpolation of the lateral displacement, while (c) providing a basis to assess the effect to commonly omitted higher distortional modes on the predicted critical moments and buckling modes. The solution is then used to conduct a systematic parametric study to quantify the reduction in critical moments due to web distortion relative to the classical non-distortional predictions in the case of simply-supported beams, cantilevers, and beams with an overhang. The solution is then used to generate interaction curves for beams with an overhang subjected to various proportions of uniformly distributed and point loads.

Authors Keywords: Thin-walled beams, finite element, lateral torsional buckling, distortional lateral torsional buckling, distortional modes, non-distortional modes

List of Notations

A_F	Area of flanges
b	Width of flanges
C_{wF}	Warping constants of flanges
C_{wW}	Warping constants of web
C_{wG}	Global warping constant
D	Flexural rigidity of the web
E	Module of Elasticity
G	Shear module
h	Web height
$\mathbf{H}$	Vector collecting cubic Hermitian polynomials
I_{yF}	Moment inertia of flanges around weak axis
I_x	Moment inertia of section around strong axis
I_{yW}	Moment inertia of web around weak axis
J_F	Saint-Venant torsional constant of flanges
J_W	Saint-Venant torsional constant of web
L	Length
M	Pre-buckling moment distribution
M_D	Distortional critical moment
M_{ND}	Non-distortional critical moment
t	Thickness of flanges
t_w	Thickness of web
u	Lateral displacement field of web
u_B	Lateral displacement of bottom flange
u_T	Lateral displacement of top flange
$\tilde{u}_i$	Deformation mode i
$\tilde{\mathbf{u}}$	Vector collecting all modes of deformation
$\tilde{\mathbf{u}}_D$	Vector collecting only distortional modes of deformation
U	Strain energy throughout buckling for bottom flanges
V	The potential energy gained by load throughout buckling
$\mathbf{Z}$	Matrix including Hermitian polynomial required for all modes
ϕ_i	Amplitude of deformation mode i
$\boldsymbol{\varphi}$	Vector collecting all amplitudes of modes
λ	Eigenvalue
θ_B	Angle of twists of bottom flanges
θ_T	Angle of twists of top flanges
σ	Normal stress due to bending
τ	Shear stress due to bending
$\boldsymbol{\Delta}_i$	Degrees of freedom associated with mode i
$\boldsymbol{\Delta}$	Vector collecting all degrees of freedom for all modes
Π	Total potential energy throughout buckling

2.1. Introduction and Literature Review

Lateral torsional buckling is a failure limit state that typically governs the resistance of long-span thin-walled members. The Vlasov beam theory [1] laid the foundation to tackle the lateral-torsional buckling of thin-walled members. The Vlasov thin-walled beam theory is based on the simplifying assumptions that (i) the cross-section does not distort during buckling, (ii) shear deformation at the mid-surface vanishes, and (iii) pre-buckling deformation effects are omitted. More advanced thin-walled beam buckling solutions have been developed to improve upon the Vlasov theory while adhering to the first Vlasov assumption. These may be classified as non-distortional buckling solutions. Within this class of solutions, shear effects induced by bending

and warping are accounted for in the works of Reissner [2], Wu and Sun [3], Lin et al. [4], Kollár [5], Erkmen and Mohareb [6, 7], Attard and Kim [8], Wu and Mohareb [9, 10], Erkmen [11], and Sahraei et al. [12]. The overarching theme in these solutions is that shear deformation effects gain significance in thin-wall members with relatively short spans and/or deep cross-sections.

Within the class of non-distortional buckling theories, the works of Roberts and Azizian [13, 14], Attard [15], and Pi and Trahair [16, 17] accounted for pre-buckling deformation effects. In steel members with open cross-sections, pre-buckling deformation effects typically lead to a minor increase in the predicted buckling resistance that depends on the span, cross-section proportions, and point of load application [13], and the symmetry of the cross-section [15-17]. The first Vlasov assumption, which omits cross-sectional distortion, may lead to non-conservative predictions in the buckling analysis of thin-walled members with short spans and/or deep cross-sections. This drawback motivated a paradigm of 1D finite element method (FEM) solutions based on the assumption that the web distorts as a thin-plate while assuming the flanges not to distort throughout buckling. Rajasekaran and Murray [18] developed a FEM solution by superimposing the distortional behavior, modeled the Kirchhoff plate bending theory on the kinematics of the Vlasov thin-walled theory. Bradford and Trahair [19] developed a FEM solution in which the lateral displacements and angles of twist of both flanges were interpolated along the longitudinal direction using Hermitian polynomials, while the lateral displacement of the web was then obtained by a cubic function along the web height. This element was extended to investigate the distortional buckling of monosymmetric I-sections beam-columns [20], and doubly symmetric I-section cantilevers [21]. Bradford and Ronagh [22] added the contribution of elastic translational and rotational restraints to the Bradford and Trahair [19] element and adopted the new feature to investigate the distortional buckling of elastically restrained beam-columns with I-section. Pezeshky and Mohareb [23] developed a FEM solution for distortional buckling that accounted for the pre-buckling deformation. In this work, the flanges follow the kinematics of Gjelsvik theory enabling the flanges to undergo local warping. Pezeshky et al. [24] investigated the distortional buckling of Gerber beams that accounts for the local warping of flanges and the load height effect.

A common theme in the above FEM solutions is the use of cubic functions to characterize the distribution of lateral displacements along the web height and the lateral displacements and the angles of twists of the flanges along the longitudinal direction. A few studies considered different interpolation schemes for developing distortional buckling FEM of doubly symmetric wide-flanges beam-columns. Bradford and Trahair [25] expressed the angles of twist for both

flanges as the superposition of the average twist for both flanges (obtained by the difference in flange lateral displacement of the flanges divided by the web height) and additional function that captures web distortion. Roberts and Jhita [26] assumed that the lateral displacement of the web follows a combination of cubic functions along the web height, each modified by trigonometric functions along the longitudinal direction. Finally, Hughes and Ma [27, 28] adopted a fifth-order polynomial to characterized the lateral displacement distribution along the web height.

In addition to FEM solutions, other approximate distortional buckling solutions were developed by adopting similar kinematic assumptions in conjunction with the Rayleigh-Ritz method [29-32]. Closed-form solutions were developed for doubly symmetric I-section beam-columns [33], and elastically restrained monosymmetric I-section beam-columns [34, 35] for simply-supported members.

The third class of distortional buckling theories is based on the Generalized beam theory (GBT). In GBT, the buckled configuration of the thin-walled members is expressed as a linear combination of pre-defined cross-sectional deformations modes with longitudinally varying amplitudes. As a 1D augmented model, the GBT can account for the distortion of both the web and flanges in the context of wide-flange beams. A non-exhaustive survey of GBT developments in the context of the present study is presented herein. Schardt [36] devised the GBT in its original format, which was introduced to the English speaking world by the outstanding works of Davies and his co-workers [37, 38]. Schardt [39] showed the usefulness of GBT for the buckling behavior of thin-walled members with open unbranched cross-sections. Together with Davies' introductory paper [40], this work gave rise to further research on the buckling behavior of thin-walled members. Camotim and Silvestre and their team at the Technical University of Lisbon made significant advances in the GBT-based distortional buckling research. Examples of their work include the buckling behavior of thin-walled with C and Z-sections [40, 41], arbitrary branched open-cross sections [42], multi-cell closed cross-section [43], closed or partially closed sections [43], and T- and cruciform sections [44], and flat-walled with arbitrary cross-sections [45].

The earliest works on distortional buckling began with 3D FEM solutions [46]. Although these solutions led to accurate predictions, they involve a large number of degrees of freedom, and consequently, high computational power at the time. In addition to 1D augmented solutions, finite strip methods (FSM) were shown to provide a computationally efficient solution for the distortional buckling of thin-walled members [47]. Unlike GBT-based solutions, FSM, in its initial form, was unable to separate the cross-sectional deformation modes. This limitation was

addressed in the works of Ádány and Schafer [48, 49], who developed the constrained finite strip method (cFSM). The authors implemented constraints into the classic FSM, thus capturing distortional modes in a manner akin to the GBT treatment. Following a similar approach, Ádány et al. [50, 51] also developed the constrained finite element method (cFEM) solution.

As mentioned, the majority of distortional buckling formulations treat the flanges as non-distorting elements while considering the web to distort according to a cubic distribution along the web height. In a manner similar to previous studies, the present work retains the non-distorting assumption for the flanges. In contrast to past studies, web distortion is assumed to follow a more general distribution for the lateral displacement along the web height. Thus, the present study develops a family of finite element solutions that adopt a superior characterization of the lateral displacement distribution based on the superposition of two linear (non-distortional) modes with any number of user-specified Fourier terms to capture distortional effects along the web height accurately. The proposed displacement distribution is shown to converge to the classical non-distortional lateral-torsional buckling (LTB) solutions when the distortional Fourier terms are omitted. Also, it provides a benchmark to assess the accuracy of other distortional LTB solutions based on cubic lateral displacements. The solution is then used to conduct a parametric study to quantify the reduction in critical moments due to web distortion relative to the classical non-distortional solutions.

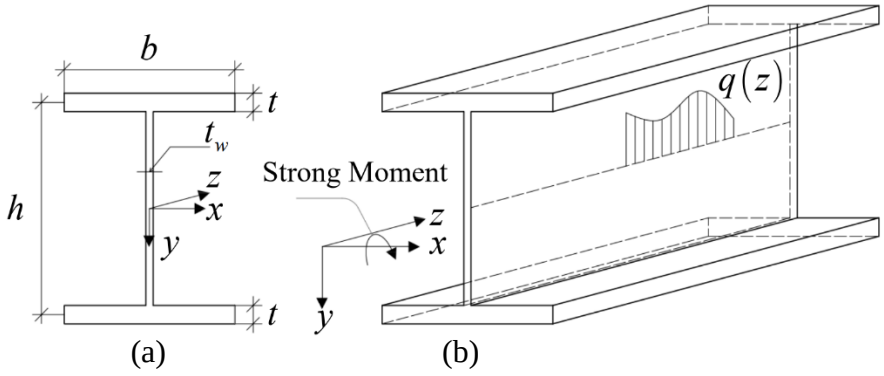

Fig. 2-1. (a) Cross-section geometric parameters (b) Loading scheme

2.2. Problem Statement

A doubly-symmetric beam with a wide flange cross-section has flanges of width b and thickness t. The web height is h, and its thickness is t_W. A right-handed coordinate system is defined on the web mid-height (Fig. 2-1). Fig. 2-2 shows the undeformed configuration of the beam in stage 1. A reference load $q(z)$ is applied to the web mid-height of the beam, and it moves to stage 2. As the load increases to a threshold value $\lambda q(z)$, the beam is assumed to

undergo a proportional transverse deformation $\lambda v(z)$ and reach stage 3. In this stage, the beam is in neutral equilibrium. Hence, an infinitesimal increase in $\lambda q(z)$ will cause the beam to buckles laterally and go to stage 4.

As a convention, all subscripts W denote the web, T denotes the top flange, and B denotes the bottom flange. The lateral displacement field of the web $u(y,z)$ characterizes the buckling configuration of the beam. The lateral displacement of the flanges $u_T(z)$ and $u_B(z)$, and their angles of twists are related to $u(y,z)$ through compatibility equations (Eq.2.6). It is required to determine the critical load $\lambda q(z)$, by which the beam tends to buckle.

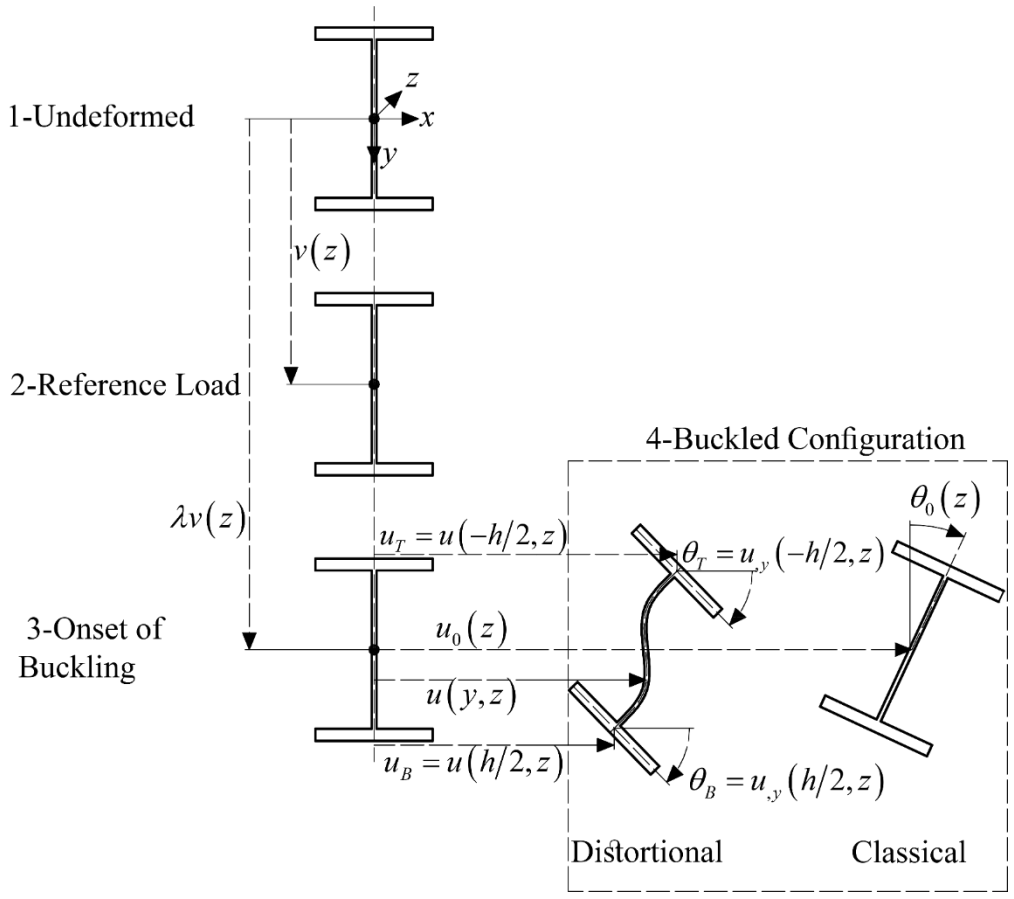

Fig. 2-2. Stages of deformation

2.3. Assumptions

The present formulation is based on the following assumptions

1. Beam cross-section is a doubly symmetric wide flange
2. Material is linearly elastic isotropic
3. Pre-buckling strains are small

4. Flanges are stocky, so that their distortion is negligible. As such, each flange can be idealized as a Vlasov beam.
5. The classical Vlasov thin-walled beam theory omits web distortion [1]. In the present solution, this assumption is relaxed, and the web is assumed free to distort. The present solution models the web using the kinematics of the classical Kirchhoff plate theory [52].

2.4. Pre-buckling Analysis

The pre-buckling analysis is conducted based on a two-node Euler-Bernoulli beam. The pre-buckling normal stress $\sigma(y,z)$ and the shear stress distributions in the web $\tau(z)$ are given by

$$\sigma(z,y)=\frac{M(z)y}{I_x};\qquad \tau(z)=\frac{V(z)}{ht_w} \tag{2.1a-b}$$

in which I_x is the strong axis moment of inertia, and $M(z)$ is the internal bending moments. $V(z)$ is the internal shear force. Both $M(z)$ and $V(z)$ are linearly interpolated from the pre-buckling internal forces M_1, M_2, V_1 and V_2 at both ends of the element, i.e.,

$$M(z)=\frac{M_1(L-z)-M_2 z}{L};\qquad V(z)=\frac{V_1(L-z)-V_2 z}{L} \tag{2.2a-b}$$

From Eq.(2.2a-b) by substituting into (2.1a-b), the normal stress in the section and the shear stresses in the web takes the following forms

$$\sigma(z,y)=\frac{M_1}{LI_x}y(L-z)-\frac{M_2}{LI_x}yz;\qquad \tau(z)=\frac{V_1}{Lht_w}(L-z)-\frac{V_2}{Lht_w}z \tag{2.3a-b}$$

2.5. Buckling Formulation

The total potential energy of the beam throughout buckling (i.e., in going from stage 3 to stage 4 in Fig. 2-2), Π is the sum of the internal strain energy U stored and the potential energy V gained by the loads. Both the internal strain energy U and the potential energy V gained consists of three contributors corresponding to (i) the web, (ii) the bottom flange, and (iii) the top flanges. Thus, the total potential energy of the beam is

$$\Pi=(U_W+U_B+U_T)-\lambda(V_W+V_B+V_T) \tag{2.4}$$

Let $u(y,z)$ denote the lateral displacement of the web. The web is modeled as a thin plate. Hence, its contribution, as given in, e.g. [25, 53], is

$$U_W = \frac{D}{2}\int_0^L \int_{-h/2}^{h/2} \left(u_{,yy}^2 + u_{,zz}^2 + 2\mu u_{,yy} u_{,zz} + 2(1-\mu) u_{,yz}^2 \right) dy\, dz$$
$$V_W = \frac{t_w}{2}\int_0^L \int_{-h/2}^{h/2} \left(\sigma(z,y) u_{,z}^2 + 2\tau(z) u_{,y} u_{,z} \right) dy\, dz \qquad \text{(2.5a-b)}$$

in which μ is the Poisson's ratio; $\sigma(z,y)$ and $\tau(z)$ are pre-buckling stresses as given by Eq.2.3a-b. The flexural rigidity of the web is $D = Et_W^3 / 12(1-\mu^2)$. As a convection, all commas denote the partial derivative of the leading field with respect to the argument coordinates. The lateral displacements and angles of twists of the bottom and top flanges are related to $u(y,z)$ using compatibility relations, i.e.

$$u_B(z) = u(y = h/2, z); \qquad u_T(z) = u(y = -h/2, z)$$
$$\theta_B(z) = -u_{,y}(h/2, z); \qquad \theta_T(z) = -u_{,y}(-h/2, z) \qquad \text{(2.6a-d)}$$

Based on assumption 4 (Section 2.3), the flanges are modeled based on the Vlasov thin-wall beam theory. Combining Eq.(2.6a-d) and the Vlasov beam energy terms [54], one obtains

$$U_B = \frac{1}{2}\int_0^L \left(EI_{yF} u_{,zz}^2 + EC_{wF} u_{,yzz}^2 + GJ_F u_{,yz}^2 \right)_{y=h/2} dz$$
$$V_B = \frac{1}{2}\int_0^L \sigma(z, h/2) \left(A_F u_{,z}^2 + I_{yF} u_{,yz}^2 \right)_{y=h/2} dz$$
$$U_T = \frac{1}{2}\int_0^L \left(EI_{yF} u_{,zz}^2 + EC_{wF} u_{,yzz}^2 + GJ_F u_{,yz}^2 \right)_{y=-h/2} dz \qquad \text{(2.7a-d)}$$
$$V_T = \frac{1}{2}\int_0^L \sigma(z, -h/2) \left(A_F u_{,z}^2 + I_{yF} u_{,yz}^2 \right)_{y=-h/2} dz$$

where G is the shear modulus, E is Young's modulus, A_F is the area of the flanges, I_{yF} is the weak axis moment of inertia for the flanges; C_{wF}, warping constant of the flanges, and J_F is the Saint-Venant torsional constant for the flanges. These sectional properties are determined by $(A_F, I_{yF}, C_{wF}, J_F) = (bt,\ b^3 t/12,\ b^3 t^3/144, bt^3/3)$.

2.6. Finite Element Formulation

The lateral displacement field of the web $u(y,z)$ is assumed to take the form

$$u(y,z) = \sum_{i=1}^{m} \tilde{u}_i(y) \phi_i(z) \qquad \text{(2.8)}$$

where $\tilde{u}_i(y)$ $i=1,2,\ldots,m$ are deformation modes characterizing the variation of the lateral displacement along the web height. Functions $\phi_i(z)$ provide the amplitudes of the deformation modes $\tilde{u}_i(y)$. It is convenient to express Eq.2.8 in a vector form, i.e.,

$$u(y,z)=\tilde{\mathbf{u}}^T(y)\boldsymbol{\varphi}(z) \tag{2.9}$$

where

$$\begin{aligned}\tilde{\mathbf{u}}^T(\mathbf{y})&=\langle \tilde{u}_1(y) \quad \tilde{u}_2(y) \quad \ldots \quad \tilde{u}_m(y)\rangle\\ \boldsymbol{\varphi}^T(\mathbf{z})&=\langle \phi_1(z) \quad \phi_2(z) \quad \ldots \quad \phi_m(z)\rangle\end{aligned} \tag{2.10a-b}$$

2.6.1. Distribution of Lateral Displacement along the Height – Scheme 1:

In distortional buckling solutions (e.g., [18-25, 29-35, 55]), it is common to adopt Hermitian polynomials to relate the displacement field $u(y,z)$ to the lateral displacement and the angle of twist of the top and bottom flanges $u_T(z)$, $\theta_T(z)$, $u_B(z)$, $\theta_B(z)$. This displacement scheme can be recovered as a special case of Eq.2.8, by setting the number of terms $m=4$, i.e.,

$$u(y,z)=\sum_{i=1}^{4}\tilde{u}_i(y)\phi_i(z) \tag{2.11}$$

and setting the displacement functions $\tilde{u}_i(y)$ equal to the Hermitian polynomials, i.e.,

$$\begin{aligned}\tilde{u}_1(y)&=\frac{1}{2}-\frac{3y}{2h}+\frac{2y^3}{h^3}, & \tilde{u}_2(y)&=\frac{h}{8}-\frac{y}{4}-\frac{y^2}{2h}+\frac{y^3}{h^2}\\ \tilde{u}_3(y)&=\frac{1}{2}+\frac{3y}{2h}-\frac{2y^3}{h^3}, & \tilde{u}_4(y)&=\frac{-h}{8}-\frac{y}{4}+\frac{y^2}{2h}+\frac{y^3}{h^2}\end{aligned} \tag{2.12}$$

In this case, functions $\phi_i(z)$ represent the displacements and the angles of twist at the bottom and top of the web, i.e., $\phi_1(z)=u_B(z)$, $\phi_2(z)=\theta_B(z)$, $\phi_3(z)=u_T(z)$, and $\phi_4(z)=\theta_T(z)$. The interpolation scheme of Eq.2.12 has been implemented to serve as a benchmark solution against the more elaborate interpolation scheme proposed under Section 2.6.2.

2.6.2. Distribution of Lateral Displacement along the Height – Scheme 2:

The commonly adopted lateral displacement distribution (Section 2.6.1) has two limitations: (1) there are no direct means to recover the conventional non-distortional LTB solution (e.g., [2, 6, 7, 9, 10, 12, 13, 56-58]) as a special case from the distortional solution, and (2) Web

distortion is characterized by only four parameters $\phi_i(z), i=1,2,3,4$, with no direct means to improve the lateral displacement distribution along the web height. Within this context, the scheme proposed herein offers a generalized lateral displacement distribution that addresses both limitations. The non-distortional web deformation modes (Fig. 2-3a-b), represented by modes 1 and 2, are captured by adopting linear interpolation to relate the lateral displacements of the top and bottom web-flanges junctions, i.e.,

$$\tilde{u}_1(y)=\frac{1}{2}+\frac{y}{h}; \qquad \tilde{u}_2(y)=\frac{1}{2}-\frac{y}{h} \tag{2.13a-b}$$

The distortional deformation modes (Fig. 2-3c-f) are represented by higher modes $2<i<m$ and are assumed to take the form

$$\tilde{u}_i(y)=\begin{cases}\cos\left[\pi(i-2)y/h\right] & i=\text{odd}\\ \sin\left[\pi(i-2)y/h\right] & i=\text{even}\end{cases} \qquad 2<i<m \tag{2.14}$$

The number of distortional modes n is related to the total number of modes m through $n=m-2$. The amplitudes $\phi_i(z), i=1,2,...m$ are related to the degrees of freedom $\boldsymbol{\Delta}_i$ at the end of the element using the Hermitian polynomials, yielding

$$\phi_i(z)=\mathbf{H}^T(z)\boldsymbol{\Delta}_i \tag{2.15}$$

in which

$$\boldsymbol{\Delta}_i^T=\left\langle \phi_i(0) \quad \phi_{i,z}(0) \quad \phi_i(L) \quad \phi_{i,z}(0)\right\rangle \tag{2.16}$$

$$\mathbf{H}^T(z)=\left\langle \left(1-\frac{3z^2}{L^2}+\frac{2z^3}{L^3}\right) \quad \left(z-\frac{2z^2}{L}+\frac{z^3}{L^2}\right) \quad \left(\frac{3z^2}{L^2}-\frac{2z^3}{L^3}\right) \quad \left(-\frac{z^2}{L}+\frac{z^3}{L^2}\right)\right\rangle \tag{2.17}$$

From Eq.2.15 , by substituting into Eq.(2.9), one obtains

$$u(y,z)=\tilde{\mathbf{u}}^T(y)\mathbf{Z}(z)\boldsymbol{\Delta} \tag{2.18}$$

in which

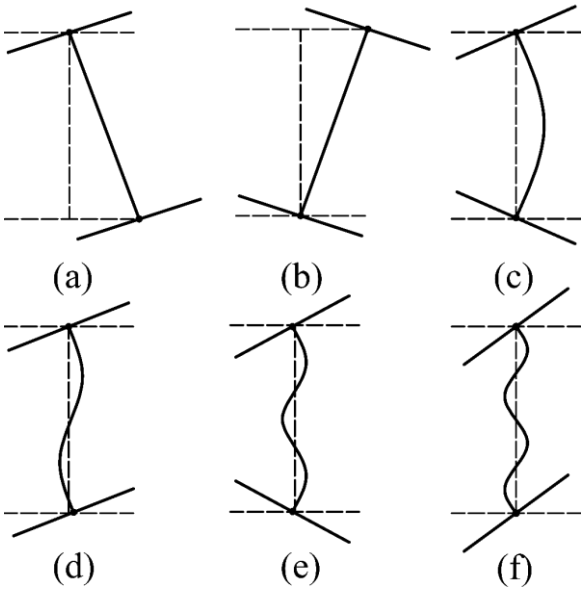

Fig. 2-3. (a) and (b) global deformation modes, (e) to (f) first four distortional modes

$$\tilde{\mathbf{u}}^T(y) = \left\langle (1/2 + y/h) \quad (1/2 - y/h) \;\vdots\; \cos(\pi y/h) \quad \sin(2\pi y/h) \quad \dots \right\rangle_{1\times m}$$

$$\mathbf{Z}(z) = \begin{bmatrix} \mathbf{H}^T(z) & & & \\ & \mathbf{H}^T(z) & \dots & \\ & \vdots & & \\ & & & \mathbf{H}^T(z) \end{bmatrix}_{m\times 4m} \qquad (2.19a\text{-}c)$$

$$\boldsymbol{\Delta}^T = \left\langle \boldsymbol{\Delta}_1^T \;\vdots\; \boldsymbol{\Delta}_2^T \;\vdots\; \dots \;\vdots\; \boldsymbol{\Delta}_m^T \right\rangle_{1\times 4m}$$

By taking the appropriate derivatives of Eq.2.18 , substituting into the total potential energy terms for the web (Eq.2.5 a-b) and the flanges (Eq.2.7a-d), and applying the compatibility equations (Eq.2.6a-d), one obtains

$$U_W = \frac{1}{2}\boldsymbol{\Delta}^{\mathbf{T}} D \int_0^L \int_{-h/2}^{h/2} \left(\sum_{i=1}^{5} \tilde{\mathbf{K}}_i \right) dy dz\, \boldsymbol{\Delta}; \qquad V_w = \frac{1}{2}\boldsymbol{\Delta}^{\mathbf{T}} t_w \int_0^L \int_{-h/2}^{h/2} \left(\sum_{i=1}^{3} \tilde{\mathbf{G}}_i \right) dy dz\, \boldsymbol{\Delta}$$

$$U_B = \frac{1}{2}\boldsymbol{\Delta}^{\mathbf{T}} \int_0^L \left(\sum_{i=3}^{5} \tilde{\mathbf{K}}_i \right) dz \boldsymbol{\Delta}; \qquad V_B = \frac{1}{2}\boldsymbol{\Delta}^{\mathbf{T}} \int_0^L \left(\sum_{i=4}^{5} \tilde{\mathbf{G}}_i \right) dz\, \boldsymbol{\Delta} \qquad (2.20a\text{-}f)$$

$$U_T = \frac{1}{2}\boldsymbol{\Delta}^{T} \int_0^L \left(\sum_{i=4}^{6} \tilde{\mathbf{K}}_i \right) dz \boldsymbol{\Delta}; \qquad V_T = \frac{1}{2}\boldsymbol{\Delta}^{T} \int_0^L \left(\sum_{i=5}^{7} \tilde{\mathbf{G}}_i \right) dz\, \boldsymbol{\Delta}$$

in which matrices $\tilde{\mathbf{K}}_i$ and $\tilde{\mathbf{G}}_i$ are defined as

$$\tilde{\mathbf{K}}_1 = \mathbf{Z}\tilde{\mathbf{u}}_{,yy}\tilde{\mathbf{u}}_{,yy}^T\mathbf{Z}^T; \quad \tilde{\mathbf{K}}_2 = \mathbf{Z}_{,zz}\tilde{\mathbf{u}}\tilde{\mathbf{u}}^T\mathbf{Z}_{,zz}^T; \quad \tilde{\mathbf{K}}_3 = \mu\mathbf{Z}\tilde{\mathbf{u}}_{,yy}\tilde{\mathbf{u}}^T\mathbf{Z}_{,zz}^T$$

$$\tilde{\mathbf{K}}_4 = \mu\mathbf{Z}_{,zz}\tilde{\mathbf{u}}\tilde{\mathbf{u}}_{,yy}^T\mathbf{Z}^T; \quad \tilde{\mathbf{K}}_5 = 2(1-\mu)\mathbf{Z}_{,z}\tilde{\mathbf{u}}_{,y}\tilde{\mathbf{u}}_{,y}^T\mathbf{Z}_{,z}^T; \quad \tilde{\mathbf{K}}_6 = \left(EI_{yF}\mathbf{Z}_{,zz}\tilde{\mathbf{u}}\tilde{\mathbf{u}}^T\mathbf{Z}_{,zz}^T\right)_{y=\frac{h}{2}}$$

$$\tilde{\mathbf{K}}_7 = \left(EC_{wF}\mathbf{Z}_{,zz}\tilde{\mathbf{u}}_{,y}\tilde{\mathbf{u}}_{,y}^T\mathbf{Z}_{,zz}^T\right)_{y=\frac{h}{2}}; \quad \tilde{\mathbf{K}}_8 = \left(GJ_F\mathbf{Z}_{,z}\tilde{\mathbf{u}}_{,y}\tilde{\mathbf{u}}_{,y}^T\mathbf{Z}_{,z}^T\right)_{y=\frac{h}{2}}; \quad \tilde{\mathbf{K}}_9 = \left(EI_{yF}\mathbf{Z}_{,zz}\tilde{\mathbf{u}}\tilde{\mathbf{u}}^T\mathbf{Z}_{,zz}^T\right)_{y=\frac{-h}{2}}$$

$$\tilde{\mathbf{K}}_{10} = \left(EC_{wF}\mathbf{Z}_{,zz}\tilde{\mathbf{u}}_{,y}\tilde{\mathbf{u}}_{,y}^T\mathbf{Z}_{,zz}^T\right)_{y=\frac{-h}{2}}; \tilde{\mathbf{K}}_{11} = \left(GJ_F\mathbf{Z}_{,z}\tilde{\mathbf{u}}_{,y}\tilde{\mathbf{u}}_{,y}^T\mathbf{Z}_{,z}^T\right)_{y=\frac{-h}{2}}; \quad \tilde{\mathbf{G}}_1 = \sigma\mathbf{Z}_{,z}\tilde{\mathbf{u}}\tilde{\mathbf{u}}^T\mathbf{Z}_{,z}^T \quad (2.21a\text{-}$$

$$\tilde{\mathbf{G}}_2 = \tau\mathbf{Z}\tilde{\mathbf{u}}_{,y}\tilde{\mathbf{u}}^T\mathbf{Z}_{,z}^T; \quad \tilde{\mathbf{G}}_3 = \tau\mathbf{Z}_{,z}\tilde{\mathbf{u}}\tilde{\mathbf{u}}_{,y}^T\mathbf{Z}^T; \quad \tilde{\mathbf{G}}_4 = \left(\sigma A_F\mathbf{Z}_{,z}\tilde{\mathbf{u}}\tilde{\mathbf{u}}^T\mathbf{Z}_{,z}^T\right)_{y=\frac{h}{2}}$$

$$\tilde{\mathbf{G}}_5 = \left(I_{yF}\sigma\mathbf{Z}_{,z}\tilde{\mathbf{u}}_{,y}\tilde{\mathbf{u}}_{,y}^T\mathbf{Z}_{,z}^T\right)_{y=\frac{h}{2}}; \quad \tilde{\mathbf{G}}_6 = \left(\sigma A_F\mathbf{Z}_{,z}\tilde{\mathbf{u}}\tilde{\mathbf{u}}^T\mathbf{Z}_{,z}^T\right)_{y=\frac{-h}{2}}; \quad \tilde{\mathbf{G}}_7 = \left(I_{yF}\sigma\mathbf{Z}_{,z}\tilde{\mathbf{u}}_{,y}\tilde{\mathbf{u}}_{,y}^T\mathbf{Z}_{,z}^T\right)_{y=\frac{-h}{2}}$$

r)

2.7. Separation of Variables:

Consider, for example, matrix $\tilde{\mathbf{K}}_1(y,z) = \mathbf{Z}(z)\tilde{\mathbf{u}}_{,yy}(y)\tilde{\mathbf{u}}_{,yy}^T(y)\mathbf{Z}^T(z)$ arising in Eq.2.21a. When performing the integral $\int_{z=0}^{z=L}\int_{y=-h/2}^{y=h/2}\tilde{\mathbf{K}}_1(y,z)\,dydz$, one would need first to perform the matrix multiplication $\tilde{\mathbf{K}}_1(y,z) = \mathbf{Z}(z)\tilde{\mathbf{u}}_{,yy}(y)\tilde{\mathbf{u}}_{,yy}^T(y)\mathbf{Z}^T(z)$ and then perform double integration over y and z for each of the resulting matrix elements. The operation can be considerably simplified by using the Kronecker product operation for two matrices (subsequently denoted by the symbol $\otimes$). The matrix $\tilde{\mathbf{K}}_1(y,z)$ can be expressed as $\tilde{\mathbf{K}}_1 = \left[\tilde{\mathbf{u}}_{,yy}(y)\tilde{\mathbf{u}}_{,yy}^T(y)\right]\otimes\left[\mathbf{H}(z)\mathbf{H}^T(z)\right]$. The first matrix $\left[\tilde{\mathbf{u}}_{,yy}(y)\tilde{\mathbf{u}}_{,yy}^T(y)\right]$ is a function solely of variable y, while the second matrix $\left[\mathbf{H}(z)\mathbf{H}^T(z)\right]$ is a function solely of variable z, enabling a separation of variables y and z thus transforming the double integral into the product of two single integrals (Appendix A), i.e.,

$$\int_{z=0}^{z=L}\int_{y=-h/2}^{y=h/2}\tilde{\mathbf{K}}_1(y,z)dydz = \int_{y=-h/2}^{y=h/2}\left[\tilde{\mathbf{u}}_{,yy}(y)\tilde{\mathbf{u}}_{,yy}^T(y)\right]dy\otimes\int_{z=0}^{z=L}\left[\mathbf{H}(z)\mathbf{H}^T(z)\right]dz$$

Repeated application of the Kronecker product for each of the terms arising in Eq.2.21 enables the separation of variables x and y for all $\tilde{\mathbf{K}}_i$ and $\tilde{\mathbf{G}}_i$. From the expressions of the normal stresses σ and the shearing stresses τ appearing in Eq.2.3a-b, by substituting into Eq.2.20a-f and applying the Kronecker product rule, one obtains

$$\Pi = \frac{1}{2}\boldsymbol{\Delta}^T\left[\sum_{i=1}^{11}\mathbf{K}_i - \lambda\sum_{j=1}^{14}\mathbf{G}_j\right]\boldsymbol{\Delta} \qquad (2.22)$$

in which $\mathbf{K}_i = a_i \mathbf{A}_i \otimes \mathbf{B}_i$ and $\mathbf{G}_j = b_j \mathbf{E}_j \otimes \mathbf{F}_j$ are respectively the entries of the stiffness and the geometric stiffness matrices. a_i, $\mathbf{A}_i$, $\mathbf{B}_i$ are defined in Table 2-1, and b_i, $\mathbf{E}_j$, $\mathbf{F}_j$ are defined in

Table 2-2. Appendix B provides the matrix definitions for $\mathbf{A}_i, \mathbf{B}_i, \mathbf{E}_j, \mathbf{F}_j$. By evoking the stationary condition of Eq.2.22, one obtains

$$\left[\sum_{i=1}^{11} \mathbf{K}_i - \lambda \sum_{j=1}^{14} \mathbf{G}_j\right] \boldsymbol{\Delta} = \mathbf{0} \tag{2.23}$$

The non-trivial solution of Eq.2.23 is provided by setting to zero the determinant of the bracketed matrix, yielding the eigenvalue λ and the corresponding buckling mode $\boldsymbol{\Delta}$.

Table 2-1: Entries of the stiffness matrix

i	a_i	$\mathbf{A}_i$	$\mathbf{B}_i$
1	D	$\int_{-h/2}^{h/2} \tilde{\mathbf{u}}_{,yy}(y)\tilde{\mathbf{u}}_{,yy}^T(y)dy$	$\int_0^L \mathbf{H}(z)\mathbf{H}^T(z)dz$
2	D	$\int_{-h/2}^{h/2} \tilde{\mathbf{u}}(y)\tilde{\mathbf{u}}^T(y)dy$	$\int_0^L \mathbf{H}_{,zz}(z)\mathbf{H}_{,zz}^T(z)dz$
3	μD	$\int_{-h/2}^{h/2} \tilde{\mathbf{u}}_{,yy}(y)\tilde{\mathbf{u}}^T(y)dy$	$\int_0^L \mathbf{H}\ (z)\mathbf{H}_{,zz}^T(z)dz$
4	μD	$\int_{-h/2}^{h/2} \tilde{\mathbf{u}}(y)\tilde{\mathbf{u}}_{,yy}^T(y)dy$	$\int_0^L \mathbf{H}_{,zz}(z)\mathbf{H}^T(z)dz$
5	$2D(1-\mu)$	$\int_{-h/2}^{h/2} \tilde{\mathbf{u}}_{,y}(y)\tilde{\mathbf{u}}_{,y}^T(y)dy$	$\int_0^L \mathbf{H}_{,z}(z)\mathbf{H}_{,z}^T(z)dz$
6	EI_{yF}	$\tilde{\mathbf{u}}(h/2)\tilde{\mathbf{u}}^T(h/2)$	$\int_0^L \mathbf{H}_{,zz}(z)\mathbf{H}_{,zz}^T(z)dz$
7	GJ_F	$\tilde{\mathbf{u}}_{,y}(h/2)\tilde{\mathbf{u}}_{,y}^T(h/2)$	$\int_0^L \mathbf{H}_{,z}(z)\mathbf{H}_{,z}^T(z)dz$
8	EC_{wF}	$\tilde{\mathbf{u}}_{,y}(h/2)\tilde{\mathbf{u}}_{,y}^T(h/2)$	$\int_0^L \mathbf{H}_{,zz}(z)\mathbf{H}_{,zz}^T(z)dz$
9	EI_{yF}	$\tilde{\mathbf{u}}(-h/2)\tilde{\mathbf{u}}^T(-h/2)$	$\int_0^L \mathbf{H}_{,zz}(z)\mathbf{H}_{,zz}^T(z)dz$
10	GJ_F	$\tilde{\mathbf{u}}_{,y}(-h/2)\tilde{\mathbf{u}}_{,y}^T(-h/2)$	$\int_0^L \mathbf{H}_{,z}(z)\mathbf{H}_{,z}^T(z)dz$
11	EC_{wF}	$\tilde{\mathbf{u}}_{,y}(-h/2)\tilde{\mathbf{u}}_{,y}^T(-h/2)$	$\int_0^L \mathbf{H}_{,zz}(z)\mathbf{H}_{,zz}^T(z)dz$

Table 2-2: Entries of the geometric stiffness matrix

j	b_j	$\mathbf{E_j}$	$\mathbf{F}_i$
1	$M_1 t_W / (LI_x)$	$\int_{-h/2}^{h/2} y\tilde{\mathbf{u}}(y)\tilde{\mathbf{u}}^T(y)dy$	$\int_0^L (L-z)\mathbf{H}_{,z}(z)\mathbf{H}_{,z}^T(z)dz$
2	$-M_2 t_W / (LI_x)$	$\int_{-h/2}^{h/2} y\tilde{\mathbf{u}}(y)\tilde{\mathbf{u}}^T(y)dy$	$\int_0^L z\mathbf{H}_{,z}(z)\mathbf{H}_{,z}^T(z)dz$
3	$V_1/(hL)$	$\int_{-h/2}^{h/2} \tilde{\mathbf{u}}_{,y}(y)\tilde{\mathbf{u}}^T(y)dy$	$\int_0^L (L-z)\mathbf{H}\ (z)\mathbf{H}_{,z}^T(z)dz$
4	$-V_2/(hL)$	$\int_{-h/2}^{h/2} \tilde{\mathbf{u}}_{,y}(y)\tilde{\mathbf{u}}^T(y)dy$	$\int_0^L z\mathbf{H}\ (z)\mathbf{H}_{,z}^T(z)dz$
5	$V_1/(hL)$	$\int_{-h/2}^{h/2} \tilde{\mathbf{u}}(y)\tilde{\mathbf{u}}_{,y}^T(y)dy$	$\int_0^L (L-z)\mathbf{H}_{,z}(z)\mathbf{H}^T(z)dz$
6	$-V_2/(hL)$	$\int_{-h/2}^{h/2} \tilde{\mathbf{u}}(y)\tilde{\mathbf{u}}_{,y}^T(y)dy$	$\int_0^L z\mathbf{H}_{,z}(z)\mathbf{H}^T(z)dz$
7	$A_F hM_1/(2I_x L)$	$\tilde{\mathbf{u}}(h/2)\tilde{\mathbf{u}}^T(h/2)$	$\int_0^L (L-z)\mathbf{H}_{,z}(z)\mathbf{H}_{,z}^T(z)dz$
8	$-A_F hM_2/(2I_x L)$	$\tilde{\mathbf{u}}(h/2)\tilde{\mathbf{u}}^T(h/2)$	$\int_0^L z\mathbf{H}_{,z}(z)\mathbf{H}_{,z}^T(z)dz$
9	$I_{yF} hM_1/(2I_x L)$	$\tilde{\mathbf{u}}_{,y}(h/2)\tilde{\mathbf{u}}_{,y}^T(h/2)$	$\int_0^L (L-z)\mathbf{H}_{,z}(z)\mathbf{H}_{,z}^T(z)dz$
10	$-I_{yF} hM_2/(2I_x L)$	$\tilde{\mathbf{u}}_{,y}(h/2)\tilde{\mathbf{u}}_{,y}^T(h/2)$	$\int_0^L z\mathbf{H}_{,z}(z)\mathbf{H}_{,z}^T(z)dz$
11	$-A_F hM_1/(2I_x L)$	$\tilde{\mathbf{u}}(-h/2)\tilde{\mathbf{u}}^T(-h/2)$	$\int_0^L (L-z)\mathbf{H}_{,z}(z)\mathbf{H}_{,z}^T(z)dz$
12	$A_F hM_2/(2I_x L)$	$\tilde{\mathbf{u}}(-h/2)\tilde{\mathbf{u}}^T(-h/2)$	$\int_0^L z\mathbf{H}_{,z}(z)\mathbf{H}_{,z}^T(z)dz$
13	$-I_{yF} hM_1/(2I_x L)$	$\tilde{\mathbf{u}}_{,y}(-h/2)\tilde{\mathbf{u}}_{,y}^T(-h/2)$	$\int_0^L (L-z)\mathbf{H}_{,z}(z)\mathbf{H}_{,z}^T(z)dz$
14	$I_{yF} hM_2/(2I_x L)$	$\tilde{\mathbf{u}}_{,y}(-h/2)\tilde{\mathbf{u}}_{,y}^T(-h/2)$	$\int_0^L z\mathbf{H}_{,z}(z)\mathbf{H}_{,z}^T(z)dz$

2.8. Recovering the Classical Non-distortional Lateral-Torsional Buckling Solution

It is of interest to investigate whether the classical (non-distortional) lateral-torsional buckling (LTB) solution can be recovered as a special case from the present solution (Section 2.6.2). By retaining the first two modes, which represent the non-distortional modes (Eq.2.13a-b), and

substituting into Eq.2.8, and from the application of the compatibility equations (Eq.2.6a-b), one obtains

$$u(y,z)=\left(\frac{1}{2}+\frac{y}{h}\right)u_T(z)+\left(\frac{1}{2}-\frac{y}{h}\right)u_B(z) \tag{2.24}$$

Eq.2.24 can be cast in the form

$$u(z,y)=u_0(z)+\theta_0(z)\,y \tag{2.25}$$

in which $u_0(z)=\left[u_B(z)+u_T(z)\right]/2$ is the displacement at web mid-height and $\theta_0(z)=\left[u_B(z)-u_T(z)\right]/h$ is the angle of twist of the section (Fig. 2-2). From Eq.2.25, by substituting into the internal strain energy and the potential energy terms associated with the web (Eq.2.5a-b) and the flanges (Eq.2.7a-d), and their summation, one obtains the total potential energy as (see Appendix C)

$$\Pi=\frac{1}{2}\int_0^L\left[E\overline{I}_y u_{0,zz}^2+E\overline{C}_w\theta_{0,zz}^2+G\overline{J}\theta_{0,z}^2\right]dz-\int_0^L\left(Mu_{0,zz}\theta_0\right)dz \tag{2.26}$$

in which $\overline{I}_y$, $\overline{C}_w$ and $\overline{J}_s$ are the sectional properties of the flanges and the web, which are defined as

$$\begin{aligned}\overline{I}_y&=2I_{yF}+I_{yW}/\left(1-\mu^2\right)\\ \overline{C}_w&=C_{wG}+2C_{wF}+C_{wW}/\left(1-\mu^2\right)\\ \overline{J}&=J_W+2J_F\end{aligned} \tag{2.27a-c}$$

and the sectional properties of the web are $\left(I_{yW},C_{wW},J_W\right)=\left(ht_w^3/12,\ h^3t_w^3/144,ht_w^3/3\right)$. The global warping constant is $C_{wG}=2I_{yF}\left(h/2\right)^2$. The sectional properties derived from the present solution also give rise to the local warping constant for the flanges C_{wF} and for the web C_{wW}. Eq.2.26 is similar to that obtained under the classical non-distortional LTB formulations (e.g., Barsoum and Gallagher [56]). The only difference lies in the fact that the weak axis moment of inertia $\overline{I}_y$, and the warping $\overline{C}_w$ involve the Poisson's ratio μ. Nevertheless, the following numerical investigation shows that this dependence is rather weak.

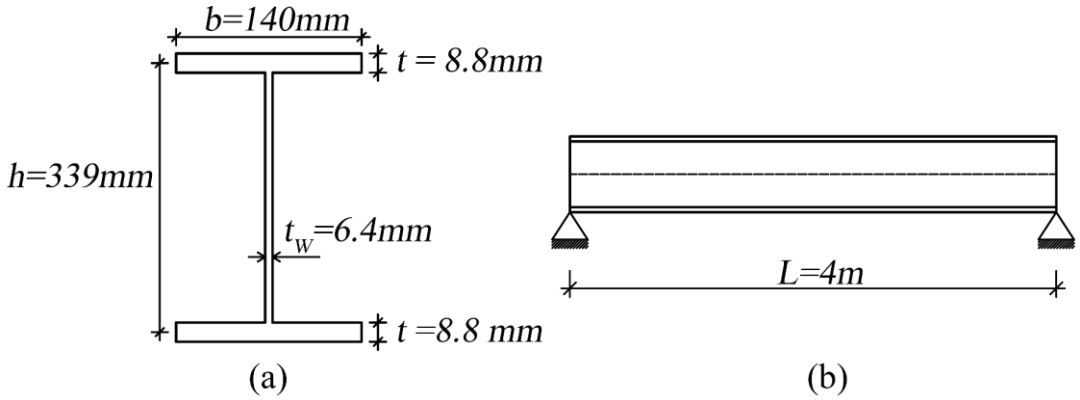

Fig. 2-4: (a) the reference beam cross-section and (b) the boundary conditions of the reference beam

Consider a simply-supported wide-flange I-beam with W410x39 cross-section ($h = 339mm$, $b = 140\,mm$, $t = 8.8\,mm$ and $t_W = 6.4\,mm$) (Fig. 2-4a). The span of this beam is 4 meters (Fig. 2-4b). The Young's module taken is taken as $E = 200\,GPa$. The Poisson's ratio μ is taken 0.3 unless mentioned otherwise. In this work, we refer to this geometry as the reference beam.

The reference beam is subjected to a mid-span point load acting at its centroid. Four cases are generated by varying the Poisson's ratio $\mu \in \langle 0,\ 0.1,\ 0.2,\ 0.3 \rangle$. The beam is discretized by 20 elements, and the lateral displacement of the flanges is restrained at the supports. For each case, the non-distortional LTB critical moments are determined by (i) the present solution M_{ND} by retaining only the first two non-distortional modes as computed by a Matlab program developed based on the formulation herein (Appendix D) and (ii) the classical finite element solution provided Barsoum and Gallagher [56] M_{BG}. The ratio M_{ND}/M_{BG} versus μ is shown in Fig. 2-5.

It is observed that the present model coincides with the Barsoum and Ghallagher element [56] when $\mu = 0$. As μ increases, the present model yields critical moment predictions that are slightly smaller than those predicted by the Barsoum and Gallagher formulation. Nevertheless, the maximum difference, which occurs at $\mu = 0.3$, is well within 0.002%, suggesting that the present model predictions practically coincide with those predicted by the Barsoum and Ghallagher elements.

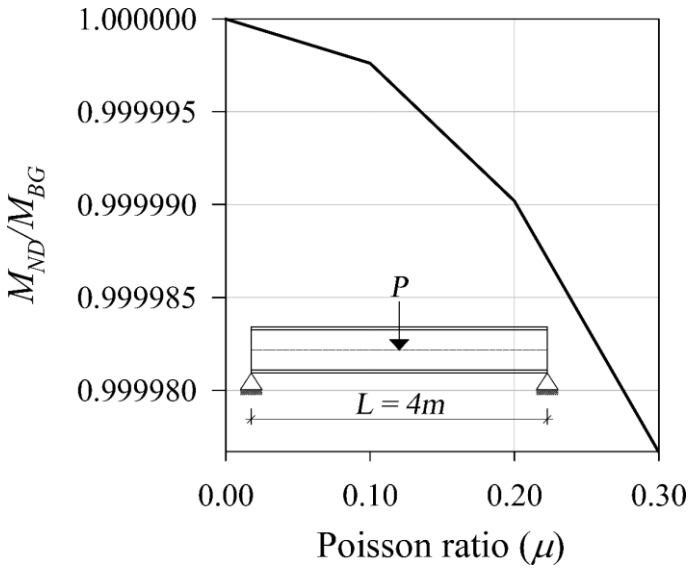

Fig. 2-5: Comparison of the non-distortional lateral torsional buckling obtained by the present study and the classical finite element solution developed by Barsoum and Gallagher [56] by the variation of μ

2.9. Number of Modes needed for Convergence

The reference beam (Fig. 2-4) is investigated under three loading cases (a) uniform moment, (b) reverse curvature moment, and (c) mid-span point load at its shear center. Throughout the finite element buckling formulation (Section 2.6.2), we recall that the web shape function was assumed to consist of a combination of deformation modes, including two non-distortional modes and n distortional modes. The critical moments for the reference beam are obtained by varying n from zero to 12. The critical moments are compared against (a) the predictions of a shell element model under Abaqus and (b) against the Hermitian Distortional model (Section 2.6.1).

For the 1–D models (i.e., the present solution and Hermitian Distortional model), the reference beam is discretized by 9 elements. This discretization leads to convergent results for both models. The boundary conditions are imposed by restraining the lateral displacement of the top and bottom flanges at both ends.

The shell model is based on the S4R element in the Abaqus library, which is a quadrilateral element with four nodes with six degrees of freedom per node and reduced integration. The beam is meshed using 150 elements along the span and six elements along both flanges and along the web. The lateral nodal displacements at the flange-to-web junctions at both ends are restrained. A mesh study indicated that the discretization scheme provides convergent results for all the models. For loading cases involving end moments, equal and opposite longitudinal

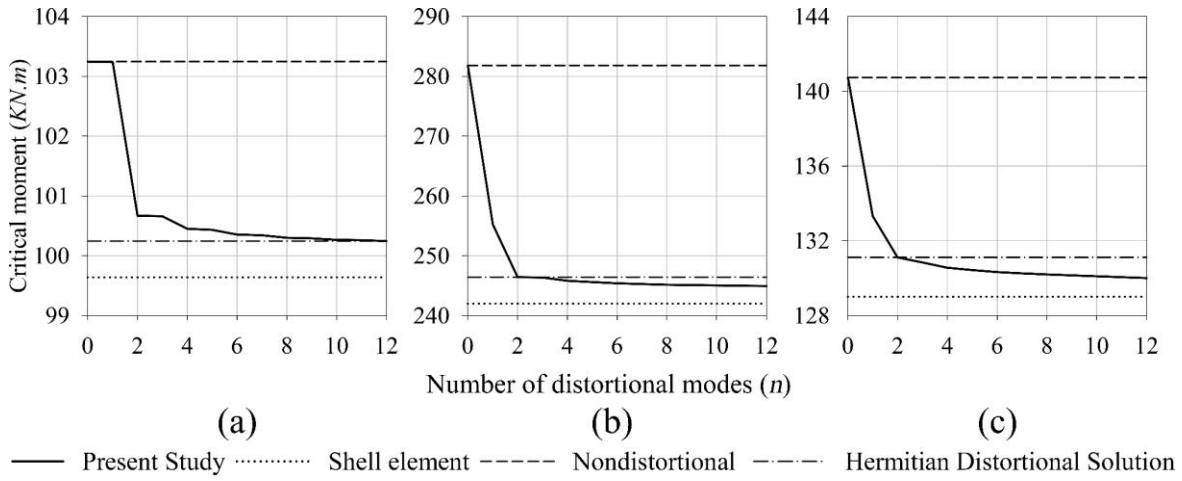

Fig.2-6: The effect of distortional modes for (a) uniform moment (b) reverse curvature moment (c) mid-span point load

forces were applied at the flange–to–web junctions, and for load case (c), the mid-span point load was equally split between both the flanges to avoid localized deformation of the web.

As discussed in Section 2.8, the non-distortional LTB solution is recovered when the distortional modes are excluded, i.e., $n = 0$, which provides an upper bound critical moment, as shown in Fig.2-6. Also, the critical moments obtained by the shell model also represent a lower bound as it captures the distortion in the web and in the flanges. Increasing the number of distortional modes leads to the higher flexibility of the web and reduces the critical moments predicted accordingly. Moreover, when taking a larger number of distortional modes, the present model predicts critical moments smaller than those based on the Hermitian distortional model described under Section 7.2.

The results indicate that higher distortional modes $n \geq 4$ have a negligible effect on the critical moment predictions. However, this conclusion cannot be generalized for other cases, as the number of distortional modes needed for convergence is expected to depend on the boundary conditions, loading conditions, cross-sectional geometry, and span.

2.10. Contributions of Distortional Modes

The reference beam is revisited (Fig. 2-4) by discretizing it into 40 subdivisions. The boundary conditions and loading cases are similar to those of the previous section. The total number of the deformation modes is taken as 14, consisting of the two non-distortional modes $\tilde{u}_1(y)$, $\tilde{u}_2(y)$ and an additional 12 distortional modes $\tilde{u}_3(y), \tilde{u}_4(y), \ldots, \tilde{u}_{14}(y)$. A buckling analysis is conducted for all three loading cases. Recalling that the amplitudes corresponding to each mode are defined by 4 degrees of freedom at both ends of the element and longitudinally

interpolated using cubic Hermitian polynomials between two nodes, we extract the amplitude functions $\phi_i(z), i = 1, 2, \ldots 14$ for all nodes corresponding to the first buckling eigenmode. Fig. 2-7 shows the normalized amplitudes for each mode $\phi_i(z), i = 1, 2, \ldots 14$ versus the longitudinal coordinate z. For the three loading cases considered, the comparatively small amplitudes associated with modes $i = 3, 4, \ldots, 14$ suggest that the non-distortional modes predominantly characterize the buckling behavior of the beam $i = 1, 2$. Under uniform moments, the contribution of the odd distortional modes is negligible. For the reverse curvature moment case, pronounced web distortion is observed near the supports as manifested by the spike of the distortional amplitudes in the neighborhood of the supports. Conversely, the presence of mid-span point load induces significant web distortions in the neighborhood of the section of load application.

Where the reference beam (Fig. 2-4) is subjected to mid-span point load, Fig. 2-8a depicts the lateral displacements of the bottom and top flanges as characterized by the superimposition of $\phi_1(z)$ and $\phi_2(z)$, whose linear combination represents the non-distortional LTB portion of the response. The individual contributions of the first three distortional modes (modes 3 to 5) are depicted in Fig. 2-8b-d. Fig. 2-9 provides a comparison between the non-distortional LTB response (Fig. 2-9a) based on the superimposition of modes 1 and 2, and the distortional LTB response (Fig. 2-9b) based on the superimposition of modes 1 to 14.

2.11. Parametric Study

2.11.1. Effect of Geometric Parameters on Distortional Buckling

Based on the geometrical and the mechanical properties of the reference beam (Fig. 2-4a), four cases are investigated: (1) a simply-supported beam subjected to mid-span point load; (2) a simply-supported beam subjected to a uniform distributed load; (3) a cantilever subjected to a point load acting at the tip; and (4) a simply-supported beam with an overhang subjected to a tip point load.

For all cases, the beams are discretized using 20 elements in the longitudinal direction, which is expected to yield convergent results. Both flanges are restrained laterally at the supports. In Cases (1)-(3), the span L varied, and for Case 4, the length of the overhang is taken as $4h$ ($h = 339mm$), and the back–span to cantilever span ratio α is varied.

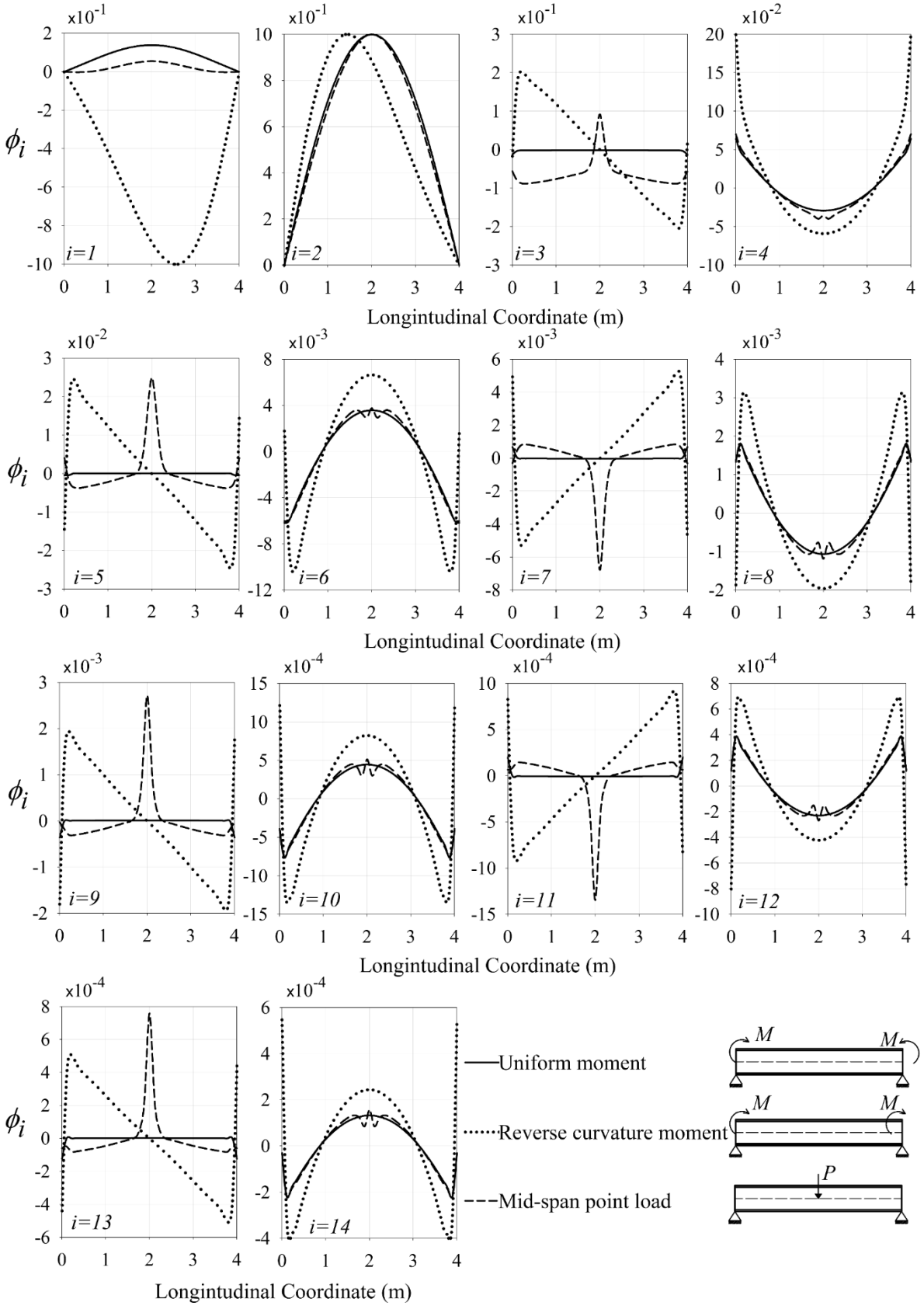

Fig. 2-7.The variation the amplitude function in the longitudinal direction

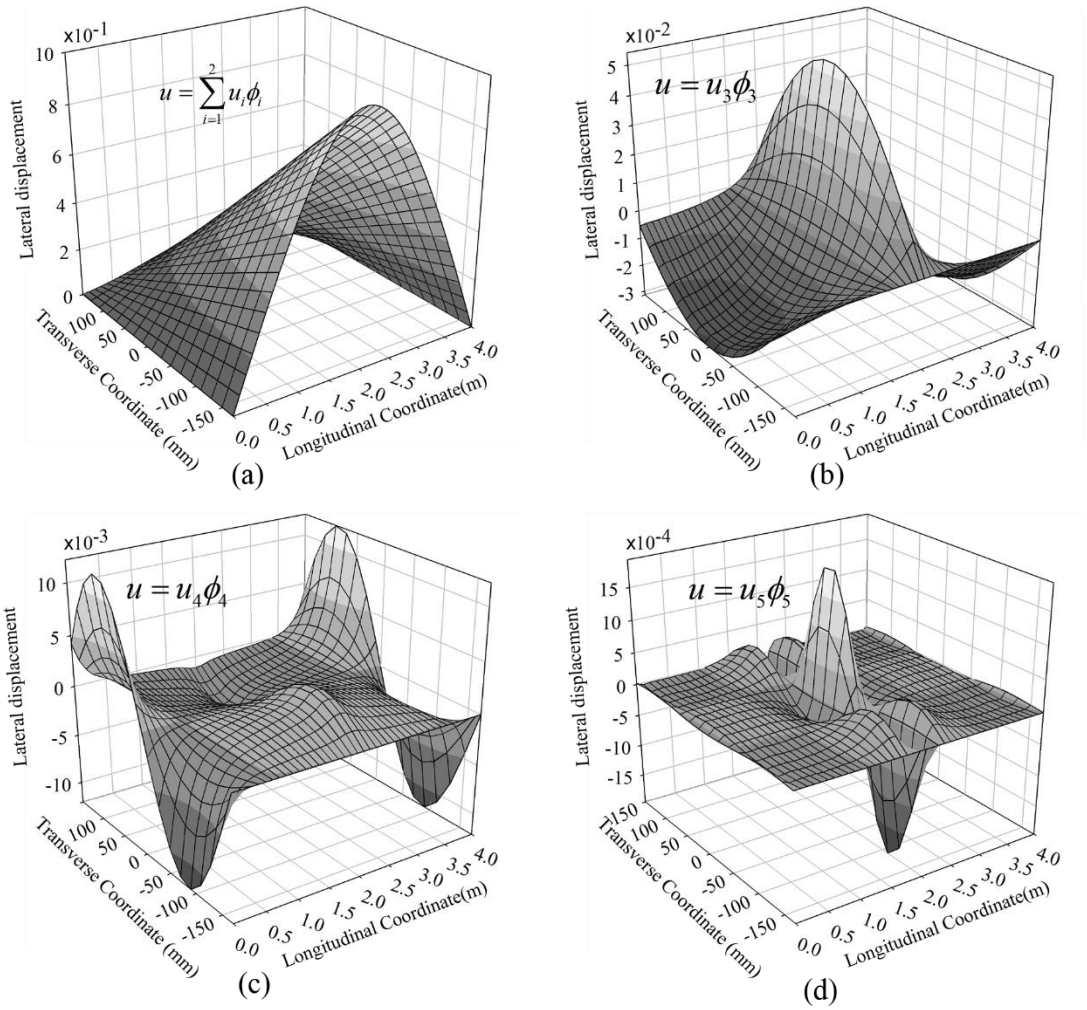

Fig. 2-8. Contribution to the buckled configuration (mid-span load case) of (a) combination of non-distortional modes, and (b) mode 3 (c) mode 4, and (d) mode 5 individually

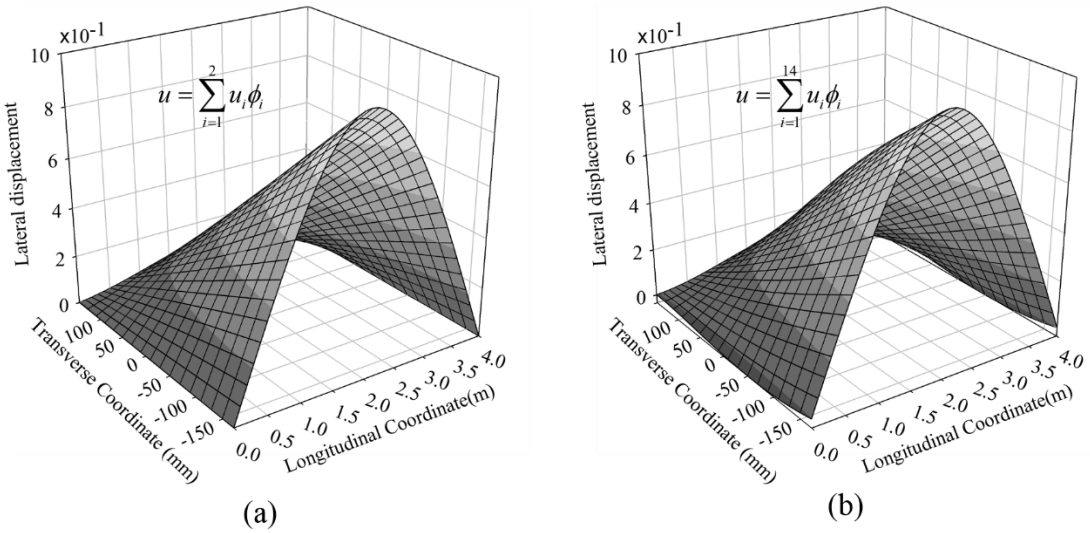

Fig. 2-9. Buckled configuration of the web (mid-span loading case) based on the superposition of (a) non-distortional modes, and (b) all modes

It is required to investigate the effect of web slenderness h/t_w, flange slenderness b/t, section aspect ratio b/h, the span to depth ratio L/h, and back-span to cantilever span ratio α on the critical moment ratio M_D/M_{ND}. The cross-section height h is kept constant at $339mm$, and the span L is varied for Cases 1, 2, and 3 so as to vary the L/h ratio. For Case 4, the span ratio α is varied. Parameters b/h, h/t_w and b/t were individually varied while keeping the dimensionless parameters equal to those of the reference beam. The ranges for h/t_w, b/t, b/h, L/h, and α, are based on the practical considerations and common section proportions, as summarized in Table 2-3.

Table 2-3: the constants and variables used in the parametric study

Objective	Constant parameters	Variable parameters		
		Cases 1 and 2	Case 3	Case 4
Effect of web slenderness	$h=339mm$ $b=140mm$ $t=6.4mm$	$5 \le L/h \le 30$ $25 \le h/t_W \le 65$	$3 \le L/h \le 15$ $25 \le h/t_W \le 65$	$1 \le \alpha \le 6$ $25 \le h/t_W \le 65$
Effect of flange slenderness	$h=339mm$ $b=140mm$ $t_W=8.8mm$	$5 \le L/h \le 30$ $4 \le b/t \le 26$	$3 \le L/h \le 15$ $4 \le b/t \le 26$	$1 \le \alpha \le 6$ $4 \le b/t \le 26$
Section aspect ratio	$h=339mm$ $t_W=8.8mm$ $t=6.4mm$	$5 \le L/h \le 30$ $0.2 \le b/h \le 1.0$	$3 \le L/h \le 15$ $0.2 \le b/h \le 1.0$	$1 \le \alpha \le 6$ $0.2 \le b/h \le 1.0$

A total of 1340 runs were conducted. For each run, the distortional and non-distortional critical moments M_D and M_{ND} are obtained. In order to determine M_D, a total of 18 modes were taken, including the two non-distortional modes and an additional 16 distortional modes. For determining M_{ND}, all distortional modes are suppressed. The relationships of M_D/M_{ND} versus the dimensionless span L/h and α were plotted for different h/t_w, b/t, and b/h values in Fig. 2-10 for Cases 1 and 2, and in Fig. 2-11 for Cases 3 and 4.

The ratio M_D/M_{ND} is indicative of the influence of web distortion on the critical moment, i.e., when the ratio M_D/M_{ND} is close to unity, the effect of web distortion is negligible, and when M_D/M_{ND} is significantly below unity, the effect of web distortion gains significance.

A theme common to the plots in Fig. 2-10, and Fig. 2-11 is that distortional effects gain significance (a) as the web slenderness h/t_W increases, (b) as the flange slenderness b/t decreases, (c) as the section aspect ratio b/h increases, or (d) as the span to depth ratio L/h and α decreases.

Fig. 2-10 a, b, d, and e depict similar trends for the mid-span point and uniformly distributed loading cases. For large spans (i.e., $L/h \geq 25$), the critical moment ratio approaches unity, irrespective of h/t_w or b/h suggesting that web distortion has a negligible effect on the critical moments beyond a certain point.

Interestingly, Fig. 2-10 c, d indicate that for comparatively thicker flanges with $b/t \leq 10$, the critical moment ratio M_D/M_{ND} is significantly smaller than unity, suggesting that web distortion has a more pronounced effect on the critical moment, even for spans as large as $L/h = 30$. This finding was corroborated against the predictions of S4R shell element model under Abaqus for Case 1. A section with $h = 339mm$, $t_W = 8.8mm$, $b = 140mm$ was considered with a comparatively large span ratio $L/h = 20$. By considering the extreme case of a thick flange with $b/t = 3$ the critical moments $M_{D-\text{s4r}}$ as predicted by the Abaqus shell model, M_D as predicted by the present distortional solution and the non-distortional critical moment M_{ND} (Section 2.8) were determined. The specifics of the Abaqus shell model are comparable to those described under Section 2.9. The critical moment ratios obtained are $M_{D-\text{s4r}}/M_{ND} = 0.42$ based on Abaqus versus $M_D/M_{ND} = 0.43$ based on the present model.

In a manner analogous to simply-supported beams, Cantilevers (Case 3) and beams with overhangs (Case 4) of relatively large spans, (i.e., with $L/h > 15$ and $\alpha > 6$, respectively), the web slenderness h/t_w has moderate influence on the web distortion, and the critical moment ratio M_D/M_{ND} under these conditions approaches unity (Fig. 2-11 a, d). In contrast to simply-supported beams, for cantilevers (Case 3) and beams with overhangs (Case 4), the influence of web distortion on the critical moment ratio largely depends on the section aspect ratio b/h (Fig. 2-11 b and e), as reflected by the relatively low M_D/M_{ND} ratios for $L/h \leq 15$ and $\alpha \leq 6$.

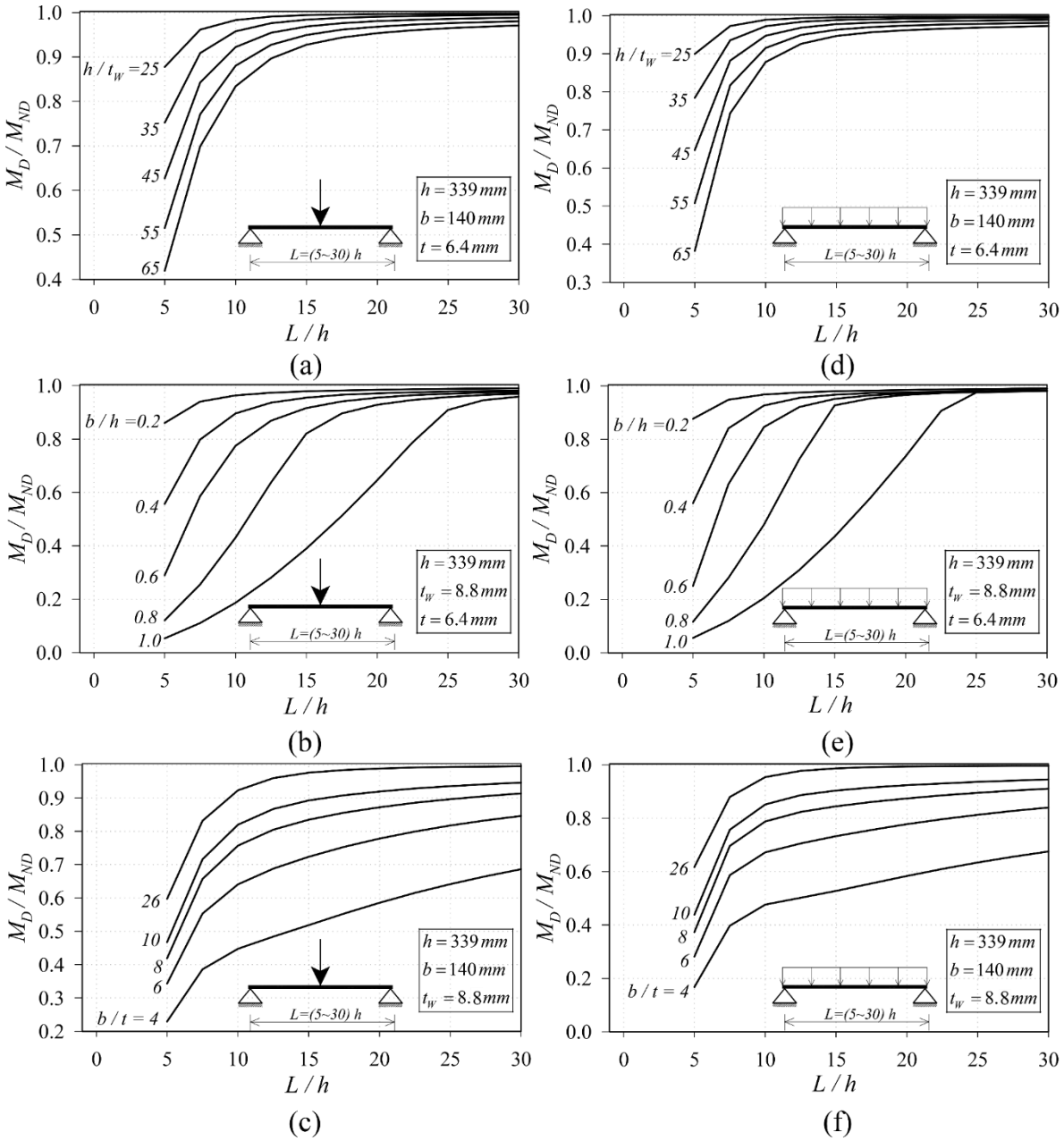

Fig. 2-10: Critical moment ratio M_D/M_{ND} for Case 1 simply-supported beam under mid-span point load (a) effect of web slenderness h/t_w, (b) effect of section aspect ratio b/h, (c) effect of flange slenderness b/t, and for Case 2 under uniformly distributed load (d) effect of web slenderness h/t_w, (e) effect of section aspect ratio b/h, and (f) effect of flange slenderness b/t.

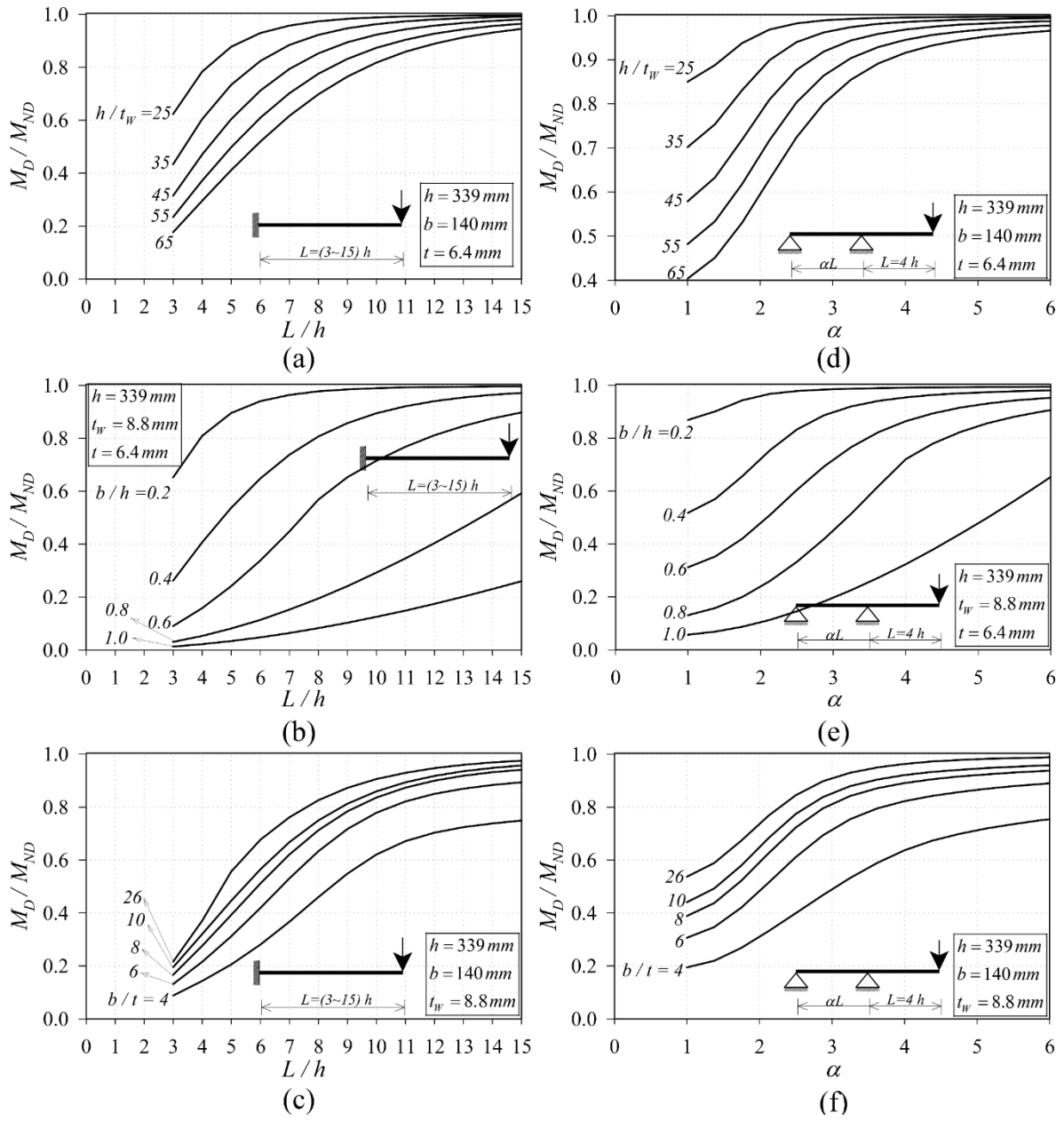

Fig. 2-11: Critical moment ratio M_D/M_{ND} for Case 3-cantilever subjected to tip point load (a) effect of web slenderness h/t_w, (b) effect of section aspect ratio b/h, (c) effect of flange slenderness b/t, and Case 4-simply-supported beam with overhang subjected a tip point load (d) effect of web slenderness h/t_w, (e) effect of section aspect ratio b/h, and (f) effect of flange slenderness b/t.

Fig. 2-11c, f suggest that cantilevers and beams with overhangs with stockier flanges exhibit pronounced web distortion, and consequently, a reduction in M_D/M_{ND}, even within practical span ranges (i.e., $L/h \le 15$ and $\alpha \le 6$). The selection of wide-flange I-beams with a lower aspect ratio and slender flanges would optimize material utilization in these cases.

2.11.2. Example 1: Buckled Configuration of Cantilevers

The previous section has shown that cantilevers exhibit high web distortional sensitivity as indicated by the reduction in critical moment ratio M_D/M_{ND} as the cantilever span is reduced. In this section, we examine the buckled configuration of the web as the span is varied. The sectional dimensions of the reference beam (Fig. 2-4a) are assigned to a cantilever subjected to a tip point load. The span is varied from 2m to 4m. The cantilevers are discretized by 40 elements in the longitudinal direction, providing convergent results. The lateral displacements of both flanges and their rotation about the y-axis are restrained at the cantilever root. Two critical moments are obtained from (i) a non-distortional LTB solution based only on the first two modes and (ii) a distortional LTB solution based on 18 modes (i.e., 2 non-distortional modes with 16 distortional modes).

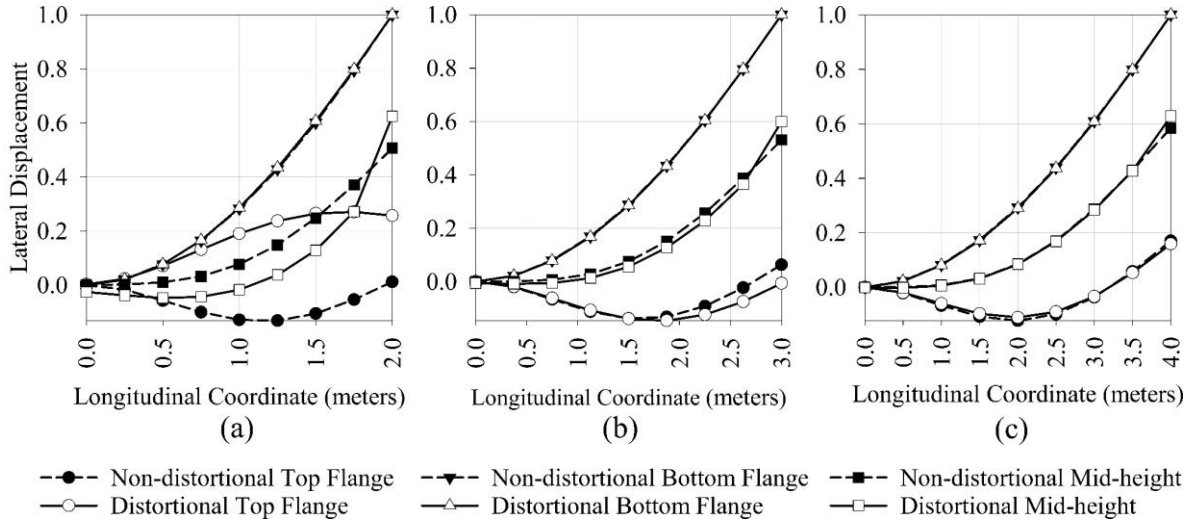

Fig. 2-12. Buckling modes for W410x39 cantilever. Spans are (a) 2m (b) 3m and (b) 4m

The lateral displacements at the bottom and top flanges and at the section mid-height are computed based on the normalized buckling mode as characterized by the combination of modes taken in each case, as discussed in Section 2.10. Fig. 2-12(c) shows that for the 4m span cantilevers, little to no distortion is observed in the web as the lateral displacements at both flanges and web mid-height based on the distortional LTB solution essentially coincide with those of non-distortional LTB solution and the corresponding critical moment ratio is $M_D/M_{ND} = 0.93$ close to unity. In contrast, the 2m span cantilever (Fig. 2-12a) exhibits significantly more distortion as evidenced by the large difference observed between the mid-height lateral displacements of the distortional LTB and non-distortional LTB solutions, leading to a lower critical moment ratio of $M_D/M_{ND} = 0.63$. A moderate amount of distortion

is observed for the 3m span cantilever (Fig. 2-12b), leading to a critical moment ratio of $M_D/M_{ND} = 0.84$ which lies in between those of the 2m and 4m spans.

2.12. Example 2: Interaction Curve of simply-supported Beam with Overhang

Consider a simply-supported beam with a single overhang. The cross-section of this beam is W690x125 ($h = 678mm, b = 253mm, t_W = 11.7mm, t = 16.3mm$). This beam is subjected to a uniformly distributed load w, and a concentrated point load P applied on the tip of the overhang. Both loads are acting at the beam centroid. The beam is laterally braced at the overhang's tip, and the supports for both top and bottom flanges. The cantilever span is taken as $L = 2m$, and that of the back-span is αL (Fig. 2-13a), where the seven cases have been investigated. The beams are discretized using 20 elements, and the number of distortional taken for the buckling analysis is taken as16.

Changes in the forces P and w result in a change in the distribution of moments in the pre-buckling analysis, and consequently, the distortional LTB critical forces. The critical load P_o in the absence of the distributed load is obtained by setting w to zero. In this case, the beam is subjected only to tip-placed loads, and the critical force P_o is obtained through the buckling analysis. Also, the other limiting case for the critical distributed load w_o is obtained by setting $P = 0$ (Table 2-4). In order to obtain the interaction curves for a given back-span to cantilever span ratio α thorough variations in P and w, the reference value w is set to unity, and the corresponding reference value for P is increased. The buckling analysis predicts the critical load combination (P_{cr}, w_{cr}) at which distortional buckling takes place. Fig. 2-13b shows the interaction curves for normalized critical distributed load w_{cr}/w_0 versus the corresponding normalized critical point load P_{cr}/P_0 for various α and w_o for various back-span to cantilever span ratios α. It is observed that the shape of the interaction curves depends on α. For the present problem, the interaction curves can be accurately approximated by a linear interpolation when $\alpha \geq 4.0$, while for other back-span to cantilever span ratios α, non-linear interpolation is expected to describe the interaction curves.

Table 2-4: Limiting values for the critical loads for various back-span to cantilever span ratios

α	$P_o\,(KN)$	$w_o\,(KN/m)$
2	2138.7	1381.5
2.5	1806.8	744.5
3.0	1480.5	391.2
3.5	1210.4	221.5
4.0	1005.8	134.7
4.5	849.5	87.0
5.0	728.9	59.0

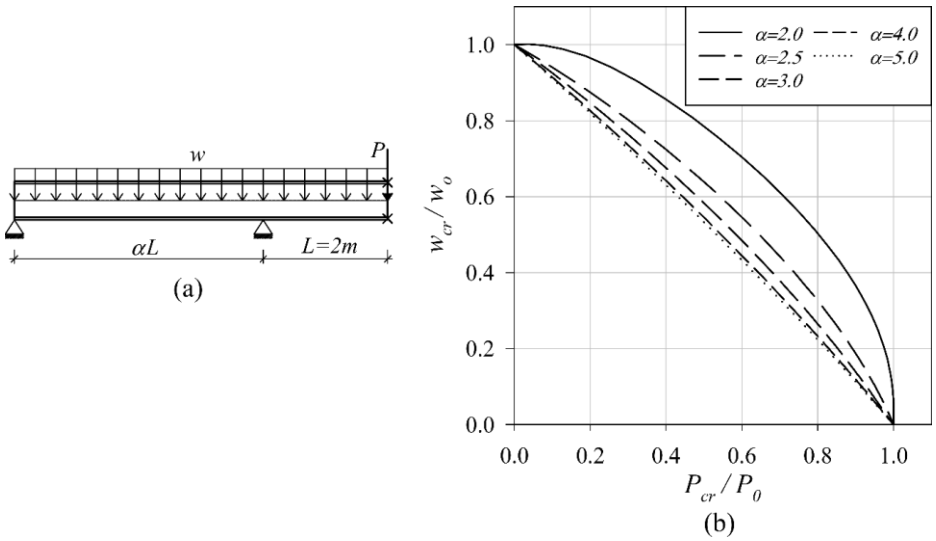

Fig. 2-13: simply-supported beam with a single overhang (a) load and geometry (b) Buckling Interaction Curves

2.13. Summary and Conclusions

The present study developed a finite element formulation for the lateral distortional buckling of doubly symmetric beams. Comparisons against classical non-distortional solutions, other distortional theories, and shell finite element analysis models indicate that the model reliably predicts the elastic buckling capacity and mode shapes. The element was employed to conduct a comprehensive parametric study to assess the effect of web distortion on the critical moment for simply-supported beams, cantilevers, and simply-supported beams with overhangs. The main findings of the research are:

1. A moderate increase in the number of distortional modes enables the present solution to yield distortional LTB critical moments smaller than those predicted by the Hermitian distortional model and closer to shell finite element predictions.
2. In the case studies investigated in the present work, four distortional modes were found to accurately predict the distortional buckling capacity and buckling modes for doubly symmetric I-beams.
3. The presence of mid-span concentrated point load induces significant web distortions in the neighborhood of the load application section. This localized effect is successfully captured the present solution.
4. For simply-supported beams subjected to mid-span point load, uniform moment, or reverse curvature moments, the amplitude of the distortional modes along the longitudinal direction is shown to be either symmetric or anti-symmetric about the mid-span section.
5. For short-span simply-supported beams subjected to mid-span point load or uniformly distributed load, the distortional effects gain significance with the increases in web slenderness h/t_w and section aspect ratio b/h, whereas for those with relatively large span $L \geq 25h$, the distortional effects are found insignificant.
6. For cantilevers and simply-supported beams with an overhang subjected to a tip point load, the distortional effect is highly susceptible to the increase in section aspect ratio b/h. When $b/h \geq 0.7$, web distortion is associated with a significant drop in the predicted buckling resistance even for beams with relatively large spans. Hence, the selection of cross-section with smaller section aspect ratios would help enhance the buckling resistance of cantilevers and simply-supported beams with an overhang.

2.14. References

[1] V.Z. Vlasov, Thin-walled elastic beams, National Technical Information Service1961.
[2] E. Reissner, On lateral buckling of end-loaded cantilever beams, Zeitschrift für angewandte Mathematik und Physik ZAMP 30(1) (1979) 31-40.
[3] X.-X. Wu, C.T. Sun, Simplified theory for composite thin-walled beams, AIAA Journal 30(12) (1992) 2945-2951.
[4] Z.M. Lin, D. Polyzois, A. Shah, Stability of thin-walled pultruded structural members by the finite element method, Thin-Walled Structures 24(1) (1996) 1-18.
[5] L.P. Kollár, Flexural–torsional buckling of open section composite columns with shear deformation, International Journal of Solids and Structures 38(42) (2001) 7525-7541.
[6] R.E. Erkmen, M. Mohareb, Buckling analysis of thin-walled open members—A complementary energy variational principle, Thin-Walled Structures 46(6) (2008) 602-617.
[7] R.E. Erkmen, M. Mohareb, Buckling analysis of thin-walled open members—A finite element formulation, Thin-Walled Structures 46(6) (2008) 618-636.

[8] M.M. Attard, M.-Y. Kim, Lateral buckling of beams with shear deformations – A hyperelastic formulation, International Journal of Solids and Structures 47(20) (2010) 2825-2840.
[9] L. Wu, M. Mohareb, Buckling of shear deformable thin-walled members—I. Variational principle and analytical solutions, Thin-Walled Structures 49(1) (2011) 197-207.
[10] L. Wu, M. Mohareb, Buckling formulation for shear deformable thin-walled members—II. Finite element formulation, Thin-Walled Structures 49(1) (2011) 208-222.
[11] R.E. Erkmen, Shear deformable hybrid finite-element formulation for buckling analysis of thin-walled members, Finite Elements in Analysis and Design 82 (2014) 32-45.
[12] A. Sahraei, L. Wu, M. Mohareb, Finite element formulation for lateral torsional buckling analysis of shear deformable mono-symmetric thin-walled members, Thin-Walled Structures 89 (2015) 212-226.
[13] M. Roberts Terence, G. Azizian Zaven, Instability of Thin Walled Bars, Journal of Engineering Mechanics 109(3) (1983) 781-794.
[14] M. Roberts Terence, G. Azizian Zaven, Influence of pre-buckling displacements on the elastic critical loads of thin walled bars of open cross section, International Journal of Mechanical Sciences 25(2) (1983) 93-104.
[15] M.M. Attard, General non-dimensional equation for lateral buckling, Thin-Walled Structures 9(1-4) (1990) 417-435.
[16] Y.L. Pi, N.S. Trahair, Prebuckling deflections and lateral buckling. I: theory, Journal of structural engineering 118(11) (1992) 2949-2966.
[17] Y.L. Pi, N.S. Trahair, Prebuckling deflections and lateral buckling. II: applications, Journal of Structural Engineering 118(11) (1992) 2967-2985.
[18] S. Rajasekaran, D.W. Murray, Coupled Local Buckling In Wide-Flange Beam-Columns, 1973.
[19] M.A. Bradford, N.S. Trahair, Distortional buckling of thin-web beam-columns, Engineering Structures 4(1) (1982) 2-10.
[20] M.A. Bradford, Distortional buckling of monosymmetric I-beams, Journal of Constructional Steel Research 5(2) (1985) 123-136.
[21] M.A. Bradford, Buckling of doubly-symmetric cantilevers with slender webs, Engineering Structures 14(5) (1992) 327-334.
[22] M.A. Bradford, H.R. Ronagh, Generalized Elastic Buckling of Restrained I-Beams by FEM, Journal of Structural Engineering 123(12) (1997) 1631-1637.
[23] P. Pezeshky, M. Mohareb, Distortional lateral torsional buckling of beam-columns including pre-buckling deformation effects, Computers & Structures 209 (2018) 93-116.
[24] P. Pezeshky, A. Sahraei, M. Mohareb, Distortional Lateral Torsional Buckling Analysis of Beams with Overhangs, Journal of Structural Engineering 145(3) (2019) 04018266.
[25] M.A. Bradford, N.S. Trahair, Distortional Buckling of I-Beams, 1981.
[26] T.M. Roberts, P.S. Jhita, Lateral, local and distortional buckling of I-beams, Thin-Walled Structures 1(4) (1983) 289-308.
[27] O. Hughes, M. Ma, Lateral Distortional Buckling of Monosymmetric Beams under Point Load, 1996.
[28] M. Ma, O. Hughes, Lateral distortional buckling of monosymmetric I-beams under distributed vertical load, Thin-Walled Structures 26(2) (1996) 123-145.
[29] C. Wang, C.K. Chin, S. Kitipornchai, Parametric study on distortional buckling of monosymmetric beam-columns, 1991.
[30] Z. Vrcelj, M.A. Bradford, Elastic distortional buckling of continuously restrained I-section beam–columns, Journal of Constructional Steel Research 62(3) (2006) 223-230.

[31] W.E.I. Chen, J. Ye, Elastic Lateral and Restrained Distortional Buckling of Doubly Symmetric I-Beams, International Journal of Structural Stability and Dynamics 10(05) (2010) 983-1016.
[32] J.-s. Lei, L.-y. Li, Combined web distortional and lateral-torsional buckling of partially restrained I-section beams, International Journal of Mechanical Sciences 131-132 (2017) 107-112.
[33] G.J. Hancock, M.A. Bradford, N. Trahair, Web distortion and flexural-torsional buckling, 1979.
[34] M.A. Bradford, Buckling of elastically restrained beams with web distortions, Thin-Walled Structures 6(4) (1988) 287-304.
[35] M.A. Bradford, Stability of monosymmetric beam-columns with thin webs, Journal of Constructional Steel Research 15(4) (1990) 323-339.
[36] R. Schardt, Verallgemeinerte technische biegetheorie, Springer-Verlag, Heidelberg, 1989.
[37] J.M. Davies, P. Leach, First-order generalised beam theory, Journal of Constructional Steel Research 31(2) (1994) 187-220.
[38] J. Davies, P. Leach, D. Heinz, Second-order generalised beam theory, Journal of Constructional Steel Research 31(2-3) (1994) 221-241.
[39] R. Schardt, Generalized beam theory—an adequate method for coupled stability problems, Thin-Walled Structures 19(2) (1994) 161-180.
[40] N. Silvestre, D. Camotim, Distortional buckling formulae for cold-formed steel C and Z-section members: Part I—derivation, Thin-Walled Structures 42(11) (2004) 1567-1597.
[41] N. Silvestre, D. Camotim, Distortional buckling formulae for cold-formed steel C- and Z-section members: Part II—Validation and application, Thin-Walled Structures 42(11) (2004) 1599-1629.
[42] P.B. Dinis, D. Camotim, N. Silvestre, GBT formulation to analyse the buckling behaviour of thin-walled members with arbitrarily ‘branched’ open cross-sections, Thin-Walled Structures 44(1) (2006) 20-38.
[43] R. Gonçalves, P.B. Dinis, D. Camotim, GBT formulation to analyse the first-order and buckling behaviour of thin-walled members with arbitrary cross-sections, Thin-Walled Structures 47(5) (2009) 583-600.
[44] P.B. Dinis, D. Camotim, N. Silvestre, On the local and global buckling behaviour of angle, T-section and cruciform thin-walled members, Thin-Walled Structures 48(10) (2010) 786-797.
[45] R. Bebiano, C. Basaglia, D. Camotim, R. Gonçalves, GBT buckling analysis of generally loaded thin-walled members with arbitrary flat-walled cross-sections, Thin-Walled Structures 123 (2018) 11-24.
[46] C.P. Johnson, M.K. Will, Beam Buckling By Finite Element, 1974.
[47] G.J. Hancock, Local, distortional and lateral buckling of I-beams, 1978.
[48] S. Ádány, B.W. Schafer, Buckling mode decomposition of single-branched open cross-section members via finite strip method: Derivation, Thin-Walled Structures 44(5) (2006) 563-584.
[49] S. Ádány, B.W. Schafer, Buckling mode decomposition of single-branched open cross-section members via finite strip method: Application and examples, Thin-Walled Structures 44(5) (2006) 585-600.
[50] S. Ádány, Constrained shell Finite Element Method for thin-walled members, Part 1: constraints for a single band of finite elements, Thin-Walled Structures 128 (2018) 43-55.
[51] S. Ádány, D. Visy, R. Nagy, Constrained shell Finite Element Method, Part 2: application to linear buckling analysis of thin-walled members, Thin-Walled Structures 128 (2018) 56-70.
[52] J.N. Reddy, Theory and Analysis of Elastic Plates and Shells, CRC Press LLC, Bosa Roca, 2006.

[53] S. Timoshenko, S. Woinowsky-Krieger, Theory of Plates and Shells, New York, London, 1940, Eingegangen am 25. 10 (1956).
[54] N. Trahair, Flexural-torsional buckling of structures, E & FN Spon, London, 1993.
[55] M.L.-H. Ng, H.R. Ronagh, An Analytical Solution for the Elastic Lateral-Distortional Buckling of I-section Beams, Advances in Structural Engineering 7(2) (2004) 189-200.
[56] R.S. Barsoum, R.H. Gallagher, Finite element analysis of torsional and torsional–flexural stability problems, International Journal for Numerical Methods in Engineering 2(3) (1970) 335-352.
[57] D.A. Nethercot, K.C. Rockey, Finite element solutions for the buckling of columns and beams, International Journal of Mechanical Sciences 13(11) (1971) 945-949.
[58] S. Kitipomchai, P.F. Dux, N.J. Richter, Buckling and Bracing of Cantilevers, Journal of Structural Engineering 110(9) (1984) 2250-2262.

Chapter 3: Effect of Load and Lateral Bracing height on lateral distortional buckling

Abstract

In a recent study, a family of finite element solutions was formulated for the distortional buckling analysis of wide flange beams that characterizes the distortional behavior of the web using any number of user-specified modes. By adopting the finite element formulation as a starting point, the present study augments the formulation by two additional features aimed at enabling the analyst to account for the destabilizing effect due to the load height relative to the shear and enforcing user-defined multi-point kinematic constraints. The multi-point constraint feature is then employed to model practical design problems, including the modeling of lateral bracing that is offset from the shear center and suppressing distortion at sections with transverse stiffeners. The effect of load height, bracing height, and combined effects of load and bracing height is investigated under the new formulation. A distortional indicator is then introduced to characterize the distribution of web distortion along the beam span as the beam undergoes distortional lateral buckling. The distortional indicator is used to devise an innovative procedure aimed at locating the optimum location(s) along the beam span for transverse stiffeners, such that they would maximize the critical moment capacity.

Authors Keywords: Finite Element, Lateral Torsional Buckling, distortional lateral buckling, load height effect, lateral bracing, kinematic constraints, transverse stiffeners

List of Notations

A_F	Area of flanges
b	Width of flanges
C_{wF}	Warping constants of flanges
C_w	Warping constants of section
C_H	Load height effect coefficient
D	Flexural rigidity of the web
E	Module of Elasticity
G	Shear module
h	Web height
$\mathbf{H}$	Vector collecting cubic Hermitian polynomials
$\mathbf{G}$	Geometric Stiffness matrix of element throughout buckling
$\mathbf{G}_q$	Geometric stiffness matrix due to load height effect
$\bar{\mathbf{G}}$	Geometric stiffness matrix of structure throughout buckling
I_{yF}	Moment inertia of flanges around weak axis
I_y	Moment inertia of section around weak axis
J	Saint-Venant torsional constant of section
J_F	Saint-Venant torsional constant of flanges
$\mathbf{K}$	Stiffness matrix of the element throughout buckling
$\bar{\mathbf{K}}$	Stiffness matrix of the structure throughout buckling
L	Length
M	Pre-buckling moment distribution
M_D	Distortional lateral torsional buckling under present work
M_{cl}	Classical lateral torsional buckling simply-supported beam subjected to uniform moments
t	Thickness of flanges
t_w	Thickness of web
q	Reference transverse loading
u	Lateral displacement field of web
$\tilde{u}_i$	Deformation mode i
u_B	Lateral displacement of bottom flange
u_T	Lateral displacement of top flange
u_D	Distortional lateral displacement
$\bar{u}_D$	Distortion indicator defined in Section 3.8.1
$\tilde{\mathbf{u}}$	Vector collecting all modes of deformation
$\tilde{\mathbf{u}}_D$	Vector collecting only distortional modes of deformation
y_q	Load Height
y_a	Location of lateral bracing
U	Strain energy throughout buckling
v_q	Vertical displacement of reference load throughout buckling
V	The potential energy gained by load throughout buckling
V_q	The potential energy gained due to load height effect.
$z_{\max}$	Coordinate in longitudinal direction with maximum distortion indicator defined in Section 3.8.1
$\mathbf{Z}$	Matrix including Hermitian polynomial required for all modes
$\mathbf{Z}_D$	Matrix including Hermitian polynomial required for only for distortional modes
ϕ_i	Amplitude of deformation mode i
λ	Eigenvalue
θ_B	Angle of twists of bottom flanges
θ_T	Angle of twists of top flanges
σ	Normal stress due to bending
τ	Shear stress due to bending
$\mathbf{B}$	Matrix of user-defined coefficients related to kinematic constraints
$\mathbf{\Delta}_i$	Degrees of freedom associated with mode i
$\mathbf{\Delta}$	Vector collecting all degrees of freedom for all modes
$\bar{\mathbf{\Delta}}$	Vector collecting all degrees of structure
$\mathbf{\Delta}_D$	Vector collecting all degrees of freedom for only distortional modes
μ	Poisson's ratio

Π	Total potential energy throughout buckling	$\bar{\Pi}^*$	Augmented Total potential energy of element considering kinematic constraints
Π^*	Augmented Total potential energy of element considering load height effect throughout buckling	$\boldsymbol{\Gamma}$	Vector collecting Lagrange multipliers
$\bar{\Pi}$	Total potential energy of structure throughout buckling		

3.1. Introduction and Literature Review

Long span thin-walled beams are prone to lateral-torsional buckling, an instability phenomenon that involves lateral deflection and twist of the cross-section. The stability of beams can be improved by providing lateral or torsional bracing restraints at discrete points along the span. A class of non-distortional solutions for the bucking of restrained beams has been developed based on Vlasov first assumption, which assumes the beam cross-section remains undistorted throughout buckling. Relevant studies on doubly-symmetric cantilevers I-beams include [1], on mono-symmetric cantilevers include [2] and [3]. Additional studies include studies on doubly symmetric I-beams [4-8] and monosymmetric I-beams [9, 10].

Continuous bracing provided by floor decking may also uniformly restrain the lateral displacement of the flanges and/or twist along the beam span. Non-distortional buckling solutions dealing with continuous bracing of beams include the work of Schmidt [11], Hancock, and Trahair [12], Trahair [13]., Larue et al. [14], Khelil and Larue [15].

Distortional lateral buckling solutions that capture cross-sectional distortion constitute another class of solutions. Within this class, the effect of twist and/or translational restraints on web distortion of I-beams has been investigated in [16-19], cantilevers with tee-sections [20], and I-beams with continuous elastic restraints [21, 22]. The influence of single flange restraining has been investigated for lipped channel beams [23], symmetric I-beams [22, 24-30], and mono-symmetric I-beam [31, 32], and mono-symmetric cantilevers [33].

The overarching themes in the abovementioned investigations are that (i) the optimal location for bracing depends on the position of load along the cross-section, the degree of mono-symmetry of the cross-section, and restrain type; (ii) Lateral bracing of the compression flange provides a significant enhancement in the buckling strength of the beam; and (iii) the lateral bracing effectiveness is influenced by the bracing height, and (iv) Continuous and/or discrete bracing induce cross-sectional distortion during buckling.

The majority of the above distortional buckling formulations treat the flanges as non-distorting Vlasov beams while considering the web to distort according to a cubic distortion along the web. In recent work (Chapter 2), we retained the non-distorting assumption for the flanges. However, in contrast to past studies, the lateral displacement field of the web is based on the superposition of (a) two linear (non-distortional) modes with (b) a user-specified number of Fourier terms. Some of the limitations of past work are related to its inability to model (i) torsional bracing, (ii) lateral bracing that is offset from the flanges, (iii) load height effects, and (iv) combined effect of load height and bracing height. Towards this goal, the present study complements the past study by (a) adding a feature to enforce any number of user-specified linear kinematic constraints and (b) incorporating the additional destabilizing effect due to load offset from the mid-height.

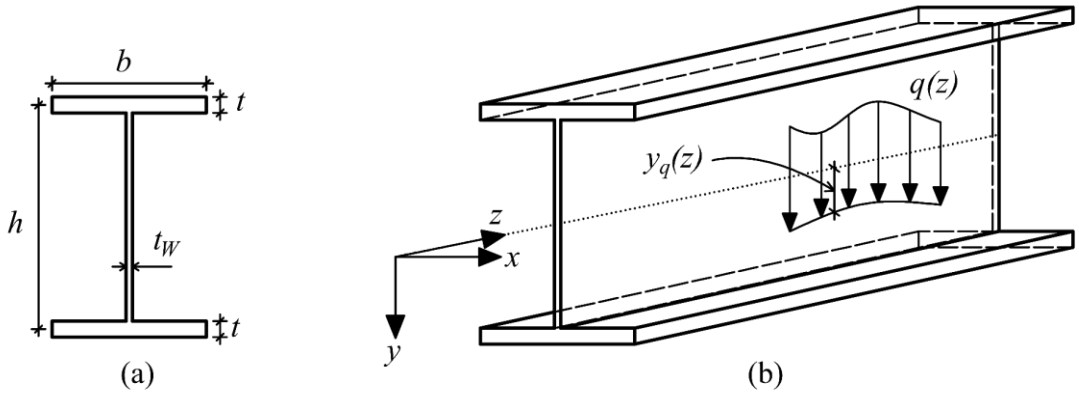

Fig. 3-1.(a) Cross-section geometric parameters (b) Loading scheme

3.2. Problem Statement

A doubly-symmetric beam with a wide flange cross-section has flanges of width b and thickness t. The web height is h, and its thickness is t_W (Fig. 3-1a). A right-handed coordinate system is defined on the web mid-height. A transverse line load $q(z)$ is applied on the beam whose line of action is defined by the curve $y_q(z)$ from the web mid-height. Load $q(z)$ induces strong axis pre-buckling bending moments (Fig. 3-1b). Fig. 3-2 shows the undeformed configuration of the beam in Stage 1. Under the effect of the reference load $q(z)$, the beam deforms to stage 2. As the load increases to a threshold value $\lambda q(z)$, the beam undergoes a proportional transverse deformation $\lambda v(z)$ and reaches stage 3. At this stage, the beam is in a neutral state of equilibrium at which the beam tends to buckle laterally by reaching stage 4 under no increase in loading.

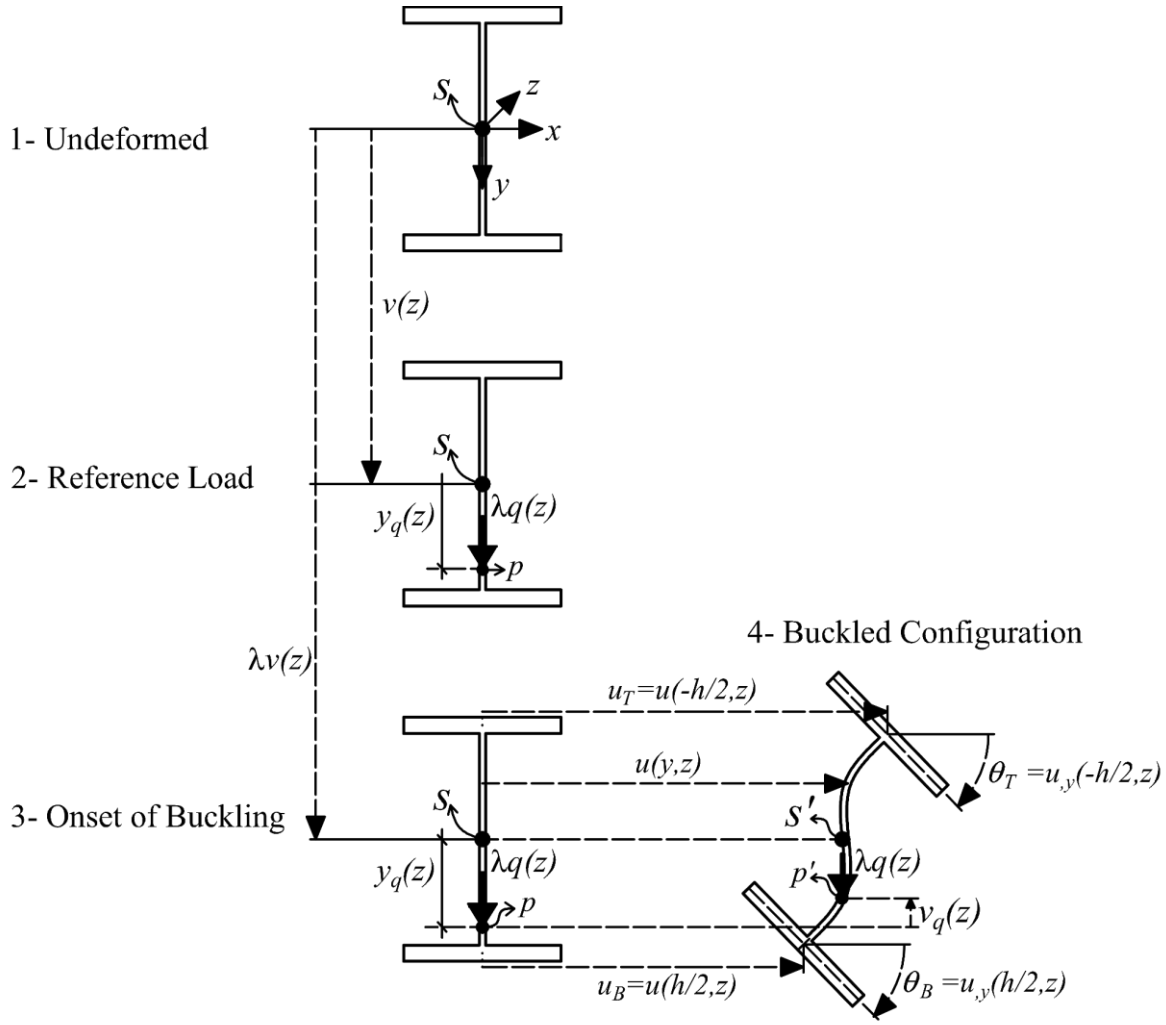

Fig. 3-2. Stages of deformation

As a convention, all subscripts W denote terms related to the web, subscript T denotes the top flange, and subscript B denotes the bottom flange. The lateral displacement field of the web $u(y,z)$ characterizes the buckling configuration of the beam. The lateral displacement of the flanges $u_T(z)$ and $u_B(z)$, and their angles of twists are related to $u(y,z)$ through compatibility relations. It is required to determine the critical load $\lambda q(z)$ under any number of user define linear kinematic constraints while accounting for the effect of load height. Towards this goal, modifications are introduced into the finite element formulation presented in Chapter 2.

3.3. Overview of Relevant Past work

In Chapter 2, a finite element method (FEM) formulation was developed for the buckling analysis of doubly symmetric wide-flange beams. In this formulation, the lateral displacement

distribution of the web was assumed to consist of a linear combination of two sets of deformation modes, namely, (i) the non-distortional modes and (ii) the distortional modes.

The formulation in Chapter 2 is limited to cases where loads are applied at the shear center. Also, it does not lend itself to enforcing some kinematic constraints associated with practical structural details, e.g., the presence of torsional restraints whereby both flanges undergo equal lateral displacements or the effect of transverse stiffeners, which would enable the non-distortional modes but suppress the distortional modes. Within this context, the present work incorporates two additional features into this finite element formulation:

1. A feature capturing the load height effects
2. The formulation is augmented to handle any number of user-defined linear kinematic constraints to model lateral braces.

3.4. Assumptions

The present formulation will follow the assumptions made in Chapter 2, i.e.,

1. Beam has a doubly symmetric wide flange cross-section
2. Material is linearly elastic isotropic
3. Pre-buckling strains are small
4. Flanges are relatively stocky, so that their distortion is negligible. As such, each flange can be idealized as a Vlasov beam.
5. The classical Vlasov thin-walled beam theory omits web distortion [34]. In the present solution, this assumption is relaxed, and the web is free to distort. The present solution will model the web using the kinematics of the classical Kirchhoff plate theory [35].

3.5. Variational Formulation

In Chapter 2, the total potential energy of a beam element throughout buckling was expressed as the sum of the potential energy Π_W associated with the web, that of the bottom flange Π_B, that of the top flange Π_T , i.e.,

$$\Pi = \Pi_W + \Pi_B + \Pi_T \tag{2.28}$$

where the energy terms for each of the contributors are

$$
\begin{aligned}
\Pi_W &= \frac{D}{2}\int_0^L\int_{-h/2}^{h/2}\left(u_{,yy}^2+u_{,zz}^2+2\mu u_{,yy}u_{,zz}+2(1-\mu)u_{,yz}^2\right)dy\,dz \\
&\quad -\frac{\lambda t_w}{2}\int_0^L\int_{-h/2}^{h/2}\left(\sigma(z,y)u_{,z}^2+2\tau(z)u_{,y}u_{,z}\right)dy\,dz \\
\Pi_B &= \frac{1}{2}\int_0^L\left(EI_{yF}u_{,zz}^2+EC_{wF}u_{,yzz}^2+GJ_F u_{,yz}^2\right)_{y=h/2}dz \\
&\quad -\lambda\frac{1}{2}\int_0^L\sigma(z,h/2)\left(A_F u_{,z}^2+I_{yF}u_{,yz}^2\right)_{y=h/2}dz \\
\Pi_T &= \frac{1}{2}\int_0^L\left(EI_{yF}u_{,zz}^2+EC_{wF}u_{,yzz}^2+GJ_F u_{,yz}^2\right)_{y=-h/2}dz \\
&\quad -\lambda\frac{1}{2}\int_0^L\sigma(z,h/2)\left(A_F u_{,z}^2+I_{yF}u_{,yz}^2\right)_{y=-h/2}dz
\end{aligned}
\qquad (2.29a\text{-}c)
$$

in which μ is the Poisson's ratio, G is the shear module, and E are the Young module of Elasticity. The normal stress distribution $\sigma(z,y)$ and the shear stress $\tau(z)$ are obtained from the pre- buckling stage. The flexural rigidity of the web is $D=Et_W^3/12(1-\mu^2)$. The sectional properties of the flanges are also determined by $\left[A_F, I_{yF}, C_{wF}, J_F\right]=\left[bt,\ b^3t/12,\ b^3t^3/144, bt^3/3\right]$. As convection, a subscript comma denotes the partial derivative with respect to the argument coordinates.

3.5.1. Interpolation Scheme

In Chapter 2, the lateral displacement field of the web $u(y,z)$ was assumed to take the form

$$
u(y,z)=\sum_{i=1}^{m}\tilde{u}_i(y)\phi_i(z) \qquad (2.30)
$$

Eq.2.30 allows for determining the lateral displacement field of the web by two schemes

Scheme 1: Hermitian Field

$$
\begin{aligned}
\tilde{u}_1(y) &= \frac{1}{2}-\frac{3y}{2h}+\frac{2y^3}{h^3}, & \tilde{u}_2(y) &= \frac{h}{8}-\frac{y}{4}-\frac{y^2}{2h}+\frac{y^3}{h^2} \\
\tilde{u}_3(y) &= \frac{1}{2}+\frac{3y}{2h}-\frac{2y^3}{h^3}, & \tilde{u}_4(y) &= \frac{-h}{8}-\frac{y}{4}+\frac{y^2}{2h}+\frac{y^3}{h^2}
\end{aligned}
\qquad (2.31)
$$

This lateral displacement field of the web has often been used in the literature (e.g., [18, 22, 23, 27, 32, 36-46]), whereby the lateral displacement of the web $u(y,z)$ is related to the lateral displacement and angle of twists of the top and bottom flanges $u_T(z)$, $\theta_T(z)$, $u_B(z)$, $\theta_B(z)$. In this case, functions $\phi_i(z), i=1,2,3,4$ represent the lateral displacements and the angles of

twist at the bottom and top of the web, i.e., $\phi_1(z)=u_B(z)$, $\phi_2(z)=\theta_B(z)$, $\phi_3(z)=u_T(z)$ and $\phi_4(z)=\theta_T(z)$. We refer to Interpolation Scheme 1 as the Hermitian distortional model subsequently.

Scheme 2: Generalized Distortional Field

$$\tilde{u}_i(y)=\begin{cases}(1/2+y/h) & i=1\\ (1/2-y/h) & i=2\\ \cos\left[\pi(i-2)y/h\right] & i=3,5,7...\\ \sin\left[\pi(i-2)y/h\right] & i=4,6,8...\end{cases} \tag{2.32}$$

where $\tilde{u}_i(y)$, $i=1,2,\ldots,m$ are deformation modes characterizing the variation of the lateral displacement along the web height. Modes 1 and 2 are the non-distortional mode, and modes $i\geq 3$ are the distortional modes. Functions $\phi_i(z), i=1,2,\ldots,m$ represent the amplitudes of the deformation modes $\tilde{u}_i(y)$ at the section z.

Under both interpolation schemes, functions $\phi_i(z)$ are related to the nodal displacements of the element $\boldsymbol{\Delta}_i^T=\langle\phi_i(0)\quad\phi_{i,z}(0)\quad\phi_i(L)\quad\phi_{i,z}(0)\rangle$ through the conventional Hermitian polynomials, i.e., $\phi_i(z)=\mathbf{H}^T(z)\boldsymbol{\Delta}_i$, in which

$$\mathbf{H}^T(z)=\left\langle\left(1-\frac{3z^2}{L^2}+\frac{2z^3}{L^3}\right)\quad\left(z-\frac{2z^2}{L}+\frac{z^3}{L^2}\right)\quad\left(\frac{3z^2}{L^2}-\frac{2z^3}{L^3}\right)\quad\left(-\frac{z^2}{L}+\frac{z^3}{L^2}\right)\right\rangle \tag{2.33}$$

Under interpolation Scheme 2, the lateral displacement field of the web $u(y,z)$ is then expressed in a matrix form as

$$u(y,z)=\tilde{\mathbf{u}}^T(y)\mathbf{Z}(z)\boldsymbol{\Delta} \tag{2.34}$$

in which

$$\tilde{\mathbf{u}}^T(y)=\langle(1/2+y/h)\quad(1/2-y/h)\;\vdots\;\cos(\pi y/h)\quad\sin(2\pi y/h)\quad\ldots\quad\rangle_{1\times m}$$

$$\mathbf{Z}(z)=\begin{bmatrix}\mathbf{H}^T(z) & & & \\ & \mathbf{H}^T(z) & \ldots & \\ & \vdots & & \\ & & & \mathbf{H}^T(z)\end{bmatrix}_{m\times 4m} \tag{2.35}$$

$$\boldsymbol{\Delta}^T=\langle\boldsymbol{\Delta}_1^T\;\vdots\;\boldsymbol{\Delta}_2^T\;\vdots\;\ldots\;\vdots\;\boldsymbol{\Delta}_m^T\rangle_{1\times 4m}$$

By taking the appropriate derivatives of Eq.2.34 and substituting them into the total potential energy term of the element appearing in Eq.2.28 and Eq.2.29, one obtains

$$\Pi = \frac{1}{2}\boldsymbol{\Delta}^T \left[\mathbf{K} - \lambda \mathbf{G}\right]\boldsymbol{\Delta} \tag{2.36}$$

in which $\mathbf{K}$ is the stiffness matrix and $\mathbf{G}$ is the geometric stiffness matrix of the element. Both matrices are of order $4m \times 4m$, and their entries have been defined in Appendix B.

3.6. Formulation

3.6.1. Modified Variational Principle

The reference load $q(z)$, applied at a height $y_q(z)$ above the shear center, undergoes the vertical displacement $v_q(z)$ throughout buckling (Stage 4 in Fig. 3-2). The corresponding potential energy gain V_q is obtained by the product of load increment $q(z)dz$ by the displacement $v_q(z) = 1/2\int_{y=0}^{y=y_q(z)} \left[u_{,y}(z,y)\right]^2 dy$. By integrating with respect to z, one recovers the total potential energy gain of the load $q(z)$ throughout buckling as

$$V_q = \lambda \int_0^L q(z) v_q(z)\, dz = \frac{\lambda}{2}\int_0^L \int_{y=0}^{y=y_q(z)} q(z)\left[u_{,y}(z,y)\right]^2 dy\, dz \tag{2.37}$$

By taking the appropriate derivatives of Eq.2.34 and substituting into Eq.2.37, one obtains

$$V_q = \frac{\lambda}{2}\boldsymbol{\Delta}^T \mathbf{G}_q \boldsymbol{\Delta} \tag{2.38}$$

in which $\mathbf{G}_q$ is the destabilizing stiffness matrix and is given by

$$\mathbf{G}_q = \int_0^L \int_{y=0}^{y=y_q(z)} q(z)\mathbf{Z}^T(z)\tilde{\mathbf{u}}_{,y}(y)\tilde{\mathbf{u}}_{,y}^T(y)\mathbf{Z}(z)\, dy\, dz \tag{2.39}$$

The total potential of the element Π^* that includes the load height effect is then given by summing the total potential energy Π (Eq.2.36) and the load height contribution (Eq.2.38), i.e.,

$$\Pi^* = \frac{1}{2}\boldsymbol{\Delta}^T \left[\mathbf{K} - \lambda\left(\mathbf{G} + \mathbf{G}_q\right)\right]\boldsymbol{\Delta} \tag{2.40}$$

3.6.2. The Imposition of Kinematic Constraint

The element stiffness matrices in Eq.2.40 are assembled using conventional techniques to form the stiffness matrix $\bar{\mathbf{K}}_{r\times r}$, and the geometric stiffness $\bar{\mathbf{G}}_{r\times r}$ of the structure, where r is the number of degrees of freedom of the structure, yielding the total potential energy expression of the structure

$$\bar{\Pi} = \frac{1}{2}\bar{\mathbf{\Delta}}^T\left[\bar{\mathbf{K}} - \lambda\bar{\mathbf{G}}_{r\times r}\right]\bar{\mathbf{\Delta}} \tag{2.41}$$

where vector $\bar{\mathbf{\Delta}}$ is the nodal displacement vector for the structure. The structure is then assumed to be subjected to a set of k multiple point constraints, written in a matrix form as

$$\mathbf{B}_{(k\times r)}\bar{\mathbf{\Delta}}_{(r\times 1)} = \mathbf{0}_{k\times 1} \tag{2.42}$$

where $\mathbf{B}_{(k\times r)}$ is a matrix of user-defined coefficients which linearly relate any set of nodal displacements. Vector $\bar{\mathbf{\Delta}}_{(r\times 1)}$ assembles all nodal displacements of the structure. It is required to evoke the stationary condition Eq.2.41 subject to the constraints in Eq.2.42. For this purpose, an augmented functional Π^{**} is constructed by pre-multiplying the constraints in Eq.2.42 by a vector of Lagrange multipliers $\mathbf{\Gamma}^T_{(k\times 1)}$, and adding it to the total potential energy of the structure, i.e.,

$$\bar{\Pi}^* = \frac{1}{2}\bar{\mathbf{\Delta}}^T_{(1\times r)}\left(\bar{\mathbf{K}}_{(r\times r)} - \lambda\bar{\mathbf{G}}_{(r\times r)}\right)\bar{\mathbf{\Delta}}_{(r\times 1)} + \mathbf{\Gamma}^T_{(1\times k)}\mathbf{B}_{(k\times r)}\bar{\mathbf{\Delta}}_{(r\times 1)} \tag{2.43}$$

By evoking the stationary conditions of Eq2.43. with respect to the nodal displacements $\partial\bar{\Pi}^*/\partial\mathbf{\Delta}_{(r\times 1)}$, and the Lagrange multipliers $\partial\bar{\Pi}^*/\partial\mathbf{\Gamma}_{(k\times 1)}$, one obtains

$$\left(\left[\begin{array}{c:c} \bar{\mathbf{K}}_{(r\times r)} & \mathbf{B}^T_{(r\times k)} \\ \hdashline \mathbf{B}_{(k\times r)} & \mathbf{0}_{(k\times k)} \end{array}\right] - \lambda\left[\begin{array}{c:c} \bar{\mathbf{G}}_{(r\times r)} & \mathbf{0}_{(r\times k)} \\ \hdashline \mathbf{0}_{(k\times r)} & \mathbf{0}_{(k\times k)} \end{array}\right]\right)\left[\begin{array}{c} \bar{\mathbf{\Delta}}_{(r\times 1)} \\ \hdashline \mathbf{\Gamma}_{(k\times 1)} \end{array}\right] = \left[\begin{array}{c} \mathbf{0}_{(r\times 1)} \\ \hdashline \mathbf{0}_{(k\times 1)} \end{array}\right] \tag{2.44}$$

The non-trivial solution of Eq.2.44 is provided by setting to zero the determinant of the bracketed matrix, yielding the load multiplier λ, the associated eigenvector $\bar{\mathbf{\Delta}}_{(r\times 1)}$, and the Lagrange multipliers $\mathbf{\Gamma}_{(k\times 1)}$.

3.7. Verification and Applications

3.7.1. Example 1: Effect of Lateral Bracing

Consider a simply-supported beam with W410x39 cross-section ($h = 339mm$, $b = 140\,mm$, $t = 8.8\,mm$ and $t_W = 6.4\,mm$) (Fig. 3-3a). The beam is subjected to uniform moments. Span is taken as 6 meters (Fig. 3-3b). Young's modulus taken is taken as $E = 200\,GPa$, and the Poisson's ratio μ is also 0.3. In this work, we refer to this geometry as the reference beam.

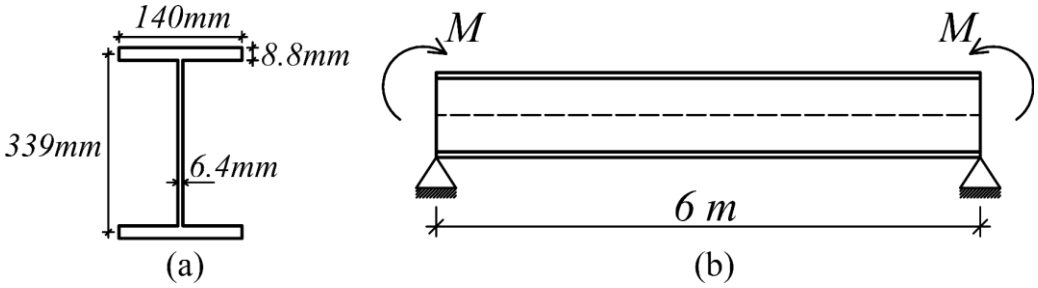

Fig. 3-3: Reference beam (a) cross-section and (b) loading

The top and bottom flanges of the reference beam are restrained at the supports. The beam is discretized using 20 elements (i.e., 21 nodes). In order to retrieve the non-distortional LTB critical moments, the distortional modes are omitted, i.e., the number of modes is set to $m = 2$. The number of degrees of freedom is thus $21\ \text{nodes} \times 2\ \text{modes} \times 4$ =168. Two scenarios are considered regarding the mid-span section: Case 1: section is laterally free, Case 2: the section is laterally restrained at mid-height.

For Case 1, the non-distortional LTB critical moments are obtained for the first six eigenmodes using the classical non-distortional formula for a simply-supported beam under uniform moments M_{cl} (Column 2 in Table 3-1),

$$M_{cl} = \frac{n\pi}{L}\sqrt{GJEI_y + \left(\frac{n\pi}{L}\right)^2 EC_w} \tag{2.45}$$

in which n is the eigenmode, which is given by the module of elasticity E, and shear module G. The sectional properties are $\left(J, I_y, C_w\right) = \left[\left(2t^3b + ht_W^3\right)/3, \left(2b^3t + ht_W^3\right)/12, I_y h^2/4\right]$. Table 3-1 shows the predictions present solution for Case 1 (Column 3 in Table 3-1). The critical moments predicted by the present solution are slightly smaller than those predicted by the classical formula, which is attributed to the minor differences in the sectional properties derived from the present solution, as has been discussed under Appendix C.

For Case 2, a single kinematic constraint is introduced to restrain the lateral displacement of mid-span at mid-height, i.e., $[y=0, z=3m \mid u=0]$. This constraint is used to form the matrix of coefficients $\mathbf{B}_{(k=1)\times(r=164)}$ (Eqs.2.42-2.44), and the resulting constrained eigenvalue problem is solved to yield load multipliers λ for the first six eigenmodes (Column 5 in Table 3-1). As can be observed from Table 3-1, the critical moments of the restrained beam with the odd eigenmodes coincide with those of the non-restrained beam with the even eigenmodes, which leads to a significant increase in the non-distortional LTB of the beam.

Table 3-1: Non-distortional LTB critical moments for simply-supported beam subjected uniform moment

Critical moment (*KN.m*)				
Case 1			Case 2	
(1) Eigenmode	(2) Classical formula (Eq.2.45)	(3) Present Solution	(4) Eigenmode	(5) Present Solution
1st	44.84	44.83		
2nd	130.54	**130.40**	1st	**130.40**
3rd	268.47	268.14	2nd	222.62
4th	460.55	**460.00**	3rd	**460.00**
5th	707.19	706.49	4th	622.60
6th	1008.50	**1008.00**	5th	**1008.00**
			6th	1235.65

3.7.2. Example 2: Effect Distortional modes on Mid-height Lateral Restraint

The reference cross-section (Fig. 3-3) is revisited. Span is taken as 4.8 meters. Similar to the previous section, two scenarios are considered regarding the mid-span section: Case 1: section is laterally free, and Case 2: section is laterally restrained at mid-height. For each case, the distortional LTB critical moment is determined by (i) present the present solution while varying the number of modes, i.e. $m \in (2,3,\ldots,14)$, (ii) The Hermitian distortional model (iii) shell model under Abaqus. (Fig. 3-4). For the 1–D models (i.e., the present solution and the Hermitian Distortional model), the reference beam is discretized into 21 elements. At both ends, the boundary conditions are imposed by restraining the lateral displacement of the top and bottom flanges.

The shell model is based on the S4R element in the Abaqus library, which is a quadrilateral element with four nodes with six degrees of freedom per node and reduced integration. The beam is meshed using 200 elements along the span, and 18 elements along flanges, and 20 elements along the web. The lateral nodal displacements at the flange-to-web junctions at both ends are restrained. A mesh study indicated that the previous discretization scheme provides convergent results for all the models. The end moments are modeled by equal and opposite longitudinal forces applied at the flange–to–web junctions.

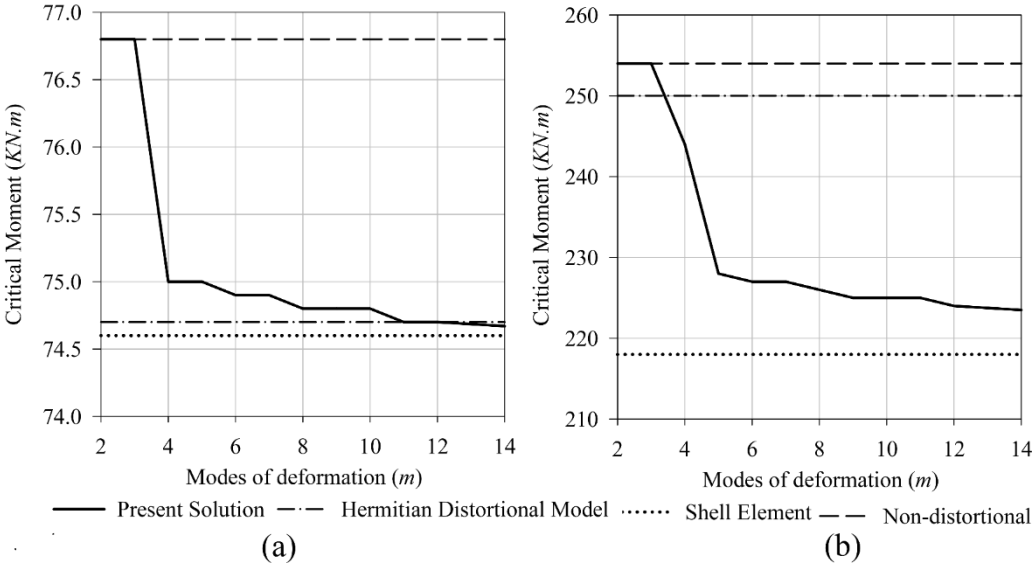

Fig. 3-4: Effect of number of modes of deformation for a simply-supported beam under uniform moments (a) beam is laterally unrestrained, and (b) the mid-span section is laterally restrained at the mid-height

For both cases, the non-distortional LTB solution is obtained by setting $m = 2$, which provides an upper bound for the critical moments. Given a large number of degrees of freedom, the shell model is more flexible, and hence it provides a lower bound critical moment. In the present solution, as the number of deformation modes m increases, the critical moment predicted decreases. For Case 1, where the mid-span section is laterally free, the Hermitian distortional model predicts critical moment slightly higher than those predicted by the present solution when enough number of modes of deformation is included, i.e., $m \geq 11$ (Fig. 3-4a).

For Case 2, where the mid-span section is restrained at mid-height, the Hermitian distortional model leads to a critical moment that is 11.0% higher than the present solution's prediction with 14 modes of deformation (Fig. 3-4b). In order to investigate this difference, the lateral displacement of the flanges and the section mid-height along the longitudinal direction are compared for the first eigenmodes of (i) the present solution with 14 modes of deformation, (ii) the Hermitian distortional model; and (iii) the first and second eigenmodes of the shell

element (Fig. 3-5). It is observed that the lateral displacement of the flanges and mid-height as predicted by the present solution coincides approximately with those predicted by the first eigenmode of the shell model.

A comparison of the second eigenmode of the shell element and the Hermitian distortional model leads to two observations: (1) the second eigenmode of the shell element model yields a critical moment of 249*KNm*, which is close to the prediction of the Hermitian distortional model of 250*KNm*, and (2) The lateral displacement of the flanges and the mid-height as predicted by the Hermitian distortional model are in close to those predicted by the second eigenmode of the shell model. These observations suggest that the Hermitian distortional model is unable to adequately account for the web distortion when the web is laterally restrained.

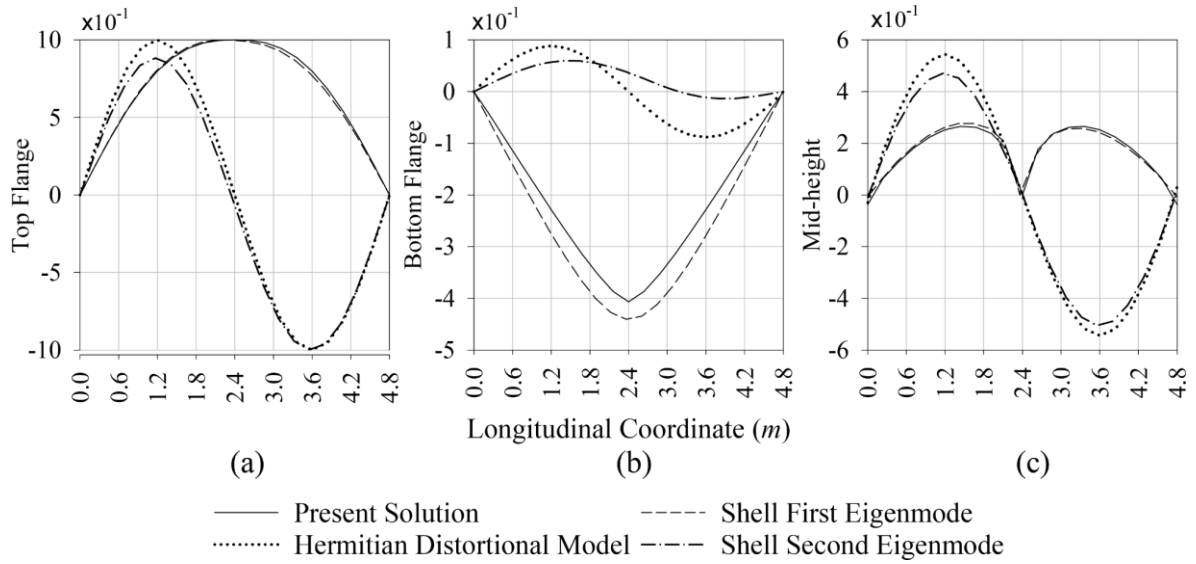

Fig. 3-5: The lateral displacement along the longitudinal direction at (a) Top Flange (b) Bottom flange, and (c) Mid-height

3.7.3. Example 3: Effect of Height of Lateral Brace

The previous example is revisited while varying the height of the mid-span lateral brace y_a, such that by retaining the web height $-0.5 \le y_a/h \le 0.50$. The critical moments are obtained by (i) the present solution with 18 modes of deformation, (ii) the non-distortional solution by setting $m = 2$, and (iii) the shell element model under Abaqus. The modeling scheme conforms to the descriptions provided in Section 3.7.2. The result of this treatment is showed in Fig. 3-6. The non-distortional LTB critical moments provide an upper-bound, and the distortional LTB critical moments predicted by the present solution and the shell element model are in good agreement.

A common theme to the plots in Fig. 3-6 is that raising the height of the lateral brace from the bottom flange (tension flange) towards the top flange (compression flange) results in an increase in the critical moment up to a threshold height after which no increase in the critical moments is observed. The threshold height predicted by the present distortional model is $y_a = -0.029h$, and that predicted by the non-distortional model as $y_a = 0.081h$.

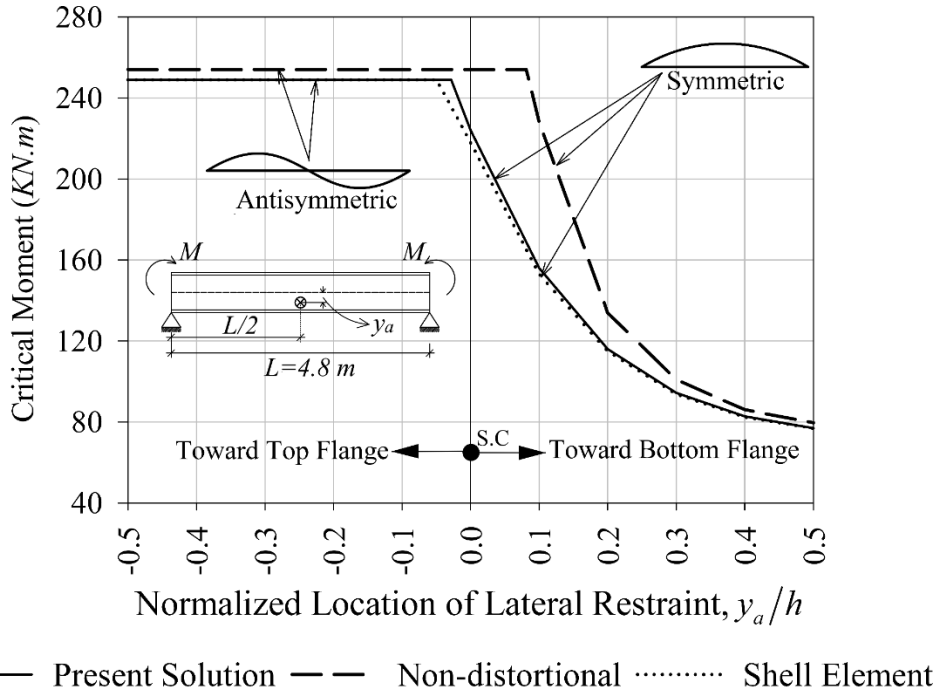

Fig. 3-6: Effect of lateral restrain height on critical moments based on the present distortional, non-distortional, and shell FEA for a simply-supported beam subjected to uniform moments

The buckled lateral displacements of the flanges and at web mid-height predicted by both distortional and non-distortional LTB model reveal an abrupt change in the buckled configuration of the beam as the lateral brace height passes through the threshold height. When the lateral brace is located below the threshold height, the buckled configuration is symmetric relative to the mid-span section. Below the threshold height, the buckled configuration becomes anti-symmetric relative to the mid-span section. This phenomenon is depicted in two representative cases where the bracing height is located $y_a = 0.3h$ solution (Fig. 3-7a and b) and $y_a = -0.3h$ (Fig. 3-7 b and d).

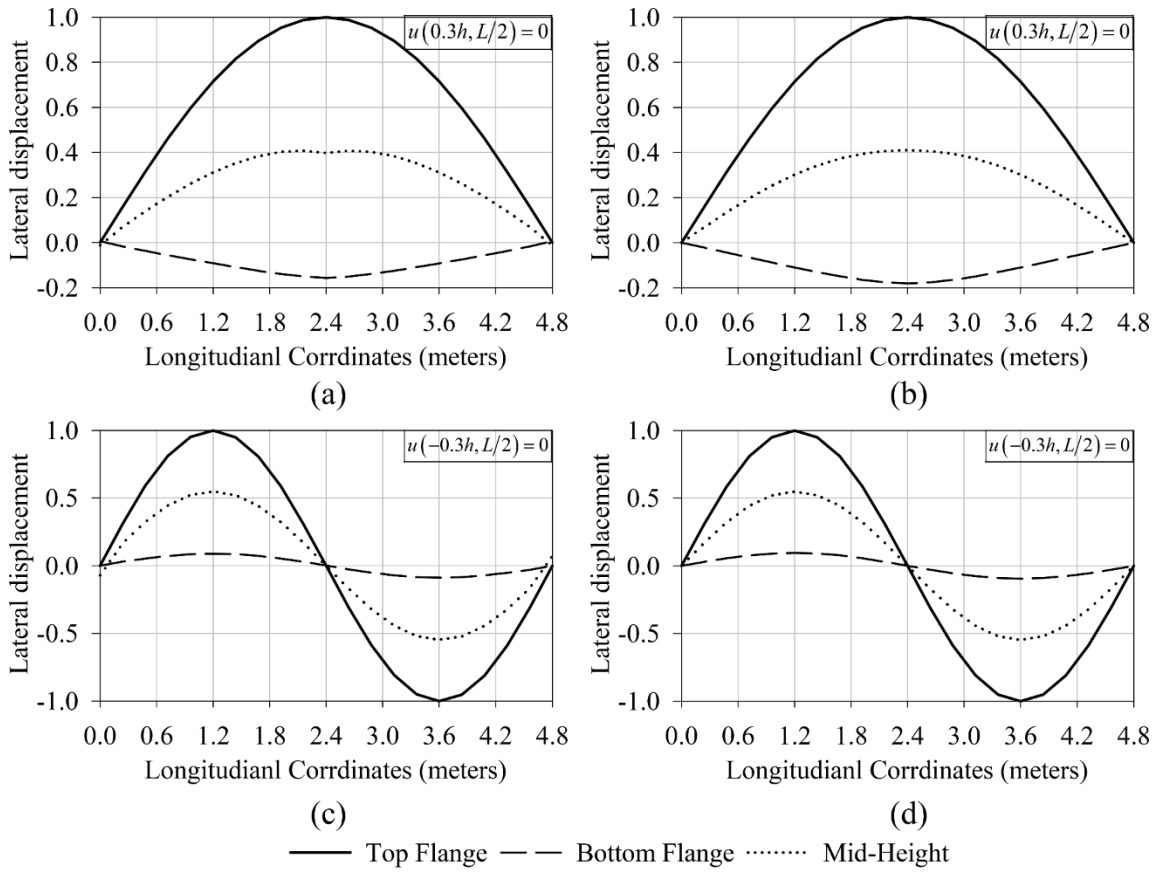

Fig. 3-7: Lateral displacement of flanges and web mid-height along longitudinal direction when the mid-span section is laterally restrained at $y_a=0.3h$, obtained by (a) the present solution and (b) the non-distortional model; and when the mid-span section is laterally restrained at $y_a=-0.3h$, obtained by (c) the present solution and (d) the non-distortional model

3.7.4. Example 4: Effect of Load Height

Consider a simply-supported beam with W310x31 cross-section ($h = 306mm$, $b = 164mm$, $t_W = 5mm$, $t = 7.4mm$) with a span $L = 6.6\,m$. The beam is subjected to a point load applied at $0.35L$ (Fig. 3-8a). It is required to investigate the effect of the load height y_q on the critical moment. The ratio y_q/h is varied from -0.5 to 0.5. For each case, the critical moments are obtained by (i) the distortional LTB moments using 18 modes of deformation $m = 18$, (ii) the non-distortional LTB by setting $m = 2$, and (iii) based predictions of the S4R shell element model under Abaqus.

For the 1-D models obtained from the present work, the beam is discretized into 20 elements. The boundary conditions are imposed by restraining the lateral displacement of the bottom and top flanges at both ends. The shell model in this section is similar to that described under Section 3.7.2.

In order to avoid localized deformation in the web in the present model and Abaqus, when applying the load P at a height y_q below the shear center $-h/2 \le y_q \le h/2$, a proportion of the load $\left(0.5+y_q/h\right)P$ is allocated to the bottom web-to-flange junction, and the remaining portion of the load $\left(0.5-y_q/h\right)P$ is allocated to the top web-to-flange junction.

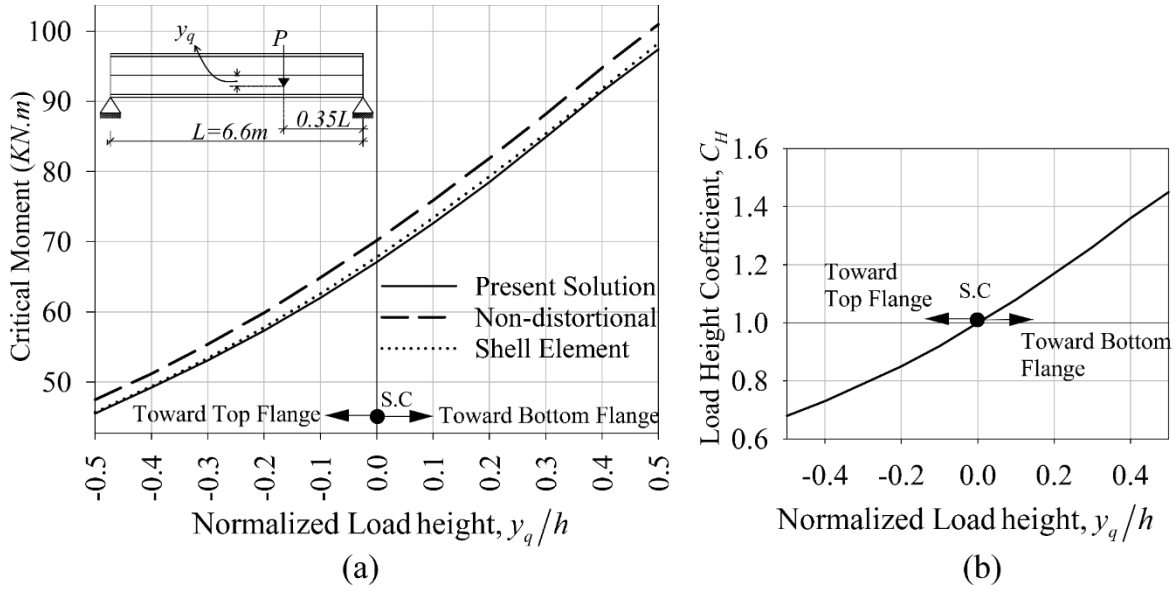

Fig. 3-8: simply-supported beam subjected to a floating-point load along the transverse direction (a) Critical moment versus normalized load height (b) Load Height Coefficient

As expected, Fig. 3-8a shows that the critical moment reduces as the point of application of the load application shifts toward the top flange. Compared to Abaqus, the non-distortional LTB grossly overpredicts the critical moments. Interestingly, the distortional LTB buckling moment predicted by the present non-distortional solution is slightly lower than those based on the shell element model. The reason is attributed to the fact that the destabilizing term (Eq.2.29) includes only the effect of longitudinal and shear stresses but omits the contribution of transverse normal stresses since the pre-bucking analysis is based on the conventional Euler-Bernoulli beam theory is unable to capture the magnitudes of pre-buckling transverse stresses.

In design, it is convenient to define the load height coefficient C_H at a height y_q as the ratio of the critical moment when the load(s) is/are applied at height y_q to the critical moment when the loads are applied at the section shear center $y_q = 0$. The load height coefficient $C_H\left(y_q\right) = M_D\left(y_q\right)/M_D\left(0\right)$ based on the present distortional model versus the normalized load height ratio y_q/h is depicted in Fig. 3-8b for the present beam and is found to vary from 0.68 when the load is applied at the top flange to 1.45 when the load is applied at the bottom

flange. Interestingly, the load height coefficient obtained from the non-distortional LTB and the shell element model approximately coincides with those of the present distortional solution.

3.7.5. Example 5: Combined Effect of Load and Lateral Brace Height

In steel construction, point loads acting on a girder can arise from smaller beams framing into the girder. Commonly, the framing beams provide a lateral brace to the girder at the point of attachment. In such a scenario, one has $y_q = y_a$, and it becomes of interest to examine the effect of load/bracing height on the critical moment.

The beam in the previous section is revisited. The location of the load application $y_q\left(z = 0.35L\right)$ is varied gradually from the bottom flange ($y_q\left(z = 0.35L\right) = 0.5h$) to the top flange ($y_q\left(z = 0.35L\right) = -0.5h$). For each case, the non-distortional LTB critical moments is obtained by omitting distortional modes, i.e., $m = 2$. The distortional LTB critical moments are also obtained by the present solution with 18 modes of deformation, i.e. $m = 18$, and the shell element model under Abaqus. The modeling specifications in the shell element and 1-D models conform to those of the previous section. However, in contrast to the previous section, the point load is applied directly at the height y_q located on the web section for the shell element model.

The corresponding critical moments are depicted in Fig. 3-9. Reasonably close agreement is obtained between the present distortional model and the shell model. In comparison, the non-distortional solution overpredicts the critical moments and under-predicts the bracing threshold height. All three solutions predict a nearly critical moment when the bracing and loads are applied within the top part of the section, after which the critical moment tends to gradually drop as the bracing/load height location gets closer to the bottom flange.

Compared to Section 3.7.4 where no lateral bracing was provided at the location of the load (Fig. 3-8a), the provision of a lateral brace at the load height is observed to significantly increase the critical moment, particularly when the load is applied at the top flange.

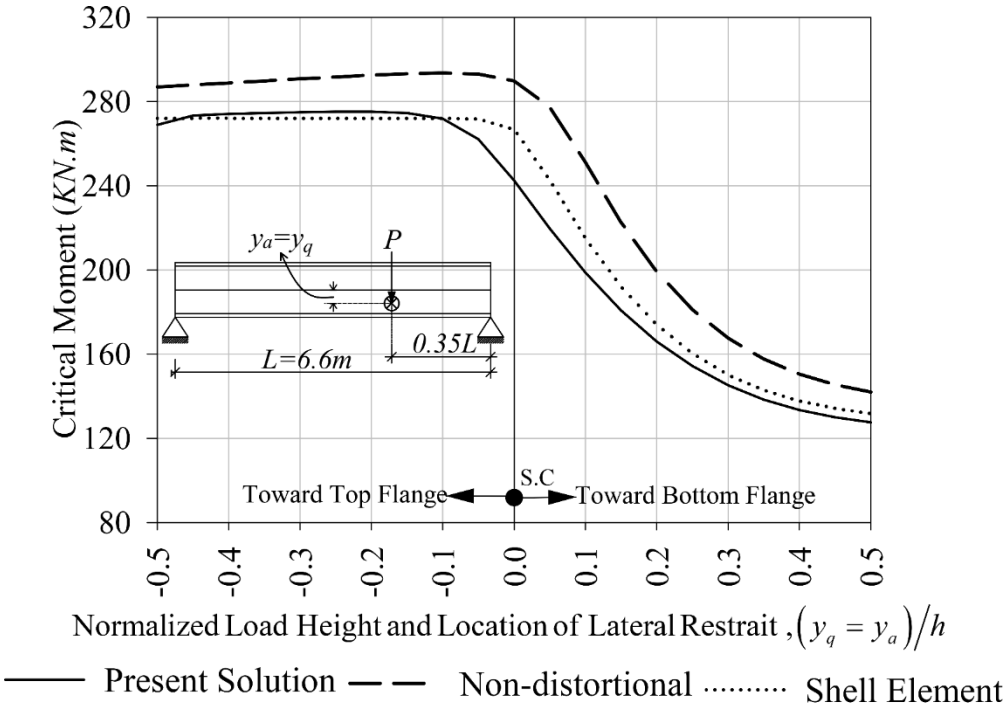

Fig. 3-9: The variation of a point load in the web height where the location of the load application is laterally restrained.

As discussed in Section 3.7.4, the use of the Euler-Bernoulli beam in pre-buckling analysis omits the contribution of transverse shear stresses; therefore, the critical moments predicted by the present study are smaller than those predicted by the shell element model.

Unlike the sharp change in the buckled configuration of the beam observed at the threshold bracing in the case where the bracing height was varied but the load height kept constant (Section 3.7.3), a more gradual transition is observed around the "threshold height" in the present problem. In order to show this gradual transition, the buckled lateral displacements are obtained from the present distortional model for three represented cases, where $y_q = y_a = -0.2h$, $y_q = y_a = -0.1h$, and $y_q = y_a = 0$ (Fig. 3-10).

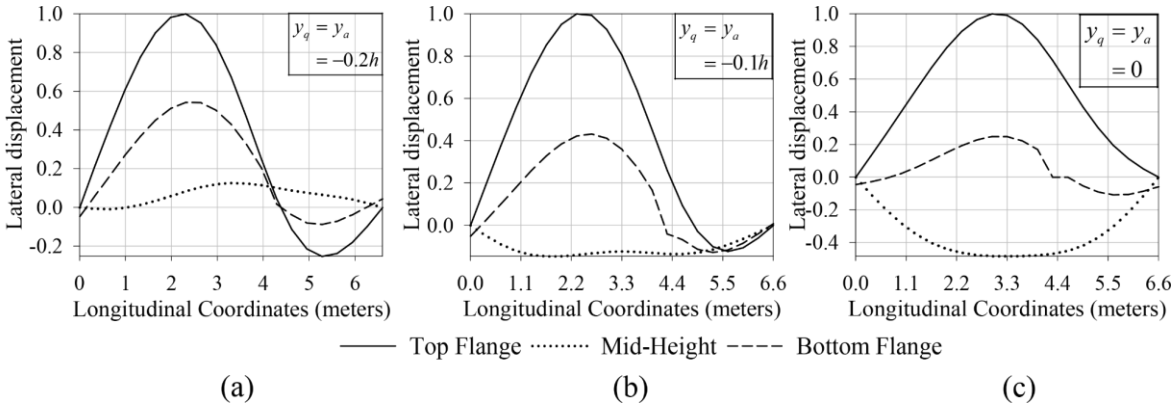

Fig. 3-10: Lateral displacement of flanges and web mid-height along longitudinal direction when load height and lateral bracing are at (a) $y_q = y_a = -0.2h$, (b) $y_q = y_a = -0.1h$, and (c) $y_q = y_a = 0$

3.8. Designing Transverse Stiffeners to Control Web Distortion

In steel construction, transverse stiffeners are used to (a) increase the web bearing capacity due to yielding or crippling when point loads or reactions act on the flanges or (b) increase the shear capacity of plate girders with slender webs through tension field action. In the context of the classical non-distortional lateral-torsional buckling, the provision of transverse stiffeners offers no advantage in increasing the critical moment capacity M_{ND} as the section is assumed to move as a rigid disk throughout LTB under the classical solution. Past investigations (Chapter 2 Section 2.11) showed that distortional modes reduce the critical moment ratio M_D/M_{ND} leading to a value below unity. From a practical viewpoint, the suppression of web distortional deformation at a given section $\bar{z}$ can be attained by providing a transverse stiffener at $\bar{z}$ (Fig. 3-11). Under the present distortional buckling model, the effect of a stiffener can be modeled by setting to zero the degrees of freedom at the section $\bar{z}$ that are associated with the distortional modes, i.e., $\boldsymbol{\Delta}^T{}_{\bar{z}} = {}_{\bar{z}}\left\langle \boldsymbol{\Delta}^T_{1\bar{z}} \;\vdots\; \boldsymbol{\Delta}^T_{2\bar{z}} \;\vdots\; \mathbf{0}^T \;\vdots\; \mathbf{0}^T \;\vdots\; \ldots \;\vdots\; \mathbf{0}^T \right\rangle_{1\times 4m}$, in which $\mathbf{0}$ is a null vector of order 4×1. This condition ensures that distortional amplitude $\phi_i(\bar{z})$ vanishes for all distortional modes $i = 3,4,\ldots m$ at section $\bar{z}$. From a design viewpoint, a designer may wish to target a critical moment ratio M_D/M_{ND} that exceeds a specified threshold value β (i.e., $M_D/M_{ND} > \beta$) by providing transverse stiffeners at optimum locations to optimize material utilization.

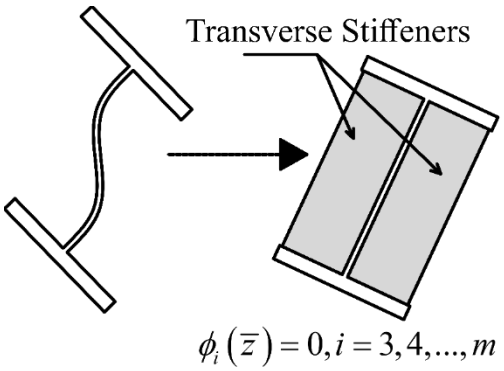

Fig. 3-11: Modeling transverse stiffeners by setting distortional modes zero

3.8.1. Distortion Indicator

Consider a beam with span L and web height h. The beam is equidistantly subdivided into $r-1$ subdivisions along the span and $s-1$ subdivisions along the web height to form an $r \times s$ grid of nodes (k, j) where $k = 1,2,....r$ and $j = 1,2,....s$. The total number of distortional modes taken to analyze the problem is m including two non-distortional modes $i = 1,2$ and the $m-2$ distortional modes $i = 3,4,...m$. The distortional lateral displacement u_D at node (k, j) with coordinates (y_k, z_j) is obtained by discarding modes 1 and 2 while retaining the distortional modes $i = 3,4,...m$ in Eq.2.18 and setting $(y, z) = (y_k, z_j)$, yielding

$$u_D(y_k, z_j) = \tilde{\mathbf{u}}_D{}^T(y_k)\mathbf{Z}_D(z_j)\boldsymbol{\Delta}_D \tag{2.46}$$

in which the following vectors and matrices have been defined:

$$\tilde{\mathbf{u}}_D{}^T(y_k) = \langle \cos(\pi y_k/h) \quad \sin(2\pi y_k/h) \quad \cos(3\pi y_k/h) \quad \sin(4\pi y_k/h) \quad \ldots \rangle_{1\times(m-2)}$$

$$\mathbf{Z}_D(z_j) = \begin{bmatrix} \mathbf{H}^T(z_j) & & & \\ & \mathbf{H}^T(z_j) & \cdots & \\ & \vdots & & \\ & & & \mathbf{H}^T(z_j) \end{bmatrix}_{(m-2)\times 4(m-2)}$$

$$\boldsymbol{\Delta}_D^T = \langle \boldsymbol{\Delta}_3^T \;\vdots\; \boldsymbol{\Delta}_4^T \;\vdots\; \ldots \;\vdots\; \boldsymbol{\Delta}_m^T \rangle_{1\times 4(m-2)}$$

We define the distortional indicator $\bar{u}_D(z_j)$ as

$$\bar{u}_D(z_j) = \sqrt{\sum_{k=1}^{k=s} u_D{}^2(y_k, z_j)} \tag{2.47}$$

in order to characterize the amount of distortion at a given section z_j . Coordinate $z_{\max}$ corresponding to the peak distortional indicator, i.e., $z_{\max} = \arg\left[\max_{j=1,2,\ldots,r}\left(\bar{u}_D\left(z_j\right)\right)\right]$, provides an indication of the optimum location for a transverse stiffener. Providing a stiffener at $z_{\max}$ would suppress the distortion at that location and would correspond to an increase in M_D/M_{ND} . The problem is then re-analyzed, and the distortional indicator is computed. The optimum location for the second stiffener is identified, and the process is repeated until M_D/M_{ND} exceeds the specified target ratio β . The design procedure can be described by the following algorithm:

Determine M_{ND} and M_D for the unstiffened beam

Loop on the following until $M_D/M_{ND} > \beta$

- Obtain $\bar{u}_D\left(z_j\right)$ for all nodes $k = 1, 2, \ldots . r$
- Identify the node(s) with peak distortion indicator(s) $z_{\max} = \arg\max_{j=1,2,\ldots,r}\left(\bar{u}_D\left(z_j\right)\right)$
- Place stiffener(s) at $z_{\max}$ by suppressing all distortional modes
- Determine M_D

End loop

The Application of the above algorithm is applied to two case studies in the following sections.

3.8.2. Case Study 1: Stiffener Design for simply-supported beam

Consider a simply-supported beam with a 4m span subjected to a mid-span point load acting at section mid-height with the cross-sectional properties of the reference beam (Fig. 2-4a). The beam is longitudinally discretized into 21 nodes. The lateral displacements of the bottom and top flanges are restrained at the supports. The non-distortional lateral-torsional buckling moment is obtained by suppressing all distortional modes, yielding $M_{ND} = 141.1 KNm$. By using 16 distortional modes, the critical moment ratio for the unstiffened beam is $M_D / M_{ND} = 0.924$. The target critical moment ratio is taken as $\beta = 98\%$. The corresponding distortional indicator vector $\bar{u}_D\left(z_j\right)$ is computed, and the optimum location $z_{\max}$ of the stiffener is determined from $\bar{u}_D\left(z_j\right)$. A single stiffener is placed at $z_{\max}$ resulting in an increase in the M_D / M_{ND} ratio. The procedure is repeated until the condition $M_D/M_{ND} > \beta$ is satisfied

(Fig. 3-12a). Table 3-2 summarizes the outcomes of the design process. In the present example, providing a single stiffener at mid-span leads to an increase in ratio M_D/M_{ND} from 0.924 to 0.952. By providing an additional two stiffeners at both ends, the ratio M_D/M_{ND} was found to increase to 0.981, which satisfies the target $\beta = 98\%$.

Table 3-2: Transverse stiffener design for a simply-supported beam under mid-span point load

#Trial	# Stiffeners	Nodes # with distortional restraint	Node(s) number corresponding to peak distortion	M_D/M_{ND}	Terminate ?
1	0	None	11	0.924	No
2	1	11	1, 21	0.952	No
3	3	1, 11, 21	—	0.981	Yes

3.8.3. Case study 2: Transverse Stiffener Design for Beam with an Overhang

Consider a simply-supported beam with an overhang. The Beam cross-section is W690x125 ($h = 678mm, b = 253mm, t_W = 11.7mm, t = 16.3mm$). The back-span is $6.4m$, and the overhang span is $1.6m$. The overhang is subjected to a tip-placed point load acting at section mid-height. The beam is discretized by 40 elements. The non-distortional LTB critical moment is found to be $1616KNm$. The target critical moment ratio is taken as $\beta = 95\%$. By taking 16 modes, the critical moment ratio M_D/M_{ND} is found to be 0.784. According to the procedure discussed in the previous section, the optimum locations of the stiffeners are obtained (Fig. 3-12b). Table 3-3 summarizes the design steps.

Table 3-3: Transverse stiffener design process for a beam with an overhang under distributed load on the overhang

Trial #	# Stiffeners	Nodes # with distortional restraint	Node(s) number corresponding to peak distortion	M_D/M_{ND}	Terminate ?
1	0	None	1	0.784	No
2	1	1	6	0.873	No
3	2	1,6	41	0.941	No
4	3	1,6,41	—	0.951	No

In practice, it is common to place transverse stiffeners at supports and possibly at the location of load application (to satisfy bearing requirements). In the present loading case, three stiffeners are placed at the overhang tip (Node 1), the middle support (node 9), and the right-side support (Node 41). The critical moment ratio M_D/M_{ND} is found to be 0.91. In order to reach the target ratio $\beta = 95\%$, an additional stiffener is to be placed at node 5. This design does not optimize material utilization since it requires four stiffeners.

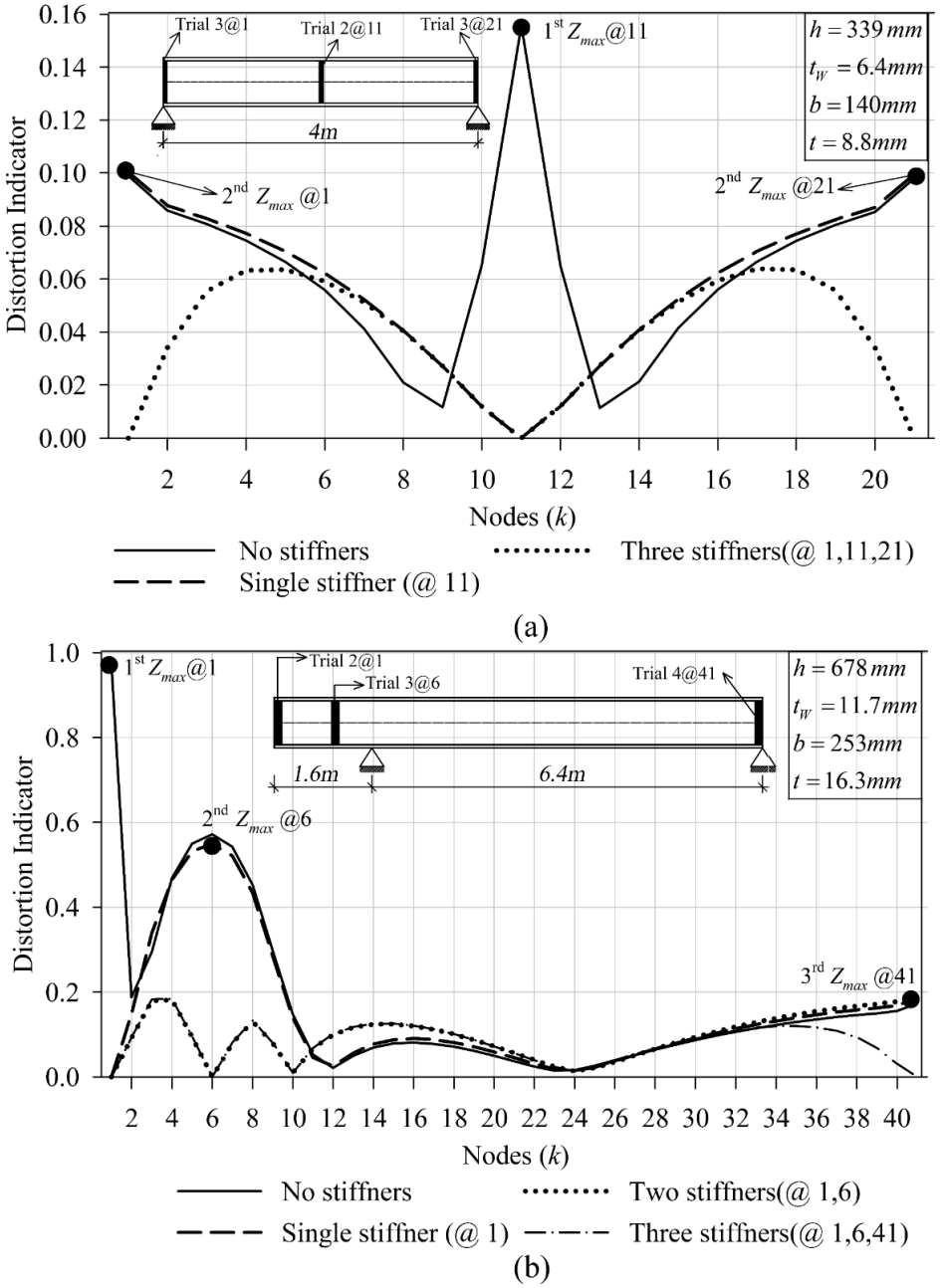

Fig. 3-12: Identification of the peak distortion and the effect of transverse stiffeners for (a) Case 1: simply-supported beam subjected to mid-span point load, and (b) Case 2: simply-supported beam with a single overhang subjected to tip-placed point load

3.9. Summary and Conclusions

In the present study, the finite element solutions developed in Chapter 2 were augmented so as to incorporate (i) the effect of load offset from the shear center and (ii) the imposition of kinematics constraints. The main conclusions of the study are:

1. The investigations on the effect of lateral bracing models reveal a significant increase in both distortional and non-distortional lateral torsional buckling resistance of doubly symmetric beam. However, for simply-supported beams whose tension flanges were discretely braced a given section, the increase in buckling resistance was moderate.
2. The presence of a lateral bracing at a given cross-section was shown to induce a significant distortional effect in the neighborhood of the point of bracing. For such cases, while the present solution accurately predicted the buckled configuration of the web when compared to the Abaqus shell model, the Hermitian distortional model failed to capture such localized effects.
3. For the problems considered, changes in the lateral bracing height showed a threshold height at which the beam's buckled configuration undergoes an abrupt modal change. Above the threshold height, the critical moment of the system remained constant.
4. In a manner consistent with past non-distortional solutions, as the point of load application shifts downwards, the critical moment capacity was found to increase. The present study, however, shows that the critical moment effects predicted by the present model are in close agreement with shell-model predictions. However, the non-distortional solution tends to over-predict the critical moments, particularly when the loads are applied near the tension flange.
5. In the case investigated where the point of load application also provides lateral bracing, as the point moves towards the top flange, the buckling resistance is observed to increase. However, no abrupt change in the buckled configuration of the beam was observed.
6. A new distortional indicator was introduced in order to characterize the distribution of web distortion along the span as the beam undergoes distortional buckling.
7. A novel technique to optimize the location of transverse stiffeners along the span was proposed. In the proposed technique, the cross-section(s) with the maximal distortion indicator were identified, and transverse stiffeners were located at the location(s) of maximum distortion. At a given cross-section with a transverse stiffener, web distortion was suppressed in the model by suppressing the distortional modes at the section.

3.10. References

[1] S. Kitipomchai, P.F. Dux, N.J. Richter, Buckling and Bracing of Cantilevers, Journal of Structural Engineering 110(9) (1984) 2250-2262.
[2] C.M. Wang, S. Kitipornchai, V. Thevendran, Buckling of braced monosymmetric cantilevers, International Journal of Mechanical Sciences 29(5) (1987) 321-337.
[3] C. Wang, K. Ang, L. Wang, Optimization of bracing and internal support locations for beams against lateral buckling, Structural optimization 9(1) (1995) 12-17.
[4] C.T. Nguyen, J. Moon, V.N. Le, H.-E. Lee, Lateral–torsional buckling of I-girders with discrete torsional bracings, Journal of Constructional Steel Research 66(2) (2010) 170-177.
[5] H.E. Lee, C.T. Nguyen, J.H. Moon, H.S. Joo, Lateral-torsional buckling of discretely-braced i-girder, Procedia Engineering 14 (2011) 264-271.
[6] C.T. Nguyen, H.-S. Joo, J. Moon, H.-E. Lee, Flexural-torsional buckling strength of I-girders with discrete torsional braces under various loading conditions, Engineering Structures 36 (2012) 337-350.
[7] F. McCann, A. Wadee, L. Gardner, Lateral stability of discretely-braced steel beams, 2012.
[8] F. McCann, L. Gardner, M.A. Wadee, Design of steel beams with discrete lateral restraints, Journal of Constructional Steel Research 80 (2013) 82-90.
[9] E. Mohammadi, S.S. Hosseini, J. AsgariMarnani, An Interactive Solution for Lateral-Torsional Buckling of the Mono-Symmetric Beam-Columns with Discrete Lateral Bracings, Structures 14 (2018) 164-177.
[10] E. Mohammadi, S.S. Hosseini, M.S. Rohanimanesh, Elastic lateral-torsional buckling strength and torsional bracing stiffness requirement for monosymmetric I-beams, Thin-Walled Structures 104 (2016) 116-125.
[11] L.C. Schmidt, A PROBLEM OF ELASTIC LATERAL STABILITY, The Quarterly Journal of Mechanics and Applied Mathematics 18(4) (1965) 501-512.
[12] G.J. Hancock, N.S. Trahair, Finite element analysis of the lateral buckling of continuously restrained beam-columns, Institution of Engineers (Australia) Civ Eng Trans (2) (1978).
[13] N. Trahair, Elastic lateral buckling of continuously restrained beam columns, The profession of a civil engineer (1979) 61-73.
[14] B. Larue, A. Khelil, M. Gueury, Elastic flexural–torsional buckling of steel beams with rigid and continuous lateral restraints, Journal of Constructional Steel Research 63(5) (2007) 692-708.
[15] A. Khelil, B. Larue, Simple solutions for the flexural-torsional buckling of laterally restrained I-beams, Engineering Structures 30(10) (2008) 2923-2934.
[16] M.A. Bradford, Lateral-Distortional buckling of steel I—Section members, Journal of Constructional Steel Research 23(1) (1992) 97-116.
[17] H.R. Ronagh, M.A. Bradford, Some notes on finite element buckling formulations for beams, Computers & Structures 52(6) (1994) 1119-1126.
[18] M.A. Bradford, H.R. Ronagh, Generalized Elastic Buckling of Restrained I-Beams by FEM, Journal of Structural Engineering 123(12) (1997) 1631-1637.
[19] J.A. Yura, Fundamentals of beam bracing, Engineering Journal, AISC (First Quarter): 11-26. (2001).
[20] M.A. Bradford, Elastic distortional buckling of tee-section cantilevers, Thin-Walled Structures 33(1) (1999) 3-17.
[21] J. Valentino, N.S. Trahair, Torsional Restraint against Elastic Lateral Buckling, Journal of Structural Engineering 124(10) (1998) 1217-1225.
[22] Z. Vrcelj, M.A. Bradford, Elastic distortional buckling of continuously restrained I-section beam–columns, Journal of Constructional Steel Research 62(3) (2006) 223-230.
[23] M.A. Bradford, N.S. Trahair, Distortional buckling of thin-web beam-columns, Engineering Structures 4(1) (1982) 2-10.

[24] R. Johnson, C. Fan, E. 4, Distortional lateral buckling of continuous composite beams, Proceedings of the Institution of Civil Engineers 91(1) (1991) 131-161.
[25] M.A. Bradford, N.S. Trahair, Lateral Stability of Beams on Seats, Journal of Structural Engineering 109(9) (1983) 2212-2215.
[26] W. Williams Fred, K. Jemah Adel, H. Lam Diem, Distortional Buckling Curves for Composite Beams, Journal of Structural Engineering 119(7) (1993) 2134-2149.
[27] M.L.-H. Ng, H.R. Ronagh, An Analytical Solution for the Elastic Lateral-Distortional Buckling of I-section Beams, Advances in Structural Engineering 7(2) (2004) 189-200.
[28] J.S. Park, J.M. Stallings, Y.J. Kang, Lateral–torsional buckling of prismatic beams with continuous top-flange bracing, Journal of Constructional Steel Research 60(2) (2004) 147-160.
[29] P. Pezeshky, A. Sahraei, M. Mohareb, Effect of Bracing Height on Lateral Torsional Buckling Resistance of Steel Beams, 2017.
[30] T. Belaid, F. Ammari, R. Adman, Influence of load position on critical lateral torsional buckling moment of laterally restrained beam at tense flange, Asian Journal of Civil Engineering 19(7) (2018) 839-848.
[31] A. Bradford Mark, Z. Gao, Distortional Buckling Solutions for Continuous Composite Beams, Journal of Structural Engineering 118(1) (1992) 73-89.
[32] M.A. Bradford, Buckling of elastically restrained beams with web distortions, Thin-Walled Structures 6(4) (1988) 287-304.
[33] A. Samanta, A. Kumar, Distortional buckling in braced-cantilever I-beams, Thin-Walled Structures 46(6) (2008) 637-645.
[34] V.Z. Vlasov, Thin-walled elastic beams, National Technical Information Service1961.
[35] J.N. Reddy, Theory and Analysis of Elastic Plates and Shells, CRC Press LLC, Bosa Roca, 2006.
[36] M.A. Bradford, N.S. Trahair, Distortional Buckling of I-Beams, 1981.
[37] S. Rajasekaran, D.W. Murray, Coupled Local Buckling In Wide-Flange Beam-Columns, 1973.
[38] G.J. Hancock, M.A. Bradford, N. Trahair, Web distortion and flexural-torsional buckling, 1979.
[39] M.A. Bradford, Distortional buckling of monosymmetric I-beams, Journal of Constructional Steel Research 5(2) (1985) 123-136.
[40] M.A. Bradford, Stability of monosymmetric beam-columns with thin webs, Journal of Constructional Steel Research 15(4) (1990) 323-339.
[41] C. Wang, C.K. Chin, S. Kitipornchai, Parametric study on distortional buckling of monosymmetric beam-columns, 1991.
[42] M.A. Bradford, Buckling of doubly-symmetric cantilevers with slender webs, Engineering Structures 14(5) (1992) 327-334.
[43] W.E.I. Chen, J. Ye, Elastic Lateral and Restrained Distortional Buckling of Doubly Symmetric I-Beams, International Journal of Structural Stability and Dynamics 10(05) (2010) 983-1016.
[44] J.-s. Lei, L.-y. Li, Combined web distortional and lateral-torsional buckling of partially restrained I-section beams, International Journal of Mechanical Sciences 131-132 (2017) 107-112.
[45] P. Pezeshky, M. Mohareb, Distortional lateral torsional buckling of beam-columns including pre-buckling deformation effects, Computers & Structures 209 (2018) 93-116.
[46] P. Pezeshky, A. Sahraei, M. Mohareb, Distortional Lateral Torsional Buckling Analysis of Beams with Overhangs, Journal of Structural Engineering 145(3) (2019) 04018266.

Chapter 4: Summary, Conclusions, and Recommendations

4.1. Summary

The present thesis has formulated a family of finite elements for the distortional lateral buckling analysis of doubly-symmetric wide flange beams subjected to general boundary conditions and loading. While the flanges are assumed to remain undistorted throughout buckling, the distribution of lateral displacements of the web along the web height is characterized by a combination of (a) two non-distortional modes that are characterized by linear functions, and (b) any number of user-specified of distortional modes characterized by Fourier terms. In the longitudinal directions, the displacement fields were characterized by cubic Hermitian interpolation.

For each cross-sectional distortional mode, there corresponds an amplitude is defined along the beam span. Following obtaining the amplitudes of the distortional modes through an eigenvalue analysis, the participation of each mode to the buckled configuration of the web is obtained by the product of distortional mode with its corresponding amplitude along the span. The summation of the participation of the non-distortional modes yields the non-distortional buckled configuration of the web. The successive superposition of the distortional modes to the non-distortional deformation leads to a smooth transition from the non-distortional buckling solution to the distortional buckled configuration of the web.

In contrast to more conventional distortional buckling theories based on a Hermitian distortional cross-section mode, where the distribution of the lateral displacement of the web is characterized by cubic polynomials, the distribution of the lateral displacement of the web in the current finite element formulation lends itself to a more accurate representation of the distortional behavior of the web. The degree of accuracy of the solution can be controlled by specifying the number of distortional modes in addition to the conventional approach of increasing the number of elements in the longitudinal direction. Specifying a large number of distortional modes provides a better predictive power in determining (i) the distortional lateral-torsional buckling strength, and (ii) the distortional buckled configuration of the web.

In the formulation, mathematical identities related to the Kronecker product matrix operation were found to facilitate the automatic superposition of any number of user-specified distortional modes and enable the seamless separation of variables, leading to simplifications and efficiencies in the numeric implementation. Thus, the resulting finite element formulation provides a robust and computationally efficient tool for (i) conducting non-distortional and distortional lateral torsional buckling analysis and (ii) quantifying the participation of non-distortional and distortional lateral torsional modes to the buckling behavior of the beam.

The present solution features a 1-D representation of the 3D distortional buckling problem without sacrificing its prediction accuracy. This enabled conducting an extensive parametric study in which both distortional and non-distortional lateral torsional buckling resistance were obtained for four classes of problems.

The Euclidian norm of the lateral displacement quantities associated with the web distortional modes was proposed as distortional indicators that characterize the variation of distortion magnitudes along the span.

One of the advantages of the present solution is the convenience in which it can suppress the distortional modes at a given cross-section to capture the effect of transverse stiffeners and hence quantify the gain in critical moment capacity achieved by the provision of stiffeners.

4.2. Conclusions

The main conclusions of the study are:

1. The study showed that beams with larger spans are less susceptible to web distortion. Interestingly, the effect of aspect ratio and the flanges slenderness was shown to significantly impact distortion, especially for cantilevers and simply-supported beams with an overhang.
2. For unbraced beams, the comparison of the current finite element formulation, the Hermitian distortional model, and Abaqus shell element revealed that the predictions of the present study for the distortional lateral torsional buckling moments are more accurate than those predicted by the distortional Hermitian model, when a sufficient number of distortional modes, typically more than two, are taken.
3. For laterally braced beams, the present solution, under its distortional modes, accurately predicts the distortional lateral torsional buckling capacity, whereas the Hermitian distortional model fails to account for the web distortion, especially in the neighborhood of the locations at lateral braces

4.3. Recommendation for Future Work

Recommendations for future work include:

1- The present finite element solution lends itself to non-distortional and distortional lateral torsional buckling of solely doubly symmetric wide flanges beams. While this solution can be utilized for thin-wall channels with minor modifications, more effort is necessary to generalize the present solution for beams with mono-symmetric cross-sections.

2- The present solution neglects the effect of pre-buckling deformation, shear deformation effects. Future extensions of the approach may consider such effects.

3- The present solution is able to restrain lateral displacement at any arbitrary point of beams. The relevant future works include continuous restrained beams.

4- The present solution is well suited for generating closed-form solutions by observing each mode's amplitude along the beam length from the finite element analysis and assigning an approximate function to each mode amplitude.

Appendix A. **Separation of Variables**

The Kronecker product of two matrices is defined as follows: For two matrices $\mathbf{T}=\left[t_{ij}\right]$ of order $(k\times l)$ and a matrix $\mathbf{M}=\left[m_{ij}\right]$ of order $(r\times s)$, the Kronecker product is defined as

$$\mathbf{T}\otimes\mathbf{M}=\begin{bmatrix} t_{11}\mathbf{M} & t_{12}\mathbf{M} & \cdots & t_{1n}\mathbf{M} \\ t_{21}\mathbf{M} & t_{22}\mathbf{M} & \cdots & t_{2n}\mathbf{M} \\ \vdots & \vdots & & \vdots \\ t_{m1}\mathbf{M} & t_{m2}\mathbf{M} & \cdots & t_{mn}\mathbf{M} \end{bmatrix} \tag{A.48}$$

where $\mathbf{T}\otimes\mathbf{M}$ is a matrix of order $\left(k\,r\times l\,s\right)$[1].

Consider two vectors $\boldsymbol{\alpha}$ and $\boldsymbol{\beta}$ of order $(k\times 1)$, $\mathbf{I}$ is the identity matrix of order $k\times k$, and $\mathbf{M}$ is another matrix of order $(k\times k)$. We show that $\left(\mathbf{I}\otimes\boldsymbol{\alpha}\right)\mathbf{M}\left(\mathbf{I}\otimes\boldsymbol{\beta}^{\mathbf{T}}\right)=\mathbf{M}\otimes\left(\boldsymbol{\alpha}\boldsymbol{\beta}^{\mathbf{T}}\right)$. Starting with the identity

$$\mathbf{M}=\mathbf{M}\otimes\left[1\right] \tag{A.49}$$

and pre-multiply both sides of Eq.A.49 by $\left(\mathbf{I}\otimes\boldsymbol{\alpha}\right)$, one obtains

$$\left(\mathbf{I}\otimes\boldsymbol{\alpha}\right)\mathbf{M}=\left(\mathbf{I}\otimes\boldsymbol{\alpha}\right)\left(\mathbf{M}\otimes\left[1\right]\right) \tag{A.50}$$

Using the mixed product property of the Kronecker product, the right side of Eq.A.50 can be expressed as

$$\left(\mathbf{I}\otimes\boldsymbol{\alpha}\right)\mathbf{M}=\left(\mathbf{I}\otimes\boldsymbol{\alpha}\right)\left(\mathbf{M}\otimes\left[1\right]\right)=\left(\mathbf{I}\,\mathbf{M}\right)\otimes\left(\boldsymbol{\alpha}\left[1\right]\right)=\mathbf{M}\otimes\boldsymbol{\alpha} \tag{A.51}$$

By post-multiplying both sides of Eq.A.51 by $\left(\mathbf{I}\otimes\boldsymbol{\beta}^{\mathbf{T}}\right)$, one obtains

$$\left(\mathbf{I}\otimes\boldsymbol{\alpha}\right)\mathbf{M}\left(\mathbf{I}\otimes\boldsymbol{\beta}^{\mathbf{T}}\right)=\left(\mathbf{M}\otimes\boldsymbol{\alpha}\right)\left(\mathbf{I}\otimes\boldsymbol{\beta}^{\mathbf{T}}\right)=\left(\mathbf{M}\mathbf{I}\right)\otimes\left(\boldsymbol{\alpha}\boldsymbol{\beta}^{\mathbf{T}}\right)=\mathbf{M}\otimes\left(\boldsymbol{\alpha}\boldsymbol{\beta}^{\mathbf{T}}\right) \tag{A.52}$$

Now consider the following double integral

$$\frac{D}{2}\int_{0}^{L}\int_{-h/2}^{-h/2}\left(\mathbf{Z}\left(z\right)\tilde{\mathbf{u}}_{,yy}\left(y\right)\tilde{\mathbf{u}}_{,yy}^{T}\left(y\right)\mathbf{Z}^{T}\left(z\right)\right)dydz \tag{A.53}$$

Using the Kronecker product, one obtains

$$\frac{D}{2}\int_0^L \int_{-h/2}^{-h/2} \left[\left(\mathbf{I} \otimes \mathbf{H}(z) \right) \left(\tilde{\mathbf{u}}_{,yy}(y) \tilde{\mathbf{u}}_{,yy}^T(y) \right) \left(\mathbf{I} \otimes \mathbf{H}^T(z) \right) \right] dydz \tag{A.54}$$

The combination of Eq.A.54 and identity A.52 gives

$$\frac{D}{2}\int_0^L \int_{-h/2}^{-h/2} \left(\tilde{\mathbf{u}}_{,yy}(y) \tilde{\mathbf{u}}_{,yy}^T(y) \right) \otimes \left(\mathbf{H}(z) \mathbf{H}^T(z) \right) dydz \tag{A.55}$$

Since the variables y and z are separated, the above dual integral changes into the Kronecker product of two single integrals

$$\frac{D}{2}\int_{-h/2}^{h/2} \tilde{\mathbf{u}}_{,yy}(y) \tilde{\mathbf{u}}_{,yy}^T(y) dy \otimes \int_0^L \mathbf{H}(z) \mathbf{H}^T(z) dy \tag{A.56}$$

Repeated application of identity A.52 simplifies all double integral into the Kronecker product of two single integrals in a similar fashion.

[1] A. Graham, Kronecker products and matrix calculus : with applications, Chichester : Horwood .New York : Halsted Press, 1981., Chichester : New York, 1981.

Appendix B. **Entries of Matrices**

The number of deformation modes used is denoted by m. Two dummy variables s and r are also set for indexing the arrays of matrices. The Kronecker delta operator is also denoted by δ_{rs}, which is defined as

$$\delta_{rs} = \begin{cases} 1 & r = s \\ 0 & r \neq s \end{cases}$$

1- Entries of Matrix $\mathbf{A}_i$ and $\mathbf{E}_i$

Let $\mathbf{A}_i$ and $\mathbf{E}_i$ be partitioned into four sub-matrices, i.e.,

$$\mathbf{A}_i = \left[\begin{array}{c|c} \mathbf{a}_{i,1} & \mathbf{a}_{i,2} \\ \hline \mathbf{a}_{i,3} & \mathbf{a}_{i,4} \end{array}\right]$$

$$\mathbf{E}_i = \left[\begin{array}{c|c} \mathbf{e}_{i,1} & \mathbf{e}_{i,2} \\ \hline \mathbf{e}_{i,3} & \mathbf{e}_{i,4} \end{array}\right]$$

Where

- $\mathbf{a}_{i,1}$ and $\mathbf{e}_{i,1}$ are matrices of size (2×2) defined in $(r=1,2 \quad s=1,2)$
- $\mathbf{a}_{i,2}$ and $\mathbf{e}_{i,2}$ are matrices of size $(2\times n)$ defined in $(r=1,2 \quad s=1,2,\ldots,n)$
- $\mathbf{a}_{i,3}$ and $\mathbf{e}_{i,3}$ are matrices $(n\times 2)$ defined in $(r=1,2,\ldots,n \quad s=1,2)$
- $\mathbf{a}_{i,3}$ and $\mathbf{e}_{i,4}$ are matrices $(n\times n)$ defined in $(r=1,2,\ldots,n \quad s=1,2,\ldots,n)$

Let us define a function to apply the periodic behavior of the arrays of matrices

$$f(c,l) = \sin(c) + (-1)^l \cos(c)$$

Using these partitions, the entries of $\mathbf{A}_i$ and $\mathbf{E}_i$ are:

$$\mathbf{a}_{1,1}^{(r,s)} = 0$$

$$\mathbf{a}_{1,2}^{(r,s)} = 0$$

$$\mathbf{a}_{1,3}^{(r,s)} = 0$$

$$\mathbf{a}_{1,4}^{(r,s)} = \frac{\pi^4}{2h^3}(r\times s)^2 \delta_{rs}$$

$$\mathbf{a}_{2,1}^{(r,s)} = \frac{h}{6}\delta_{rs} + \frac{h}{6}$$

$$\mathbf{a}_{2,2}^{(r,s)} = \frac{-h}{s\,\pi} f\left(\frac{\pi}{2}(r+s),2\right)$$

$$\mathbf{a}_{2,3}^{(r,s)} = \frac{-h}{r\,\pi} f\left(\frac{\pi}{2}(r+s),2\right)$$

$$\mathbf{a}_{2,4}^{(r,s)} = \frac{h}{2}\delta_{rs}$$

$$\mathbf{a}_{3,1}^{(r,s)} = 0$$

$$\mathbf{a}_{3,2}^{(r,s)} = 0$$

$$\mathbf{a}_{3,3}^{(r,s)} = \frac{r\,\pi}{h} f\left(\frac{\pi}{2}(r+s),2\right)$$

$$\mathbf{a}_{3,4}^{(r,s)} = \frac{-(r\times s)\pi^2}{2h}\delta_{rs}$$

$$\mathbf{a}_{4,1}^{(r,s)} = 0$$

$$\mathbf{a}_{4,2}^{(r,s)} = \frac{s\,\pi}{h} f\left(\frac{\pi}{2}(r+s),2\right)$$

$$\mathbf{a}_{4,3}^{(r,s)} = 0$$

$$\mathbf{a}_{4,4}^{(r,s)} = \frac{-(r\times s)\pi^2}{2h}\delta_{rs}$$

$$\mathbf{a}_{5,1}^{(r,s)} = \frac{2}{h}\delta_{rs} - \frac{1}{h}$$

$$\mathbf{a}_{5,2}^{(r,s)} = 0$$

$$\mathbf{a}_{5,3}^{(r,s)} = 0$$

$$\mathbf{a}_{5,4}^{(r,s)} = \frac{(r\times s)\pi^2}{2h}\delta_{rs}$$

$$\mathbf{a}_{6,1}^{(r,s)} = \delta_{rs}\left(\frac{4-r-s}{2}\right)$$

$$\mathbf{a}_{6,2}^{(r,s)} = 0$$

$$\mathbf{a}_{6,3}^{(r,s)} = 0$$

$$\mathbf{a}_{6,4}^{(r,s)} = 0$$

$$\mathbf{a}_{7,1}^{(r,s)} = \frac{2}{h^2}\delta_{rs} - \frac{1}{h^2}$$

$$\mathbf{a}_{7,2}^{(r,s)} = \frac{s\pi}{h^2} f\left(\frac{\pi(s+2r)}{2},1\right)$$

$$\mathbf{a}_{7,3}^{(r,s)} = \frac{r\pi}{h^2} f\left(\frac{\pi(r+2s)}{2},1\right)$$

$$\mathbf{a}_{7,4}^{(r,s)} = \frac{\pi^2(r\times s)}{h^2} f\left(\frac{\pi}{2}s,1\right) f\left(\frac{\pi}{2}r,1\right)$$

$$\mathbf{a}_{8,1}^{(r,s)} = \frac{2}{h^2}\delta_{rs} - \frac{1}{h^2}$$

$$\mathbf{a}_{8,2}^{(r,s)} = \frac{s\pi}{h^2} f\left(\frac{\pi(s+2r)}{2},1\right)$$

$$\mathbf{a}_{8,3}^{(r,s)} = \frac{r\pi}{h^2} f\left(\frac{\pi(r+2s)}{2},1\right)$$

$$\mathbf{a}_{8,4}^{(r,s)} = \frac{\pi^2(r\times s)}{h^2} f\left(\frac{\pi s}{2},1\right) f\left(\frac{\pi r}{2},1\right)$$

$$\mathbf{a}_{9,1}^{(r,s)} = \delta_{rs}\left(\frac{r+s-2}{2}\right)$$

$$\mathbf{a}_{9,2}^{(r,s)} = 0$$

$$\mathbf{a}_{9,3}^{(r,s)} = 0$$

$$\mathbf{a}_{9,4}^{(r,s)} = 0$$

$$\mathbf{a}_{10,1}^{(r,s)} = \frac{2}{h^2}\delta_{rs} - \frac{1}{h^2}$$

$$\mathbf{a}_{10,2}^{(r,s)} = \frac{-s\pi}{h^2} f\left(\frac{\pi}{2}(2r+s),2\right)$$

$$\mathbf{a}_{10,3}^{(r,s)} = \frac{-r\pi}{h^2} f\left(\frac{\pi}{2}(2s+r),2\right)$$

$$\mathbf{a}_{10,4}^{(r,s)} = \frac{\pi^2(r\times s)}{h^2} f\left(\frac{\pi s}{2},2\right) f\left(\frac{\pi r}{2},2\right)$$

$$\mathbf{a}_{11,1}^{(r,s)} = \frac{2}{h^2}\delta_{rs} - \frac{1}{h^2}$$

$$\mathbf{a}_{11,2}^{(r,s)} = \frac{-s\pi}{h^2} f\left(\frac{\pi}{2}(2r+s),2\right)$$

$$\mathbf{a}_{11,3}^{(r,s)} = \frac{-r\pi}{h^2} f\left(\frac{\pi}{2}(2s+r),2\right)$$

$$\mathbf{a}_{11,4}^{(r,s)} = \frac{2\pi^2(r\times s)}{h^2}\sin\left((2s+1)\frac{\pi}{4}\right)\sin\left((2r+1)\frac{\pi}{4}\right)$$

$$\mathbf{e}_{1,1}^{(r,s)} = \frac{h^2}{12}\delta_{rs}(3-r-s)$$

$$\mathbf{e}_{1,2}^{(r,s)} = \frac{h^2}{2s\pi} f\left(\frac{\pi}{2}(s+3r),2\right) + \ldots$$
$$\frac{2h^2}{s^3\pi^3}(1-\cos(s\pi)) f\left(\frac{\pi}{2}(s+2r),1\right)$$

$$\mathbf{e}_{1,3}^{(r,s)} = \frac{h^2}{2r\pi} f\left(\frac{\pi}{2}(r+3s),2\right) + \ldots$$
$$\frac{2h^2}{r^3\pi^3}(1-\cos(r\pi)) f\left(\frac{\pi}{2}(r+2s),1\right)$$

$$\mathbf{e}_{1,4}^{(r,s)} = \frac{2h^2(s\times r)}{\pi^2(s^2-r^2)^2}(\cos((s+r)\pi)-1)\times\ldots$$
$$f\left(\frac{\pi}{2}(s+r),2\right)$$

$$\mathbf{e}_{2,1}^{(r,s)} = \frac{h^2}{12}\delta_{rs}(3-r-s)$$

$$\mathbf{e}_{2,2}^{(r,s)} = \frac{h^2}{2s\pi} f\left(\frac{\pi}{2}(s+3r),2\right) - \ldots$$
$$\frac{2h^2}{s^3\pi^3}(\cos(s\pi)-1) f\left(\frac{\pi}{2}(s+2r),1\right)$$

$$\mathbf{e}_{2,3}^{(r,s)} = \frac{h^2}{2r\pi} f\left(\frac{\pi}{2}(r+3s),2\right) - \ldots$$
$$\frac{2h^2}{r^3\pi^3}(\cos(r\pi)-1) f\left(\frac{\pi}{2}(r+2s),1\right)$$

$$\mathbf{e}_{2,4}^{(r,s)} = \frac{2\,h^2\,(s\times r)}{\pi^2\left(s^2-r^2\right)^2}\left(\cos\left((s+r)\pi\right)-1\right)\times\ldots$$
$$f\left(\frac{\pi}{2}(s+r),2\right)$$

$$\mathbf{e}_{3,1}^{(r,s)} = \frac{1}{2}\delta_{rs}\left(3-r-s\right)+\frac{1}{2}\left(s-r\right)$$

$$\mathbf{e}_{3,2}^{(r,s)} = \frac{-1}{s\pi}\left(1-\cos\left(s\pi\right)\right) f\left(\frac{\pi}{2}\left(s+2r\right),1\right)$$

$$\mathbf{e}_{3,3}^{(r,s)} = \frac{1}{r\pi}\left(1-\cos\left(r\pi\right)\right) f\left(\frac{\pi}{2}\left(r+2s\right),1\right)$$

$$\mathbf{e}_{3,4}^{(r,s)} = \frac{sr}{\left(r^2-s^2\right)} f\left(\frac{\pi}{2}s,1\right)\times\left(1-\cos\left(\pi\left(s+r\right)\right)\right)$$

$$\mathbf{e}_{4,1}^{(r,s)} = \frac{1}{2}\delta_{rs}\left(3-r-s\right)+\frac{1}{2}\left(r-s\right)$$

$$\mathbf{e}_{4,2}^{(r,s)} = \frac{-1}{s\pi}\left(1-\cos\left(s\pi\right)\right) f\left(\frac{\pi}{2}\left(s+2r\right),1\right)$$

$$\mathbf{e}_{4,3}^{(r,s)} = \frac{1}{r\pi}\left(1-\cos\left(r\pi\right)\right) f\left(\frac{\pi}{2}\left(r+2s\right),1\right)$$

$$\mathbf{e}_{4,4}^{(r,s)} = \frac{sr}{\left(r^2-s^2\right)} f\left(\frac{\pi}{2}s,1\right)\left(1-\cos\left(\pi\left(s+r\right)\right)\right)$$

$$\mathbf{e}_{3,1}^{(r,s)} = \frac{1}{2}\delta_{rs}\left(3-r-s\right)+\frac{1}{2}\left(r-s\right)$$

$$\mathbf{e}_{5,2}^{(r,s)} = \frac{1}{s\pi}\left(1-\cos\left(s\pi\right)\right) f\left(\frac{\pi}{2}\left(s+2r\right),1\right)$$

$$\mathbf{e}_{5,3}^{(r,s)} = \frac{-1}{r\pi}\left(1-\cos\left(r\pi\right)\right) f\left(\frac{\pi}{2}\left(r+2s\right),1\right)$$

$$\mathbf{e}_{5,4}^{(r,s)} = \frac{sr}{\left(s^2-r^2\right)} f\left(\frac{\pi}{2}r,1\right)\times\left(1-\cos\left(\pi\left(s+r\right)\right)\right)$$

$$\mathbf{e}_{6,1}^{(r,s)} = \frac{1}{2}\delta_{rs}\left(3-r-s\right)+\frac{1}{2}\left(s-r\right)$$

$$\mathbf{e}_{6,2}^{(r,s)} = \frac{1}{s\pi}\left(1-\cos\left(s\pi\right)\right) f\left(\frac{\pi}{2}\left(s+2r\right),1\right)$$

$$\mathbf{e}_{6,3}^{(r,s)} = \frac{-1}{r\pi}\left(1-\cos\left(r\pi\right)\right) f\left(\frac{\pi}{2}\left(r+2s\right),1\right)$$

$$\mathbf{e}_{6,4}^{(r,s)} = \frac{sr}{\left(s^2-r^2\right)} f\left(\frac{\pi}{2}r,1\right)\times\left(1-\cos\left(\pi\left(s+r\right)\right)\right)$$

$$\mathbf{E}_7 = \mathbf{E}_8 = \mathbf{A}_6$$

$$\mathbf{E}_9 = \mathbf{E}_{10} = \mathbf{A}_7$$

$$\mathbf{E}_{11} = \mathbf{E}_{12} = \mathbf{A}_9$$

$$\mathbf{E}_{13} = \mathbf{E}_{14} = \mathbf{A}_{10}$$

2- Entries of Matrix $\mathbf{B}_i$ and $\mathbf{F}_i$

$$\mathbf{B}_1 = \frac{L}{420}\begin{bmatrix} 156 & 22L & 36 & -13L \\ 22L & 4L^2 & 13L & -3L^2 \\ 36 & 13L & 156 & -22L \\ -13L & -3L^2 & -22L & 4L^2 \end{bmatrix}$$

$$\mathbf{B}_2 = \mathbf{B}_6 = \mathbf{B}_8 = \frac{1}{L^3}\begin{bmatrix} 12 & 6L & -12 & 6L \\ 6L & 4L^2 & -6L & 2L^2 \\ -12 & -6L & 12 & -6L \\ 6L & 2L^2 & -6L & 4L^2 \end{bmatrix}$$

$$\mathbf{B}_3 = \frac{1}{30L}\begin{bmatrix} -36 & -33L & 36 & -3L \\ -3L & -4L^2 & 3L & L^2 \\ 36 & 3L & -36 & 33L \\ -3L & L^2 & 3L & -4L^2 \end{bmatrix}$$

$$\mathbf{B}_4 = \frac{1}{30L}\begin{bmatrix} -36 & -3L & 36 & -3L \\ -33L & -4L^2 & 3L & L^2 \\ 36 & 3L & -36 & 3L \\ -3L & L^2 & 33L & -4L^2 \end{bmatrix}$$

$$\mathbf{F}_1 = \mathbf{F}_7 = \mathbf{F}_9 \\ \mathbf{F}_{11} = \mathbf{F}_{13} = \frac{1}{60}\begin{bmatrix} 36 & 0 & -36 & 6L \\ 0 & 6L^2 & 0 & -L^2 \\ -36 & 0 & 36 & -6L \\ 6L & -L^2 & -6L & 2L^2 \end{bmatrix}$$

$$\mathbf{F}_2 = \mathbf{F}_8 = \mathbf{F}_{10} \\ \mathbf{F}_{12} = \mathbf{F}_{14} = \frac{1}{60}\begin{bmatrix} 36 & 6L & -36 & 0 \\ 6L & 2L^2 & -6L & -L^2 \\ -36 & -6L & 36 & 0 \\ 0 & -L^2 & 0 & 6L^2 \end{bmatrix}$$

$$\mathbf{F}_3 = \frac{L}{420}\begin{bmatrix} -132 & 46L & 132 & -31L \\ -24L & 2L^2 & 24L & -5L^2 \\ -78 & -11L & 78 & -4L \\ 18L & 2L^2 & -18L & 2L^2 \end{bmatrix} \qquad \mathbf{F}_4 = \frac{L}{420}\begin{bmatrix} -78 & -4L & 78 & -11L \\ -18L & -2L^2 & 18L & -2L^2 \\ -132 & -31L & 132 & 46L \\ 24L & 5L^2 & -24L & -2L^2 \end{bmatrix}$$

$$\mathbf{F}_5 = \frac{L}{420}\begin{bmatrix} -132 & -24L & -78 & 18L \\ 46L & 2L^2 & -11L & 2L^2 \\ 132 & 24L & 78 & -18L \\ -31L & -5L^2 & -4L & 2L^2 \end{bmatrix} \qquad \mathbf{F}_6 = \frac{L}{420}\begin{bmatrix} -78 & -18L & -132 & 24L \\ -4L & -2L^2 & -31L & 5L^2 \\ 78 & 18L & 132 & -24L \\ -11L & -2L^2 & 46L & -2L^2 \end{bmatrix}$$

Appendix C. Recovering the Classical Lateral Torsional Buckling Solution as a Special Case from the Distortional Buckling Solution

By expanding the lateral displacement of the web for the first two modes (non-distortional modes) , one obtains

$$u(y,z)=\tilde{u}_1(y)\phi_1(z)+\tilde{u}_1(y)\phi_1(z) \tag{C.57}$$

by substituting the global modes (appearing in Eq.2.13a-b) into Eq.C.57, one obtains

$$u(y,z)=\left[\frac{1}{2}+\frac{y}{h}\right]\phi_1(z)+\left[\frac{1}{2}-\frac{y}{h}\right]\phi_1(z) \tag{C.58}$$

By enforcing the displacement compatibility relations at the flanges, i.e.,

$$u_B(z)=u(y=h/2,z); \qquad u_T(z)=u(y=-h/2,z) \tag{C.59a-b}$$

and substituting into Eq.C.58, one obtains

$$u(y,z)=\left[\frac{1}{2}+\frac{y}{h}\right]u_T(z)+\left[\frac{1}{2}-\frac{y}{h}\right]u_B(z) \tag{C.60}$$

Eq.C.60 can be re-written as

$$u(z,y)=u_0(z)+\theta_0(z)y \tag{C.61}$$

in which $u_0(z)$ is the lateral displacement of the web at mid-height, and $\theta_0(z)$, is the angle of twist of the section defined as $u_0(z)=\left[u_B(z)+u_T(z)\right]/2$ and $\theta_0(z)=\left[u_B(z)-u_T(z)\right]/h$. Eq.C.61 shall be substituted into both the internal strain energy U and the potential energy V for all energy terms associated with the web, the top, and the bottom flanges.

<u>The internal strain energy of the web</u>

The internal strain energy for the web U_W can be expressed as

$$\begin{aligned} U_W &= U_{W1}+U_{W2}+U_{W3}+U_{W4} \\ \langle U_{W1},U_{W2},U_{W3},U_{W4}\rangle &= \frac{1}{2}\int_0^L\int_{-h/2}^{h/2} D\left\langle u_{,yy}^2,u_{,zz}^2,2\mu u_{,yy}u_{,zz},2(1-\mu)u_{,yz}^2\right\rangle dy\,dz \end{aligned} \tag{C.62}$$

For the displacement function in Eq.C.61, its second derivative $u_{,yy}$ vanishes, and hence we have $U_{W1} = U_{W3} = 0$. By performing the integrals U_{W2}, U_{W4} with respect to y and noting that $D = Et_W^3 \big/ \left[12\left(1-\mu^2\right)\right]$, and $E = 2G\left(1+\mu\right)$ one obtains

$$\begin{aligned} U_{W2} &= \frac{1}{2}\int_0^L \left[\frac{Et_W^3 h}{12\left(1-\mu^2\right)} u_{0,zz}^2 + \frac{Et_W^3 h^3}{144\left(1-\mu^2\right)} \theta_{0,zz}^2 \right] dz \\ U_{W4} &= \frac{1}{2}\int_0^L G\left(\frac{1}{3} t_W^3 h\right) \theta_{0,z}^2 \left(z\right) dz \end{aligned} \qquad \text{(C.63a-b)}$$

Recognizing that the moment inertia of the web about the y axis is $I_{yW} = t_W^3 h/12$, and the local warping constant for the web as $C_{wW} = t_W^3 h^3/144$, the Saint-Venant torsional constant for the web is $J_w = ht_W^3/3$, one can express the internal strain energy of the web as

$$U_W = U_{W2} + U_{W4} = \frac{1}{2}\int_0^L \left[\frac{E}{\left(1-\mu^2\right)} I_{yW} u_{0,zz}^2 + \frac{E}{\left(1-\mu^2\right)} C_{wW} \theta_{0,zz}^2 + GJ_W \theta_{0,z}^2 \right] dz \qquad \text{(C.64)}$$

Load potential for the web:

The load potential of the web is given by

$$V_W = \frac{1}{2}\int_0^L \int_{-h/2}^{h/2} t_W \left(\sigma u_{,z}^2\right) dy\, dz + \frac{1}{2}\int_0^L \int_{-h/2}^{h/2} t_W \left(2\tau u_{,y} u_{,z}\right) dy\, dz \qquad \text{(C.65)}$$

By differentiating Eq.C.61, substituting into Eq.C.65, and expressing the axial stress distribution due to bending as $\sigma = My/I_x$ and the shear stress as $\tau \approx V/ht_W$, one obtains

$$V_W = \frac{1}{2}\int_0^L \int_{-h/2}^{h/2} \left[\frac{t_W M}{I_x} \left(u_{0,z}^2 y + \theta_{0,z}^2 y^3 + 2y^2 u_{0,z} \theta_{0,z} \right) \right] dy\, dz + \int_0^L \int_{-h/2}^{h/2} \left[\frac{V}{h} \left(u_{0,z} \theta_0 + y\, \theta_{0,z} \theta_0 \right) \right] dy\, dz$$

By performing the integrals with respect to y and noting that the moment of inertia of the web about the x axis is $I_{xW} = t_W h^3/12$, one obtains

$$V_W = \int_0^L \left[\frac{I_{xW}}{I_x} M u_{0,z} \theta_{0,z} + V u_{0,z} \theta_0 \right] dz \qquad \text{(C.66)}$$

Equations C.64 and C.66 provide the total potential energy contribution for the web in the context of non-distortional lateral torsional buckling.

The internal strain energy of the flanges

The internal strain energy of the bottom flange is

$$U_B = \frac{1}{2}\int_0^L \left(EI_{yF} u_{,zz}^2 \right)_{y=h/2} dz + \frac{1}{2}\int_0^L \left(EC_{wF} u_{,yzz}^2 \right)_{y=h/2} dz + \frac{1}{2}\int_0^L \left(GJ_F u_{,yz}^2 \right)_{y=h/2} dz \quad \text{(C.67)}$$

in which $I_{yF} = tb^3/12$ and $C_{wF} = t^3 b^3/144$. From Eq C.61, by differentiation and substituting $y = h/2$ into Eq.C.67 , one obtains

$$U_B = \frac{1}{2}\int_0^L \left[EI_{yF} \left(u_{0,zz}^2 + \theta_{0,zz}^2 \left(\frac{h}{2} \right)^2 + h u_{0,zz} \theta_{0,zz} \right) + EC_{wF} \theta_{0,zz}^2 + GJ_F \theta_{0,z}^2 \right] dz \quad \text{(C.68)}$$

In a similar fashion, the internal strain energy of the top flange can be expressed as

$$U_T = \frac{1}{2}\int_0^L \left[EI_{yF} \left(u_{0,zz}^2 + \theta_{0,zz}^2 \left(\frac{h}{2} \right)^2 - h u_{0,zz} \theta_{0,zz} \right) + EC_{wF} \theta_{0,zz}^2 + GJ_F \theta_{0,z}^2 \right] dz \quad \text{(C.69)}$$

By summing Equations C.68 and C.69, one recovers the internal strain energy for the flanges as

$$U_F = U_B + U_T = \int_0^L \left(EI_{yF} u_{0,zz}^2 + \left(EI_{yF} h^2/4 + EC_{wF} \right) \theta_{0,zz}^2 + GJ_F \theta_{0,z}^2 \right) dz \quad \text{(C.70)}$$

Load potential energy for the flanges

The load potential energy for the top flange is

$$V_B = \frac{1}{2}\int_0^L \left(\sigma A_f u_{,z}^2 \right)_{y=h/2} dz + \frac{1}{2}\int_0^L \left(\sigma I_{fy} u_{,yz}^2 \right)_{y=h/2} dz \quad \text{(C.71)}$$

From Eq.C.61, by differentiation, and setting $y = h/2$, into Eq.C.71, one obtains

$$V_B = \frac{1}{2}\int_0^L \left[\sigma_{y=h/2} A_f \left(u_{0,z}^2 + \theta_{0,z}^2 \left(\frac{h}{2} \right)^2 + 2\left(\frac{h}{2} \right) u_{0,z} \theta_{0,z} \right) \right] dz + \frac{1}{2}\int_0^L \left[\sigma_{y=h/2} I_{fy} \left(\theta_{0,z}^2 \right) \right] dz \quad \text{(C.72)}$$

Noting that the axial stress in the bottom flange due to bending is $\sigma = (Mh)/(2I_x)$, one obtains

$$V_B = \frac{1}{2}\int_0^L \left[\frac{MA_f}{I_x} \left(u_{0,z}^2 \left(\frac{h}{2} \right) + \theta_{0,z}^2 \left(\frac{h}{2} \right)^3 + 2\left(\frac{h}{2} \right)^2 u_{0,z} \theta_{0,z} \right) + \frac{MI_{yf}}{I_x} \left(\theta_{0,z}^2 \frac{h}{2} \right) \right] dz \quad \text{(C.73)}$$

In a similar fashion, the load potential energy of the top flange is found to be

$$V_T = \frac{1}{2}\int_0^L \left[-\frac{MA_f}{I_x}\left(u_{0,z}^2\left(\frac{h}{2}\right) + \theta_{0,z}^2\left(\frac{h}{2}\right)^3 - 2\left(\frac{h}{2}\right)^2 u_{0,z}\theta_{0,z} \right) - \frac{MI_{yf}}{I_x}\left(\theta_{0,z}^2\frac{h}{2} \right) \right] dz \qquad \text{(C.74)}$$

The load potential energy for the top and bottom flanges is obtained by summing Eqs.C.73 and C.74 yielding

$$V_F = V_B + V_T = \int_0^L \frac{A_f h^2 M}{2I_x} u_{0,z}\theta_{0,z} dz \qquad \text{(C.75)}$$

From Eqs.C.64, C.66, C.70, and C.75, by summation, one can recover the total potential energy π of the system as

$$\Pi = \frac{1}{2}\int_0^L \left[E\overline{I_y} u_{0,zz}^2 + E\overline{C_w}\theta_{0,zz}^2 + G\overline{J}\theta_{0,z}^2 \right] dz + \int_0^L \left[\alpha M u_{0,z}\theta_{0,z} + V u_{0,z}\theta_0 \right] dz \qquad \text{(C.76)}$$

in which the effective sectional properties $\overline{I_y}$, $\overline{C_w}$, and $\overline{J}$ respectively represent the minor moment of inertia, the warping constant, and the Saint-Venant torsional constant arising from the present solution and are defined in Table C- 1. Also shown in the table are the sectional properties based on the Gjelsvik theory [1] for comparison. Constant α is a multiplier of the destabilizing term due to moments as predicted from the present theory. In the classical theory (e.g., Vlasov 1961), this multiplier takes the value $\alpha = 1.0$. Numerically, it can be verified that for typical sections, one has $\overline{I_y} \approx I_y$, $\overline{C_w} \approx C_w$, $\alpha \approx 1.0$, and $\overline{J} = J$.

Table C- 1: Comparison of sectional properties based on the present theory to those of the Gjelsvik theory.

Sectional properties based on		Constant definitions
Present solution	Gjelsvik theory	
$\overline{I_y} = \left(\frac{I_{yW}}{1-\mu^2} + 2I_{yF} \right)$	$I_y = \left(I_{yW} + 2I_{yF} \right)$	$I_{yW} = \frac{ht_W^3}{12}, I_{yF} = \frac{tb^3}{12}$
$\overline{C_w} = \left(C_{wG} + \frac{C_{wW}}{1-\mu^2} + 2C_{wF} \right)$	$C_w = \left(C_{wG} + C_{wW} + 2C_{wF} \right)$	$C_{wG} = 2I_{yF}\frac{h^2}{4}$ $C_{wW} = \frac{t_W^3 h^3}{144}, C_{wF} = \frac{t^3 b^3}{144}$
$\overline{J} = \left(J_W + 2J_F \right)$	$J = \left(J_W + 2J_F \right)$	$I_{xW} = \frac{t_W h^3}{12}, I_{xF} = \frac{bt^3}{12}$

$\alpha = \dfrac{I_{xW} + 2A_F\left(\dfrac{h^2}{4}\right)}{I_{xW} + 2A_F\left(\dfrac{h^2}{4}\right) + 2I_{xF}}$	$\alpha = 1.0$	$A_F = bt,$ $I_{xW} = \dfrac{t_W h^3}{12}, I_{xF} = \dfrac{bt^3}{12}$

Based on the approximation $\alpha \approx 1.0$, the load potential energy approximation can be expressed as

$$V \approx \int_0^L \left(M u_{0,z} \theta_{0,z} + V u_{0,z} \theta_0 \right) dz \tag{C.77}$$

Integration by parts of the first term yields

$$\begin{aligned} V &\approx \left[\left(M u_{0,z} \right) \theta_0 \right]_0^L + \int_0^L \left[-\left(M u_{0,z} \right)_{,z} \theta_0 + V u_{0,z} \theta_0 \right] dz \\ &= \left[\left(M u_{0,z} \right) \theta_0 \right]_0^L + \int_0^L \left[-\left(M_{,z} u_{0,z} + M u_{0,zz} \right) \theta_0 + V u_{0,z} \theta_0 \right] dz \\ &= \left[\left(M u_{0,z} \right) \theta_0 \right]_0^L - \int_0^L \left(M u_{0,zz} \theta_0 \right) dz \end{aligned} \tag{C.78}$$

At a given end, when either $M = 0$, $u_{0,z} = 0$ or $\theta_0 = 0$, the boundary terms vanish, and the destabilizing term simplifies to

$$V = -\int_0^L \left(M u_{0,zz} \theta_0 \right) dz \tag{C.79}$$

which coincides with that of the classical lateral buckling solution (e.g., [2])

$$\Pi = \frac{1}{2} \int_0^L \left[E \overline{I_y} u_{0,zz}^2 + E \overline{C_w} \theta_{0,zz}^2 + G \overline{J} \theta_{0,z}^2 \right] dz - \int_0^L \left(M u_{0,zz} \theta_0 \right) dz \tag{C.80}$$

[1] A. Gjelsvik, The Theory of Thin-Walled Bars, Wiley, New York, USA, 1981.
[2] V.Z. Vlasov, Thin-walled elastic beams, National Technical Information Service1961.

Appendix D. **The Matlab Code**

This appendix provides the computation of lateral distortional buckling for the simply-supported beam subjected to mid-span point load acting at the section mid-height. The reference geometry is selected for this beam. The span of the beam is 4 meters. The beam is discretized by 21 nodes. The beam is laterally braced at mid-span on the web mid-height. The distortional lateral torsional buckling critical moment is obtained by 6 modes of deformation.

Clear all previous information

```
clear;clc;
```

Open Directories associated with classes, functions

```
addpath(genpath('Classes'));
addpath(genpath('Functions'));
addpath(genpath('Inputs'));
```

Obtain geometric Information

```
NumberofNodes = 21; % stores number nodes and equidistantly spread them
          % along the beam length
totallength =4000; % Total length of the beam

SEC = SectionGenerator; % generates the section object
```

Boundary conditions Definition

```
PreDOFs = [1, 0 , 1;...
      21, 0, 1]; % stores pre-buckling boundary condition that stores
           % node number, transverse displacement, rotation
           % around x

BottomDOFS=[1, 0 , 1;...
      21, 0, 1];  % stores buckling boundary conditions related to the
            % te bottom flange: node, lateral displacement,
            % and rotation with respect to y.
TOPDOFS=[1, 0 , 1;...
     21, 0, 1];   % stores buckling boundary conditions related to the
            % te Top flange: node, lateral displacement,
            % and rotation with respect to y.
```

```
DisDOFs = [];      % specifies nodes at which a transverse stiffener
            % is placed
```

Definition of Lateral Bracing

```
lateralconstraints= [11 , 0];  % Store the node at a which the lateral
                % bracing is applied, and the height of the
                % bracing
```

Definition of Loads

```
LoadMatrix = [1   11    1     0     1     0     0];
```

```
LoadMatrix = LoadID, ElemID, Type, z, p, w, Height
```

Obtain The buckling stiffness and geometric stiffness matrices

```
DistortionaModes =6;      % Based on number distortional modes the
                % the buckling matrices are generated

run('MatrixEntries.m');     % the script "MatrixEntries.m" generates
                % the buckling stiffness and geometric
                % matrices

FGGG = matlabFunction(GGG);   % Handle function of buckling stiffness
                % matrix
FKKK = matlabFunction(KKK);   % Handle function of buckling Geometric
                % stiffness % matrix
FCLHE = matlabFunction(CLHE);  % Handle function load height effect for
                % concentrated loads
FDLHE = matlabFunction(DLHE);  % Handle function load height effect for
                % uniformly distributed loads
```

Define the material object

```
MAT = MaterialGenerator; % function that generate the object Material
```

Define the node object

```
[NodalDATA]= DATAGENERATOR(DisDOFs, PreDOFs, NumberofNodes,totallength ...
  ,DistortionaModes,TOPDOFS,BottomDOFS);
NOD = NodeGenerator(NodalDATA,NumberofNodes);
% This section define creates a series o objects from class "Nodes.m".
```

```
% and Store them in “NOD” variable.
% Each node objects include an ID, Coordinates, pre-buckling boundary
% conditions, and buckling boundary conditions
% For example NOD[1].PrebucklingDOFs shows the prebuckling boundary
% conditions for the node number 1.
```

Define the elements object

```
Elem = ElementGenerator(NOD , NumberofNodes);
% number of elements are equal to the number nodes minus one.
% the following section creates a series of objects for the elements and
% store thim in variable Elem.
% each object of elements include ID number, the nodes it is connected,
its
% length, the transverse displacement, nodal forces obtained by
% the pre-buckling analysis
% for example Elem[1].The length shows the length of element number 1
```

Define the loads object

```
[ Loads ] = LoadCapturere(LoadMatrix);
% the following function generates objects for transverse loads applied on
% the beam and store all of them in variable "Loads"
% Each object includes Load ID, the element at which the load is applied,
% type of loading, the location at which the load is applied, the
% magnitude of loads, and the load heigh effect
% for example "Loads[2].type" specifies the type of the 2 number load
object
```

Start of Pre-buckling Analysis

Generation the equivalent nodal forces

```
EqLoad = EquivalentLoads( Elem , LoadMatrix);
```

Generation Pre-buckling Stiffness Matrix

```
KPP = KpGenerator(Elem , MAT , SEC);
```

Stiffness Matrix Assembly

```
Total_KPP = Assembly( KPP );
```

Boundary Conditions for Pre-buckling Analysis

```
[K_refined , selection, DOFs] = PreBoundary(NOD , Total_KPP);
```

Load Assembly

```
EquivalentLoadAssembly = LoadAssembly( EqLoad, Elem , NOD );
```

Pre-buckling Analysis

```
[displacement, forces] = PreBucklingAnlysis( selection , K_refined ,
EquivalentLoadAssembly , Total_KPP);
```

Return of Displacement back to element

```
Numberofelements = size(Elem , 2);
for i = 1: Numberofelements
  DisplacementReturner(Elem(i) , displacement);
end
```

Moment and force calculator

```
for i = 1: Numberofelements
  ElementMomentandShear(Elem(i) , MAT, SEC);
end
```

Moment Distribution

```
[ Momentdistributions ] = MomentDistribution( Elem );
[ ShearDistributions ] = ShearDistribution( Elem );
```

Node Coordinates

```
[ NODECOORDINATE ] = NodeCoordinates( NOD );
```

Maximum of Moments

```
MAXMoment = max(abs(Momentdistributions));
```

Start of buckling analysis

Define Buckling stiffness matrices for each elements

```
BucklingK = StiffnessMatrixGenerator(Elem ,MAT , SEC, FKKK);
```

Define Buckling Geometric stiffness matrices for each elements

```
BucklingG = GeometricStiffnessMatrixGenerator(Elem , SEC, FGGG);
```

Calculating Load Height Effect for loads applied

```
[ LoadStif ] = LoadPotentialStifness( Elem, FCLHE, FDLHE, Loads, SEC );
```

Permutation

```
 [ PBucklingK , PBucklingG, permutation ] = Permutation( BucklingK ,...
  BucklingG);
```

Generating user-defined coefficient for apply kinematics constraints

```
[ AssembledB ] = laterallogrange( lateralconstraints, NumberofNodes, ...
  Y, H, SEC ,Elem, DistortionaModes, permutation);
```

Assembly of buckling stiffness matrices

```
Total_BGP = BAssembly( PBucklingG,DistortionaModes );
Total_BK = BAssembly( PBucklingK,DistortionaModes );
```

Applying the load Height Effect

```
[ TotalLoadStif ] = AssemblyLoadStif( LoadStif, permutation,
DistortionaModes, BucklingG);
```

Augmented matrix for Lagrange multiplier

```
[ Total_BK_agmtd, Total_BGP_agmtd ] = AugmatedMatrix( Total_BK ,
Total_BGP, AssembledB, TotalLoadStif );
```

Reinforcing buckling Boundary Conditions

```
[ Total_BGP_refined , Total_BK_refined , selection ] = BucBoundary( NOD ,
Total_BGP_agmtd,Total_BK_agmtd,DistortionaModes );
```

Eigenvalue Analysis

```
 [EigenVector, EigenValue] = eig(Total_BK_refined,Total_BGP_refined,
'qz');
% This function sorts eigenvalues from the smallest to the largest and
store
% them in the variable "BLA", and their corresponding mode in variable
"BBB"
[BLA, BBB] = sort(diag(EigenValue));
% This function obtains the smallest positive eigenvector
[ PositveBLA ] = FirstPositiveEigenvector( BLA );
% This function generates the eigenvector associated with the smallest
positive
% eigenvector
FD = EigenVector(:,BBB(PositveBLA(1,2)));
FD2 = selection * FD;
```

Sort Eigenvectors

```
%this function sorts eigenvectors such that the amplitudes of each modes
% are obtained
[ U ] = SortNodalDisplacements( FD2 ,DistortionaModes );
```

Generation of buckled configuration of the web

```
 [summodesconfiguraton, DisIndicator , RigIndicator , DisPart, RigPart]...
  = DistortionContribution( U , NODECOORDINATE , Y , SEC); %This function
combine modes of %deformation by their amplitudes in order to generate the
buckled in order to generate the % %buckled configuration of the web
```

Buckling critical moment

```
MINEigen = PositveBLA(1,1);
% smallest positive eigenvalue is multiplied with the maximum pre-buckling
% moment to generate buckling critical moment
CritcalMoemnt = MINEigen * MAXMoment;
```

Results

Maximum pre-buckling moment = 1000 *N.mm*

Smallest positive Eigenvalue = 338718.3

Buckling critical moment = 338.72 *KNm*

Node	Amplitudes of modes of deformation							
	mode 1	**mode 2**	**mode 3**	**mode 4**	**mode 5**	**mode 6**	**mode 7**	**mode 8**
1	0	0	0.000167	-3.58E-05	3.26E-07	1.72E-07	-6.75E-07	5.41E-07
2	8.03E-05	-9.75E-05	1.60E-04	-9.05E-06	5.09E-07	9.85E-07	-2.23E-07	-2.39E-07
3	1.56E-04	-1.96E-04	1.50E-04	-2.15E-06	5.93E-08	3.20E-07	-1.06E-07	-8.48E-08
4	2.23E-04	-2.94E-04	1.39E-04	2.56E-07	-1.22E-07	3.04E-08	-6.48E-08	-8.49E-09
5	2.80E-04	-3.91E-04	1.28E-04	1.31E-06	-2.22E-07	-9.56E-08	-3.50E-08	2.64E-08
6	3.26E-04	-4.85E-04	1.17E-04	2.07E-06	-3.32E-07	-1.74E-07	1.95E-09	4.81E-08
7	0.000361	-0.00057	0.000105	2.98E-06	-4.87E-07	-2.56E-07	4.99E-08	7.05E-08
8	0.000386	-0.00064	9.20E-05	4.33E-06	-7.45E-07	-3.81E-07	1.06E-07	1.04E-07
9	0.000402	-0.0007	8.12E-05	5.48E-06	-1.40E-06	-5.31E-07	1.46E-07	1.53E-07
10	0.000411	-0.00074	8.87E-05	1.56E-06	-2.07E-06	-6.64E-07	-2.66E-07	2.40E-07
11	0.000414	-0.00075	0.000144	6.01E-06	2.26E-05	-3.25E-07	3.03E-06	-1.53E-07
12	0.000411	-0.00074	9.10E-05	4.10E-07	-2.27E-06	-5.56E-07	-2.30E-07	2.09E-07
13	0.000402	-0.0007	8.06E-05	5.77E-06	-1.38E-06	-5.62E-07	1.42E-07	1.63E-07
14	0.000386	-0.00064	9.22E-05	4.37E-06	-7.27E-07	-3.78E-07	1.03E-07	1.03E-07
15	0.000361	-0.00057	0.000105	2.78E-06	-5.05E-07	-2.35E-07	5.37E-08	6.40E-08
16	0.000326	-0.00048	0.000117	1.89E-06	-3.52E-07	-1.55E-07	6.15E-09	4.28E-08
17	0.00028	-0.00039	0.000128	1.18E-06	-2.32E-07	-8.53E-08	-3.30E-08	2.36E-08
18	0.000223	-0.00029	0.000138	2.20E-07	-1.18E-07	2.83E-08	-6.62E-08	-7.59E-09
19	0.000156	-0.0002	0.000148	-2.03E-06	8.49E-08	2.99E-07	-1.12E-07	-7.85E-08
20	8.02E-05	-9.73E-05	0.000158	-8.73E-06	5.68E-07	9.43E-07	-2.35E-07	-2.28E-07
21	0	0	0.000165	-3.53E-05	4.02E-07	1.67E-07	-6.79E-07	5.32E-07

[1] AFPA-TR14, Designing for lateral-torsional stability in wood members, in: A.R. 14 (Ed.) American Forest & Paper Association, Inc., American Wood Council, 2003.
[2] FEMA273, NEHRP GUIDELINES FOR THE SEISMIC REHABILITATION OF BUILDINGS, in: B.S.S. Council (Ed.) Washington, D.C., 1997.